

University of Louisville

ThinkIR: The University of Louisville's Institutional Repository

Electronic Theses and Dissertations

8-2008

Evaluation of bone quality using novel image analyses and mechanical testing methods.

Qian Xu

University of Louisville

Follow this and additional works at: <https://ir.library.louisville.edu/etd>

Recommended Citation

Xu, Qian, "Evaluation of bone quality using novel image analyses and mechanical testing methods." (2008). *Electronic Theses and Dissertations*. Paper 1609.

<https://doi.org/10.18297/etd/1609>

This Doctoral Dissertation is brought to you for free and open access by ThinkIR: The University of Louisville's Institutional Repository. It has been accepted for inclusion in Electronic Theses and Dissertations by an authorized administrator of ThinkIR: The University of Louisville's Institutional Repository. This title appears here courtesy of the author, who has retained all other copyrights. For more information, please contact thinkir@louisville.edu.

EVALUATION OF BONE QUALITY USING NOVEL IMAGE ANALYSES AND
MECHANICAL TESTING METHODS

By

Qian Xu

B.S., Daqing Petroleum Institute, 1993
M.Eng., Beijing University of Chemical Technology, 1996

A Dissertation
Submitted to the Faculty of the
Graduate School of the University of Louisville
In Partial Fulfillment of the Requirements
For the Degree of

Doctor of Philosophy

Mechanical Engineering Department
Orthopaedic Bioengineering Laboratory
University of Louisville
Louisville, Kentucky

August 2008

EVALUATION OF BONE QUALITY USING NOVEL IMAGE ANALYSES AND
MECHANICAL TESTING METHODS

By

Qian Xu

A Dissertation Approved on

July 30th, 2008

By the following Dissertation Committee:

Dissertation Director, Dr. Michael J. Voor

Dr. William W. Pierce

Dr. William P. Hnat

Dr. Peter M. Quesada

Dr. Amir Amini

ACKNOWLEDGEMENTS

I gratefully express my gratitude to all who give me the possibility to complete this dissertation. I would very much like to thank my advisor, Dr. Michael J. Voor, who gives me the chance and opens the door for me to the field of biomechanical engineering. I am very appreciative of Dr. Voor's invaluable advices, endless support and understanding throughout my graduate research.

I also wish to express my thanks to the members of my reading committee, Dr. William M. Pierce, Dr. William P. Hnat, Dr. Peter M. Quesada, and Dr. Amir Amini, for their invaluable advices and comments.

I very gratefully acknowledge my colleagues, Mr. Seid W. Waddell, Mr. Robert L. Burden Jr., Dr. Shuo Yang, Dr. Boon. H. Kam, for their dedication, help and assistance during the research. I also gratefully acknowledge Dr. Pierce's laboratory for the help during the animal study.

Especially, I would like to give my special thanks to my husband, Zhigang Song, whose great love enables me to complete this work. I am deeply indebted to my dear children. I also want to give my thanks to my parents who help me in all the time of the research.

ABSTRACT

EVALUATION OF BONE QUALITY USING NOVEL IMAGE ANALYSES AND MECHANICAL TESTING METHODS

Qian Xu

July 30th, 2008

Osteoporosis has become a growing health threat with rising social and economic consequences. The understanding of the relationship between bone mechanical strength and bone structural quality is important for the diagnosis of osteoporosis and the evaluation of osteoporosis treatments.

A novel cancellous bone segmentation method was developed to separate cancellous bone from cortical bone automatically. The segmentation was based on the three-dimensional images. The basic idea of the method is that a contiguous three-dimensional non-bone region that is located inside the whole bone region of interest can be defined as the marrow region. Any bone material that is surrounded by the marrow region is considered cancellous bone while bone that is outside of the marrow region is cortical bone. This method is more objective, more accurate and more precise than a manual method and an established computer method (Helterbrand method).

Twenty-four female Sprague-Dawley rats, 7-8 weeks old, were used in a study of various osteoporosis drugs. After 8 weeks drug treatment, alendronate had more positive effects on cancellous bone volume fraction than 17 β -Estradiol₂, raloxifene and PTH.

This striking result may be explained by the age of the rat model because the young animals are still growing rapidly and it is possible that the ovariectomy (OVX) operation results in higher remodeling rate in young animals. When an anti-resorptive drug is given, the individuals with high baseline remodeling rate have more positive response than those with low baseline remodeling rate.

120 female Sprague-Dawley rats, 5.5 months or 6 months old, were used in three studies of experimental drugs. In the Pradama studies, sensitivity analyses and linear regression analyses were conducted. Drug effect analyses were also conducted, but this research did not focus on that.

A new mechanical indentation test was developed. The three-point breaking test and the calculation of volume fraction were also established during the research. By focusing on only Sham group and OVX group, the sensitivity analyses showed that these three new methods were much more sensitive than more traditional methods (Archimedes' density measurements and three-point bending tests).

The linear regression analyses were conducted to explore if the image processing methods can be correlated to the mechanical test methods, such as indentation testing and three-point breaking testing. The analyses showed that the volume fraction calculated from image processing methods explained most of the bone strength, but not all. The R^2 of the correlation between the indentation force and the cancellous bone volume fraction (0.542) was a little lower than that between the indentation force and the whole bone volume fraction (0.588). The correlations between the mechanical results from three-point breaking testing and the volume fractions (cancellous bone and whole bone) were

in the range of 0.504 ~ 0.552. So it is better to combine both image analysis and mechanical tests to understand osteoporosis in bone properties and structures.

TABLE OF CONTENTS

	PAGE
ACKNOWLEDGEMENTS.....	III
ABSTRACT.....	IV
TABLE OF CONTENTS.....	VII
LIST OF TABLES.....	XI
LIST OF FIGURES.....	XV
CHAPTER 1. INTRODUCTION.....	1
CHAPTER 2. BACKGROUND AND SIGNIFICANCE.....	7
2.1 ANIMAL MODEL.....	7
2.2 DRUG TREATMENTS TO OSTEOPOROSIS.....	9
2.2.1 Antiresorptive therapy.....	9
2.2.2 Anabolic therapy.....	11
2.2.3 Combination therapy.....	12
2.3 EVALUATION OF BONE QUALITY BY IMAGING METHOD.....	13
2.4 CT SCANNING.....	15
2.4.1 Illustration of CT scanning.....	15
2.5 IMAGE SEGMENTATION.....	18
2.6 EVALUATION OF BONE COMPETENCE BY MECHANICAL TESTING21	

2.7	RESEARCH TASK.....	24
CHAPTER 3.	MATERIAL AND METHODS.....	25
3.1	GENERAL DESCRIPTION.....	25
3.2	STUDY OBJECTS AND DRUG TREATMENTS.....	27
3.2.1	Alendronate study.....	27
3.2.2	Pradama study.....	28
3.3	<i>IN VIVO</i> STRUCTURAL ANALYSIS	31
3.3.1	Scanning design	31
3.3.2	Image registration	33
3.3.3	Segmentation of metaphysis from other bones.....	38
3.3.4	Segmentation of cancellous and cortical compartments (Helterbrand method).....	41
3.4	A NOVEL AUTOMATIC METHOD TO SEGMENT CANCELLOUS BONE FROM CORTICAL BONE	43
3.5	AN IMPROVED METHOD OF BONE/NON-BONE SEGMENTATION (LOCAL GLOBAL THRESHOLD).....	58
3.6	MECHANICAL PROPERTY ANALYSIS	61
3.6.1	Indentation test.....	61
3.6.2	Three-point bending test	64
3.6.3	Torsion test.....	68
3.6.4	Three-point breaking test	70
3.6.5	Femoral density via Archimedes' principle.....	72
3.7	<i>EX VIVO</i> STRUCTURAL ANALYSIS	73

3.7.1	Scanning design	73
3.7.2	Image segmentation process	74
3.8	RESULTS ANALYSIS METHODS	75
3.8.1	Validation of cancellous bone segmentation method	75
3.8.2	Data analysis of Alendronate study	76
3.8.3	Data analysis of the Pradama Study in engineering perspective	76
3.8.4	Data analysis of Pradama Study (drug effect)	78
3.8.5	Description of P-value of statistical analysis	78
CHAPTER 4.	RESULT	79
4.1	CANCELLOUS BONE SEGMENTATION.....	79
4.2	ALENDRONATE STUDY	81
4.3	SENSITIVITY ANALYSES	84
4.3.1	Pradama Exp1 (Week 11).....	84
4.3.2	Pradama Exp2 (Week 11).....	88
4.3.3	Pradama Exp3 (Week 12).....	93
4.4	LINEAR REGRESSION ANALYSES	98
4.4.1	Indentation testing vs. volume fraction.....	98
4.4.2	Three-pt breaking testing vs. volume fraction	101
4.5	PRADAMA DATA ANALYSIS (DRUG EFFECT).....	105
CHAPTER 5.	DISCUSSION.....	118
5.1	CANCELLOUS BONE SEGMENTATION METHOD.....	118
5.2	ALENDRONATE STUDY	122
5.3	SENSITIVITY ANALYSIS	124

5.4	LINEAR REGRESSION ANALYSIS	129
5.5	PRADAMA DATA ANALYSIS (DRUG EFFECT).....	132
CHAPTER 6.	CONCLUSION	135
REFERENCE.....		137
CURRICULUM VITAE.....		148

LIST OF TABLES

	PAGE
Table 3-1 Structural analysis description.....	26
Table 3-2 Mechanical test description.....	26
Table 3-3 Treatment Arrangement for Alendronate Study.....	28
Table 3-4 Treatment Arrangement for Pradama Exp1	29
Table 3-5 Treatment Arrangement for Pradama Exp2	30
Table 3-6 Treatment Arrangement for Pradama Exp3	31
Table 4-1 Cancellous bone volume (mm^3) calculated from different segmentation methods.....	79
Table 4-2 the comparison of the means (cancellous bone volume of the sham sample) between different segmentation methods.....	80
Table 4-3 The coefficient of variation (CV) of each method (%)	80
Table 4-4 the comparison of the means (cancellous bone volume of the OVX sample) between different segmentation methods.....	80
Table 4-5 The comparison of the variances between manual segmentation method and the new method	81
Table 4-6 P-value of statistical analysis of cancellous bone volume fraction (with sham data).....	82

Table 4-7 P-value of statistical analysis of cancellous bone volume fraction (without sham data)	82
Table 4-8 P-value of statistical analysis of whole bone volume fraction (with sham data)	83
Table 4-9 P-value of statistical analysis of whole bone volume fraction (without sham data).....	83
Table 4-10 Pradama Exp1 outcomes	84
Table 4-11 Pradama Exp2 outcomes	89
Table 4-12 Pradama Exp3 outcomes	94
Table 4-13 Drug effect P-value of statistical analysis results by ANOVA (Exp 3)	106
Table 4-14 P-value of statistical analysis (Exp3) of drug effect on cancellous bone volume fraction (with sham data)	107
Table 4-15 P-value of statistical analysis (Exp3) of drug effect on cancellous bone volume fraction (without sham data)	108
Table 4-16 P-value of statistical analysis (Exp3) of drug effect on cortical bone volume fraction (with sham data)	108
Table 4-17 P-value of statistical analysis (Exp3) of drug effect on cortical bone volume fraction (without sham data)	108
Table 4-18 P-value of statistical analysis (Exp3) of drug effect on whole bone volume fraction (with sham data)	109
Table 4-19 P-value of statistical analysis (Exp3) of drug effect on whole bone volume fraction (without sham data)	109

Table 4-20 P-value of statistical analysis (Exp3) of drug effect on indentation force (with sham data).....	110
Table 4-21 P-value of statistical analysis (Exp3) of drug effect on indentation force (without sham data).....	110
Table 4-22 P-value of statistical analysis (Exp3) of drug effect on breaking force (with sham data).....	111
Table 4-23 P-value of statistical analysis (Exp3) of drug effect on breaking force (without sham data).....	112
Table 4-24 P-value of statistical analysis (Exp3) of drug effect on breaking yield force (with sham data).....	112
Table 4-25 P-value of statistical analysis (Exp3) of drug effect on breaking yield force (without sham data).....	112
Table 4-26 P-value of statistical analysis (Exp3) of drug effect on breaking Eng (with sham data).....	113
Table 4-27 P-value of statistical analysis (Exp3) of drug effect on breaking Eng (without sham data).....	113
Table 4-28 P-value of statistical analysis (Exp3) of drug effect on bending force (with sham data).....	114
Table 4-29 P-value of statistical analysis (Exp3) of drug effect on bending force (without sham data).....	115
Table 4-30 P-value of statistical analysis (Exp3) of drug effect on moment of inertia (with sham data).....	115

Table 4-31 P-value of statistical analysis (Exp3) of drug effect on moment of inertia (without sham data).....	115
Table 4-32 P-value of statistical analysis (Exp3) of drug effect on cross-sectional area (with sham data).....	116
Table 4-33 P-value of statistical analysis (Exp3) of drug effect on cross-sectional area (without sham data).....	116
Table 4-34 P-value of statistical analysis (Exp3) of drug effect on maximum tensile stress (with sham data).....	116
Table 4-35 P-value of statistical analysis (Exp3) of drug effect on maximum tensile stress (without sham data).....	117

LIST OF FIGURES

	PAGE
Figure 1-1 Bone description.....	2
Figure 1-2 Phases in the skeletal life cycle.....	3
Figure 2-1 CT equipment examples.....	16
Figure 2-2 It is the brief description of how the customized micro-CT system works. The animal is fixed on part manipulator and rotated with part manipulator when scanning is performed. X-ray source-detector system is fixed all the time.	18
Figure 3-1 It is the description of the CT scanning used in the Orthopaedic Bioengineering Lab. X-ray source is on the left, part manipulator is in the middle and x-ray detector is on the right. X-ray source-detector system is fixed all the time. Before the scanning, a rat is sedated and fixed on the part manipulator. During the scanning the rat is rotates with part manipulator.	32
Figure 3-2 It is the orientation process of a floating image stack. Figure (a) shows the image with cortex opening before orientation. Figure (b) shows the orientation result. The VOI was cut from original CT image stack by a rectangular (figure (c)).....	35
Figure 3-3 Description of the registration parts and the reslice parts	36
Figure 3-4 The position of the image of the tibia was moved from one side of the rectangle to another side of the rectangle when the image slices were checked from top of	

the tibia to the bottom of the tibia because the tibia was not in the vertical position when it was scanned.	37
Figure 3-5 Whole bone segmentation.....	40
Figure 3-6 Helterbrand method was used to segment cancellous bone from cortical bone	42
Figure 3-7 The dilating-filling-eroding process was used to find WholeBoneMask. The non-bone elements that were covered by WholeBoneMask were treated as cavity elements and were used to create 3D cavity model.	44
Figure 3-8 CancellousMask was created by eroding the dilated marrow region to its original size.....	46
Figure 3-9 Illustration of whole matrix method and overlapping method.....	48
Figure 3-10 An example to check openings on the cortex (There is an opening in the current image slice).....	50
Figure 3-11 An example to check openings on the cortex (There is no opening in the current image slice).....	51
Figure 3-12 Better WholeBoneMask was created. No false elements existed in cavity image (Figure f).	53
Figure 3-13 WholeBoneMask was not good if the value of WholeBoneErodeDilateDiff was set too large.....	54
Figure 3-14 CancellousMask and cancellous bone were determined with MarrowDiffS = 2 and MarrowDiffL=6	56
Figure 3-15 3D segmentation result.....	57
Figure 3-16 The illustration of the local global threshold method	60

Figure 3-17 The comparison of the bone/non-bone segmentation results from the local global threshold method and from the single global threshold method.....	60
Figure 3-18 The bone sample was embedded in Bondo and was CT scanned.....	62
Figure 3-19 The top part of the proximal metaphysis was trimmed by the diamond saw.....	63
Figure 3-20 Description of indentation test	64
Figure 3-21 Typical curve of the indentation result (Exp2, I_Red).....	64
Figure 3-22 Description of <i>ex vivo</i> CT scanning	65
Figure 3-23 Illustration of Bone area and moment inertia calculation	66
Figure 3-24 Three point bending test and the typical curve of the test result.....	67
Figure 3-25 Force-displacement Curve (Exp2, C_Green2).....	68
Figure 3-26 Torsion test.....	69
Figure 3-27 The typical curve of the test result (Exp1, A_Black)	70
Figure 3-28 Three-point breaking test and the typical curve of the test result (Exp2, G_Green).....	72
Figure 4-1 The results of cancellous bone volume (mm^3) from different segmentation methods.....	79
Figure 4-2 Bone volume fraction results of Alendronate study.....	81
Figure 4-3 Bone fraction results of Exp 1 from 3D image analysis.	85
Figure 4-4 Indentation testing results of Exp 1.....	85
Figure 4-5 Three-point breaking testing results of Exp 1.....	86
Figure 4-6 Three-point bending testing results of Exp 1	87
Figure 4-7 Torsion testing results of Exp 1	87
Figure 4-8 Density results of Exp 1 by Archimedes method.....	88

Figure 4-9 Bone fraction of Exp 2 from 3D image analysis.....	90
Figure 4-10 Three-dimensional images (Exp2) of the tibial metaphysis of an OVX and sham-operated animal (mean from each group) at the time of week 0 and week 11 after operation: all images are aligned manually using VGStudio MAX to illustrate the internal cancellous bone structure.....	90
Figure 4-11 Indentation testing results of Exp 2.....	91
Figure 4-12 Three-point breaking testing results of Exp 2.....	91
Figure 4-13 Three-point bending testing results of Exp 2.....	92
Figure 4-14 Density results of Exp 2 by Archimedes method.....	93
Figure 4-15 Three-dimensional images (Exp3) of the tibial metaphysis of an OVX and sham-operated animal (mean from each group) at the time of week 12 after operation: all images were aligned manually using VGStudio MAX to illustrate the internal cancellous bone structure.....	94
Figure 4-16 Bone fraction of Exp 3 from 3D image analysis.....	95
Figure 4-17 Three-point breaking testing results of Exp 3.....	96
Figure 4-18 Indentation testing results of Exp 3.....	96
Figure 4-19 Three-point bending testing results of Exp 3.....	97
Figure 4-20 Density results of Exp 3 by Archimedes method.....	98
Figure 4-21 Regression analysis of Exp2: Indentation force vs. BV/TV.....	99
Figure 4-22 Regression analysis of Exp3: Indentation force vs. BV/TV.....	100
Figure 4-23 Regression analysis of volume fractions (Exp2).....	100
Figure 4-24 Regression analysis of volume fractions (Exp3).....	101
Figure 4-25 Regression analysis of Exp2: Breaking force vs. BV/TV.....	101

Figure 4-26 Regression analysis of Exp3: Breaking force vs. BV/TV.....	102
Figure 4-27 Regression analysis of Exp2: Breaking yield force vs. BV/TV	103
Figure 4-28 Regression analysis of Exp3: Breaking yield force vs. BV/TV	103
Figure 4-29 Regression analysis of Exp2: Breaking Energy vs. BV/TV	104
Figure 4-30 Regression analysis of Exp3: Breaking Energy vs. BV/TV	105
Figure 4-31 Bone fraction of Exp 3 from 3D image analysis.....	106
Figure 4-32 Three-dimensional images (Exp3) of the tibial metaphysis of an OVX and sham-operated animal (mean from each group) at the time of week 12 after operation: all images were aligned manually using VGStudio MAX to illustrate the internal cancellous bone structure.....	107
Figure 4-33 Indentation testing results of Exp 3.....	110
Figure 4-34 Three-point breaking testing results of Exp 3	111
Figure 4-35 Three-point bending testing results of Exp 3	114

CHAPTER 1. INTRODUCTION

Bones are extremely dense connective tissues that, in various shapes, constitute the skeleton. The principal functions of the skeleton are mechanical support and protection, maintenance of calcium homeostasis and haematopoiesis in the bone marrow. Bone must be stiff, so it can support loads, such as body weight, jumping and running, etc, and protect the soft tissues, such as brain, heart and liver, etc. Bone must also maintain a degree of elasticity, so it can deform slightly without cracking to absorb energy when it is in compression or in tension.

There are two main forms of bone: one is cortical bone, also known as compact bone; the other is cancellous bone, also known as trabecular bone or spongy bone (Figure 1-1a). Cortical bone is dense, solid structure that plays an important role to the supportive and protective function of the skeleton. It is found primary in the shaft of long bones and forms the outer shell around cancellous bone at the ends of bones near joints and also in the vertebrae. Cancellous bone fills the end of long bones and also makes up the majority of vertebral bodies. Cancellous bone has honeycomb structure that consists of rods and plates. It is believed to distribute and dissipate the energy from articular contact loads. About 20% of the total skeletal mass in the adult human skeleton is cancellous bone and about 80% of the total skeletal mass is cortical bone. However, cancellous bone has a much greater surface area than cortical bone. Within the skeleton, cancellous bone

contributes about 67% of the total skeletal surface area in the adult human skeleton while cortical bone contributes the remaining 33% (Bronner F et al., 1999).

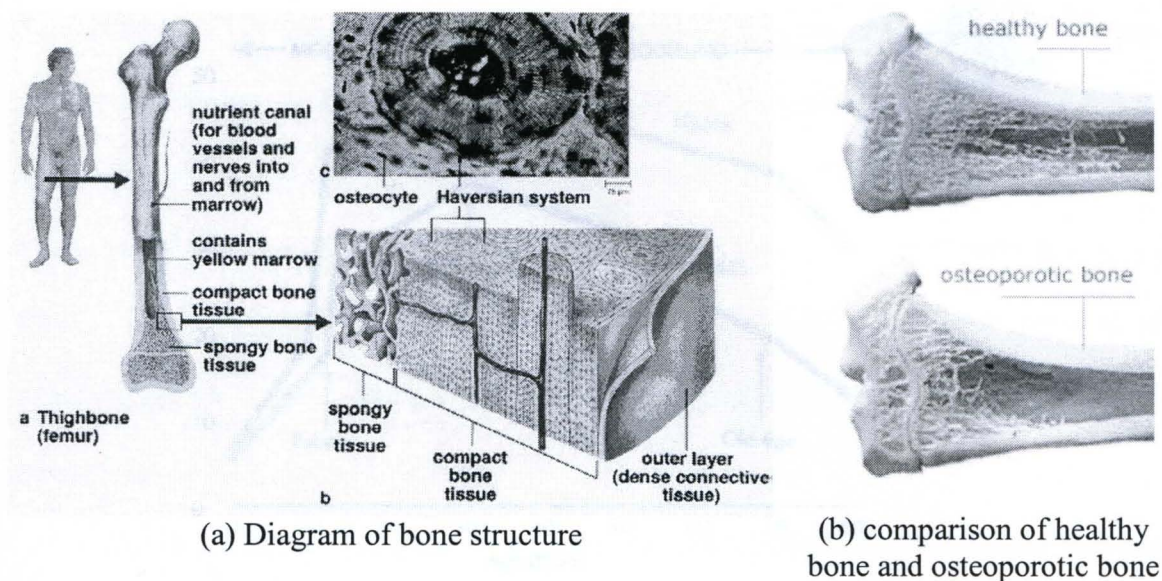


Figure 1-1 Bone description

Bone is living, self-repairing tissue constantly being replaced and renewed. Old bone is removed from the skeleton and new bone is added. Early in life, there is a positive bone balance, that is, new bone is added faster than old bone is removed. As a result, bones become larger, heavier, and denser, and the impact of bone loss related to aging is reduced. By about age 30, bone reaches its maximum density and strength, or "peak bone mass." After this peak, bone removal begins to outpace formation of new bone, which, over time, leads to bone loss (Figure 1-2). In general, the older you are, the lower the total bone mass and the greater the risk for osteoporosis. For women, the rate of bone loss is greatest in the first few years after menopause. After that, bone loss continues but more slowly. Because bone formation and bone loss only happen on the

surface of bone, cancellous bone is lost much more rapidly than cortical bone when bone turnover gets out of balance.

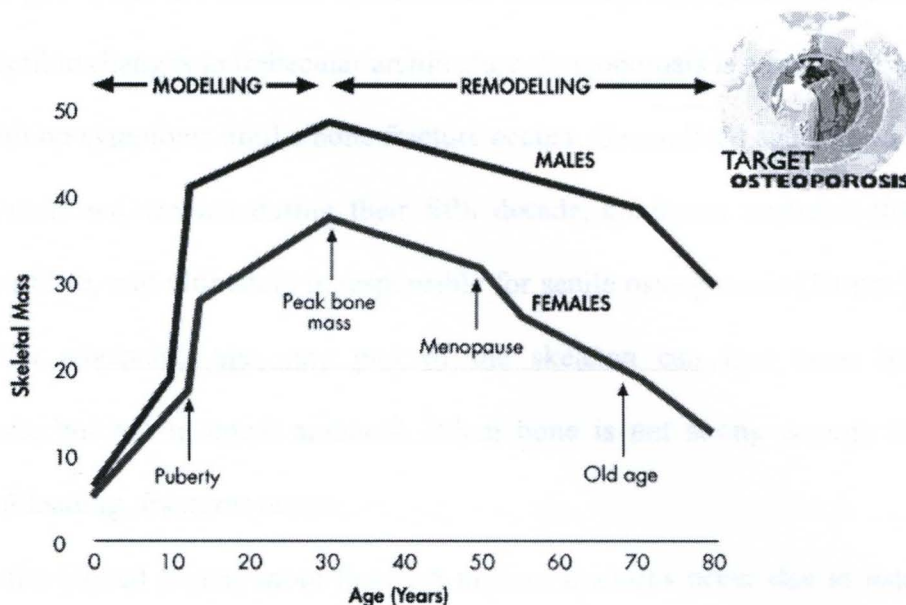


Figure 1-2 Phases in the skeletal life cycle

Estrogen deficiency (e.g., after menopause) increases the rate of remodeling and the volume of bone that is resorbed by prolonging the life span of osteoclasts. It also decreases the volume of bone that is formed by reducing the life span of osteoblasts, thereby aggravating the negative bone balance in the bone multicellular unit (Manolagas SC, 2000). It is why menopausal and post-menopausal women have accelerated bone loss and bone structural decay.

Osteoporosis has been described as “a skeletal disease characterized by low bone mass and microarchitectural deterioration of bone tissue, with a consequent increase in bone fragility and susceptibility to fracture” (Consensus Development Conference, 1991). The deterioration of bone tissue is shown in different aspects, such as cortical bone

becomes more porous and thinner, trabeculae are lost and penetrated, bone material becomes more brittle, etc. The comparison of healthy bone and osteoporotic bone is shown in Figure 1-1b, in which the loss of bone mass in the osteoporotic bone is apparent with perceptible changes in trabecular architecture. Osteoporosis is a progressive, chronic disease with no symptoms until a bone fracture occurs. Generalized age-related bone loss begins in men and women during their fifth decade, continues unabated through the remainder of life, and ultimately is responsible for senile osteoporosis (Turner RT et al., 2001). With advancing age, any part of the skeleton can lose bone because of osteoporosis, but not in equal amounts. When bone is not strong enough to support mechanical loading, fractures occur.

In the United States, more than 1.5 million fractures occur due to osteoporosis each year (Orsini LS et al., 2005). The fractures lead to considerable pain, decreased quality of life, loss of independence and mortality. Residual lifetime fracture risk in a person aged 60 years with average life expectancy was 29% for males and 56% for females (Jones G et al., 1994). The study by Melton LJ et al (1997) shows that, above age 45, 70-80% of all distal radius fractures in women, and 40-45% of all radius fractures in men are due to osteoporotic bone changes. Osteoporotic vertebral fractures are common in the elderly, occurring in about 20% of individuals older than 70 years of age (Turner AS, 2001). Women who develop a vertebral fracture are at substantial risk for additional fracture in the future (Klotzbuecher CM et al., 2000; Melton LG et al., 1999). For example, about 20% of postmenopausal women with a vertebral fracture will develop a new vertebral fracture of bone in the following year (Lindsay R et al., 2001). The most serious osteoporotic fracture is that of the hip. The risk for fractures of the femoral neck

increases 13-fold from ages 60 to 80 (De Laet CE et al., 1997). Long term nursing home care is needed for up to 30% of patients (NIH report, 2001). Twenty-five percent of patients 50-year-old and older die within 1 year after a hip fracture (US Congress OoTA, 1994). The National Osteoporosis Foundation (1996) estimates that one in two women and one in eight men are at risk of suffering osteoporosis-related fractures during their lifetime. Furthermore, osteoporotic bone heals ~30% more slowly than normal bone (Lill CA et al., 2002).

Health care expenditures attributable to osteoporotic fractures in 1995 were estimated at \$13.8 billion in the United States (Ray NF et al., 1997). Within 50 years the cost of hip fracture alone in the United States may exceed \$240 billion (Lindsay R, 1995). Because elderly people are the fastest growing population in the world and, as people age, bone mass declines and the risk of fractures increases (Cummings SR et al., 2002), osteoporosis has become a growing health threat with rising social and economic consequences. Because bone strength is the ultimate measure of bone quality and none destructive methods (imaging) are indirect measures of the bone quality, the understanding of the relationship between bone mechanical strength and bone structural quality is important for the diagnosis of osteoporosis and the evaluation of osteoporosis treatment.

The objective of this dissertation project is to develop new methods for the controlled evaluation of bone quality during experiments designed to test the efficacy of various treatments for osteoporosis using animal models. This dissertation includes both mechanical testing and high resolution imaging. Because bone strength is the ultimate measure of bone quality and none destructive methods (imaging) are indirect measures of

the bone quality, the understanding of the relationship between bone mechanical strength and bone structural quality is important for the diagnosis of osteoporosis and the evaluation of osteoporosis treatment.

CHAPTER 2. BACKGROUND AND SIGNIFICANCE

2.1 ANIMAL MODEL

Osteoporosis is a slowly progressive disease, necessitating a study of several years' duration to allow for a response to therapy (Turner AS, 2001). The high cost and the long time frame of clinical testing makes it reasonable to use animals before initiating a clinical trial in a post-menopausal osteoporosis study. Laboratory animals can provide useful information for the understanding of the pathogenesis of the osteoporosis, the extensive testing of potential therapies and evaluation of prosthetic devices in osteoporotic bone.

An appropriate animal model for any research should meet the following criteria: "1) appropriateness as an analog, 2) transferability of information, 3) genetic uniformity of organisms where applicable, 4) background knowledge of biological properties, 5) cost and availability, 6) generalizability of the results, 7) ease and adaptability to experimental manipulation, 8) ecological considerations, and 9) ethical and societal implications" (Davidson MK et al., 1987). Unfortunately, it is hard to meet all criteria for osteoporosis studies, in part because fracture risk has not been reproduced in animals, and it has proven difficult to ascertain the true degree of correspondence between the mechanisms which lead to the bone changes in the animal model and its human counterpart (Turner RT et al., 2001). Although no single animal model can precisely replicate a human

condition of osteoporosis, even a model with a small representation of human functions may be of use for some aspect of the human condition under examination (Hazzard DG et al., 1992).

The pathogenesis of osteoporosis has been investigated based on various animal models, such as dogs (Kimmel DB, 1991; Harvey EJ et al., 1999; Monier-Gaugere M-C et al., 1996; Boyce RW et al., 1990), rats and mice (Li XJ et al., 1991; Faugere MC et al., 1986; Peng Z et al., 1994; Peng Z-Q et al., 1997; Baldock PAJ et al., 1998), rabbits (Gilsanz V et al., 1988; Grardel B et al., 1994), pigs (Maier GW et al., 1997; Lafage H-M et al., 1995; Borah B et al., 2000), sheep (Lill CA et al., 2002;) and primates (Turner CH et al., 1999; Binkley N et al., 1998; Balena R et al., 1993).

The ovariectomized rat is an established model of osteopenia and osteoporosis (Li XJ et al., 1991; Wronski TJ et al., 1991; Frost HM et al., 1992), because skeletal loss after estrogen deprivation closely parallels the early rapid phase of bone loss characteristic of postmenopausal humans (Clifford JR, 2004). These include increased bone turnover, unequal bone resorption and formation, a greater loss of trabecular than cortical bone, and a rapid initial phase of bone loss followed by a slower phase (Kalu DN, 1991). With the fast generation time, rodents are often a starting point for preliminary screenings, efficacy and toxicity of new pharmacological agents or therapeutic modality, followed by verification in other species, before undertaking clinical trials in human patients (Aerssens et al., 1998). Rodents are also inexpensive and easy to house, which makes them the widely used animal model for osteoporosis studies.

Ovariectomy results in rapid loss of cancellous bone mass in some specific bone sites. From previous studies it is well known that the degree of osteoporosis is best

determined at the metaphyseal femur or tibia of the rat (Wronski TJ et al., 1985). For example, the earliest statistically significant time of cancellous bone loss in the proximal tibial metaphysis occurs at 14 days and slowing down at 90 days (Wronski TJ et al., 1988; Wronski TJ et al., 1989).

2.2 DRUG TREATMENTS TO OSTEOPOROSIS

There are three kinds of drug therapies to osteoporosis: antiresorptive therapy, anabolic therapy and combination therapy.

2.2.1 Antiresorptive therapy

Osteoporosis is the consequence of bone loss due to an imbalance in bone remodeling such that bone resorption exceeds bone formation. Because lost bone structure cannot be replaced, osteoporosis is currently managed with a range of antiresorptive therapies (Reid, 1999), which prevent further bone loss. Antiresorptive agents include bisphosphonates, calcitonin, Selective Estrogen Receptor Modulator (SERM), and estrogen.

Bisphosphonates are synthetic versions of pyrophosphate, a salt that human body manufactures to help with energy metabolism. Bisphosphonates are similar enough to bind strongly to existing bone and become embedded in the skeleton. They prevent further bone loss and create a "protective layer" that slows down osteoclast activity from dissolving tissue on the bone's surface. This can prevent the development of osteoporosis. If osteoporosis already has developed, slowing the rate of bone loss reduces the risk of

broken bones. Alendronate is the nitrogen-containing bisphosphonate. The action of alendronate in inhibiting bone resorption has been shown in large clinical trials with postmenopausal osteoporotic women with and without prevalent fractures (Black et al, 1996; Hosking et al, 1998; Li et al, 1997; McClung et al, 1998; Pols et al, 1999). Alendronate also increases degree and uniformity of mineralization in cancellous bone and decreases the porosity in cortical bone of osteoporotic women (Roschger et al, 2001).

Calcitonin is another medication used to decrease bone loss. It is a naturally occurring hormone, which helps regulate calcium levels in human body and is involved in the process of bone building. Calcitonin is used in women with osteoporosis to reduce bone loss. In Bruyere's study (2003), it shows that calcitonin reduces spinal bone (vertebrae) fractures when taken by postmenopausal women for at least 1 year. But calcitonin does not appear to be as effective as other medicines, such as alendronate, at building bone mass and reducing the risk of fractures (Abramowicz et al, 2002).

Selective Estrogen Receptor Modulators (SERMs) are "designer" drugs that activate the estrogen receptors, but have different effects on different tissues. In other words, SERMs select specific estrogen receptors in the body and either stimulate or depress an estrogen-like response. They increase bone mass, decrease the risk of spine fractures and lower the risk of breast cancer. One of SERMs, raloxifene, provides promising benefits for women with osteoporosis. Ettinger et al (1999) reported that raloxifene increased bone mineral density by 2%-3% and reduced the incidence of new vertebral fractures by 30% and 50% (in women with and without prevalent vertebral fractures, respectively) compared to placebo.

Hormone replacement therapy (HRT) is a means of continuing to provide estrogen (the female sex hormone) after its production by the ovaries has started to fail at the menopause. When estrogen levels fall therefore, the bones become thin or brittle with the result that fractures are more likely to occur. HRT is therefore used to maintain bone density and thereby reduce the risk of fractures in post-menopausal women or younger women without ovaries.

Although antiresorptive drugs slow the bone loss and decrease the risk of osteoporotic fractures by inhibiting osteoclast-mediated bone resorption, they cannot rebuild bone. In fact, because resorption and reformation occur naturally as a continuous process, blocking resorption may eventually also reduce bone formation.

2.2.2 Anabolic therapy

In anabolic therapy, both bone resorption and bone formation are stimulated. Anabolic therapy results in activation of remodeling units that leads to enhancement in bone formation over bone resorption. The primary anabolic agent is parathyroid hormone (PTH), which is administered as subcutaneous injections. There are various forms of PTH. In 2002 the FDA approved recombinant PTH 1-34, with a chemical name of teriparatide. A large multinational study of women with osteoporosis showed that treatment with teriparatide increased spinal and femoral neck bone mineral density and total body bone mineral content, and reduced the risk of vertebral and nonvertebral osteoporotic fractures by 65% and 53%, respectively (Neer et al, 2001). Moreover, what is most intriguing is that teriparatide administration leads to improvement in skeletal microarchitecture in both animals (Turner CH et al, 1999) and humans (Dempster DW et

al, 2001). Marcus (2003) showed that the skeletal response to teriparatide is largely independent of age, initial bone mineral density, and prevalent vertebral fractures in postmenopausal women with osteoporosis.

Fluoride is another bone-building agent. Its side effects were: gastrointestinal disturbances (34%), gastric ulcers (4.4%), stress fractures (6.9%), very common arthralgias (34%), and sometimes overdosages (fluorosis) (Franke J, 1988). It has also been shown to only improve bone density, but not strength. It is not commonly used because of these limitations.

2.2.3 Combination therapy

It is tempting to consider the possibility that combination therapy with different drugs, either through additive effects on suppression of bone turnover or through other as yet unknown mechanisms, might provide benefits over and above what could be achieved with either one alone. There have been and will be more clinical trials to test this hypothesis.

Johnell *et al.* (2002) reported on their study of combination therapy with alendronate and raloxifene in postmenopausal women with osteoporosis. The results of this well-designed clinical trial indicated that the combined use of these two drugs was associated with increased bone density and lower bone turnover markers than one can achieve with either drug alone. Rittmaster RS *et al.* (2000) have reported that postmenopausal osteoporotic women, who have been treated with alendronate given sequentially for 1 year after intact PTH therapy, responded with an overall increase of 14.6% at the spine together with significant increments in the femoral neck and total

body calcium. However, the study of Black et al. (2003) showed that the combination of PTH and alendronate blunted the anabolic effect of PTH on spine BMD.

Combination therapy is used on most chronic diseases. For osteoporosis, further studies are needed to determine the proper drug combination and the optimal therapeutic window.

2.3 EVALUATION OF BONE QUALITY BY IMAGING METHOD

Dual-energy X-ray Absorptiometry (DXA) is considered the clinical gold standard for measuring bone quality, and quantitative measures of bone mass (bone mineral content (BMC)) can be derived directly at all sites of interest (Genant HK et al., 1996). In World Health Organization (WHO) Technical report series 843 (year 1994), bone mineral density was used to define osteoporosis because the reduction of bone mass appears in most osteoporotic changes. Approximately 55% of the variability of femoral bone strength in side impact and vertical loading are explained by site-specific (femoral) DXA, with no other technique being able to reach a similar degree of prediction (Lochmuller EM et al., 2003). The disadvantage of the DXA is, however, that DXA provides 2D projection images, which cannot detect the details of the bone structure except projection area and length.

Although bone mineral density is used conventionally to diagnose osteoporosis, the quality of bone, such as bone structure and bone material quality etc, also plays an important role in the bone strength. It is easily explained from a mechanical perspective that the strength of a structure is determined not only by the amount and the quality of the material, but also by the spatial arrangement of the material. Geometrical measures such

as bone size, cross-sectional area or area moment of inertia have frequently shown to predict up to 70-80% of whole bone strength (Augat P et al., 2006). This explains why older women, with worse bone quality, have a much higher fracture rate than younger women with the same bone density (Heaney RP et al., 1998). Thus, detailed analysis of both trabecular and cortical bone is necessary (Peng Z-Q et al., 1997).

There are two ways to measure three-dimensional (3D) architecture of bone. One is a destructive way, such as serial milling, which uses PC-based image processing system and a digital camera to record digitized image of the cut surface (Odgaard A et al., 1989). The other is a nondestructive way, such as X-ray computed tomography (CT) and magnetic resonance imaging (MRI), which can generate a three-dimensional image of internal anatomy from a large series of two-dimensional images. It is clear that the nondestructive method is superior to the destructive one. The nondestructive method allows the specimen to be used for other measurements, such as analysis in different planes which is very desirable because the anisotropic nature of cancellous bone or the further mechanical testing which can reveal the relationship between the structural and the mechanical characteristics. When used *in vivo*, the real 3D images make it possible to catch the bone structural changes during the osteoporotic process, and also make it possible to study cortical bone and cancellous bone separately. Many structural parameters have been proposed in previous papers, such as trabecular thickness, trabecular spacing, trabecular number, bone surface, and structure model index (SMI). More studies need to be done to create a full understanding of relationships between these parameters and bone competence and fracture resistance.

2.4 CT SCANNING

2.4.1 Illustration of CT scanning

In 1895, a new radiant energy that was named as X-ray was observed and recorded by Wilhelm Conrad Rontgen. X-ray can be used to examine internal organs nondestructively and create two-dimensional images. Godfrey Hounsfield and Allan Cormack invented computed tomography (CT) in 1972 and made it possible to combine x-ray images with a computer to provide information about the tissue density across the cross-section of the tissue, which facilitates quantitative 3D architectural analysis. With continuing improvements in CT equipment and computer technology, CT became widely available by about 1980. There are now about 6,000 CT scanners installed in the U.S. and about 30,000 installed worldwide (<http://www.imaginis.com/ct-scan/history.asp>) (Figure 2-1).

A peripheral quantitative computed tomography (pQCT) scanner has been designed to examine peripheral bones such as the radius or the tibia (Kohlbrener A et al., 1997) (Figure 2-1b). Because of the relatively lower resolution ($\sim 150 \mu\text{m}$) the individual trabeculae is not easy to be recognized by the system. The pQCT is available for research scans only. It is not available yet for clinical purposes as there is no pediatric reference database (normal range) available for interpretation.

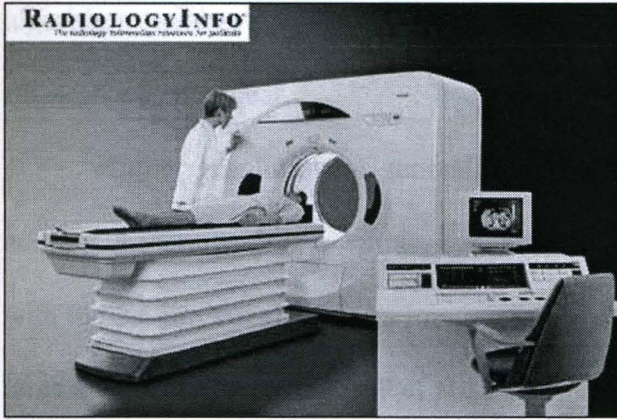


Figure (a) Abdominal and Pelvic CT

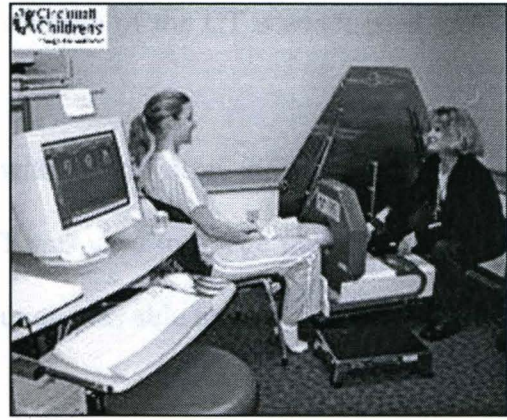


Figure (b) pQCT

Figure 2-1 CT equipment examples

Micro CT was first illustrated by Feldkamp et al. (Feldkamp LA et al., 1989; Kuhn JL et al., 1990). The system created a 3D object with image resolution of $50 \mu\text{m}$ by using a microfocus X-ray tube as a source, and image intensifier as a 3D detector, and a cone-beam reconstruction. Instead of rotating the X-ray source and detectors during data collection as in clinical CT, the specimen is rotated at various angles. The spatial resolution of $\approx 60 \mu\text{m}$ clearly visualized individual trabeculae of human, allowing a three-dimensional analysis of trabecular network (Genant HK et al., 2006). However, the resolution that appears suitable to human trabecular network is not good enough to the small animal model, such as rat, where the trabecular widths average about $50 \mu\text{m}$ and trabecular separations average $150 \mu\text{m}$ or less (Kinney JH et al., 1995). Another in vitro micro-CT scanner has been developed (Rueggsegger P et al., 1995; Rueggsegger P et al., 1996). They scanned a volume of interest that was of $4 \times 4 \times 4 \text{ mm}^3$ and represented in $14 \times 14 \times 14 \mu\text{m}^3$ voxels. The true resolution was a function of detector size, reconstruction

algorithm, number of projection, etc. The true resolution of the CT scanner used in the research was not clear.

Higher resolution is generally achieved with synchrotron μ CT and can assess additional features. For example, synchrotron μ CT was used to image trabecular surface with the 1.4 μ m voxel size. An image of this resolution was able to show a cavity inside a large trabecular strut (Peyrin F et al., 1998).

Pixel or voxel dimensions may result in a “pseudo”-resolution that typically overestimates the physically “correct” resolution by a factor of 2-4 (Jiang Y et al., 2005). Therefore, to image individual trabeculae in the rat model in which the trabecular widths average about 50 μ m, the “correct” resolution must be at least 50 μ m, requiring pixel/voxel size of 25 μ m or smaller according to Nyquist’s theorem (Engelke K et al., 1998). Peyrin’s work showed that a voxel size of 14 μ m is sufficient for most morphometric parameters (Peyrin F et al., 1998).

The micro-CT is customized to scan small animal models with a nominal resolution of 14 μ m. Similar resolution has been used in other studies, such as 13 μ m in McNamara’s study (McNamara LM et al., 2006) and 15 μ m in Boyd’s study (Boyd SK et al., 2006). The CT equipment (ACTIS 150/225 system, BIR Inc., Lincolnshire, IL) that was used in this study contains a Fein Focus 225kV microfocus x-ray system (x-ray source), a custom part manipulator and 150 mm x-ray image intensifier with DALSA 1k x 1k cooled CDD camera (x-ray detector) (Figure 2-2). The animal is fixed on the part manipulator and rotated with the part manipulator when scanning is performed. The X-ray source-detector system is fixed at all times.

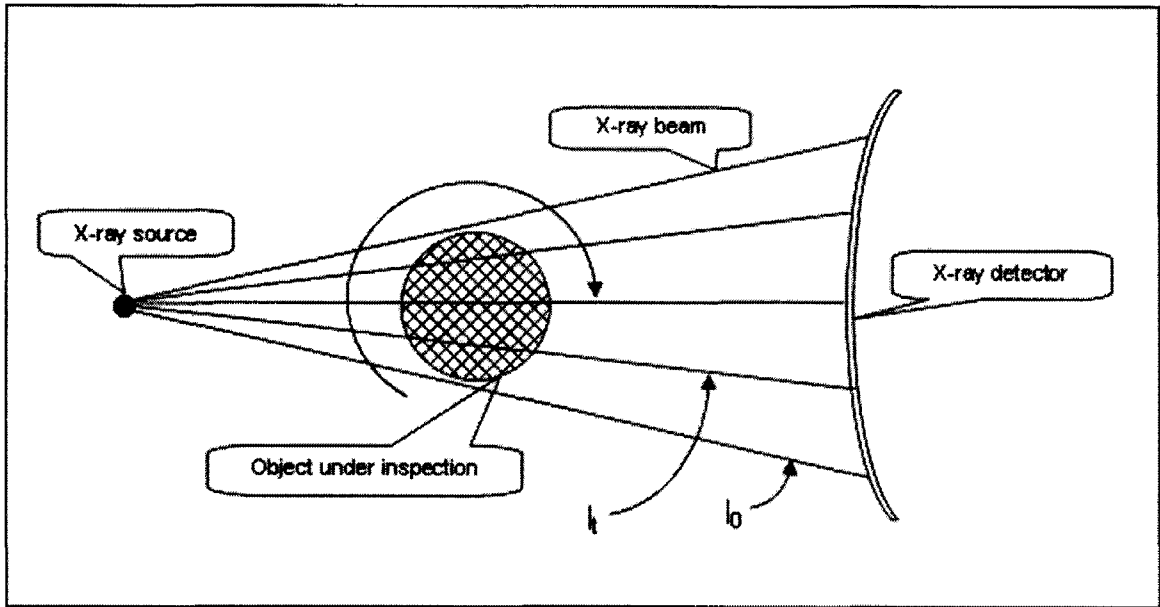


Figure 2-2 It is the brief description of how the customized micro-CT system works. The animal is fixed on part manipulator and rotated with part manipulator when scanning is performed. X-ray source-detector system is fixed all the time.

2.5 IMAGE SEGMENTATION

Segmentation methods are important to the image interpretation. There are two different segmentations: bone/non-bone segmentation and cancellous bone segmentation.

Bone/non-bone segmentation is a process to separate bone from soft tissue and the background. The CT image is composed of pixels with different gray values. The gray values of the pixels that represent bone are greater than that of the pixels that represent soft tissues and the background. The bone pixels are brighter than the soft tissue and background pixels. The analysis of bone structural parameters, such as bone volume, trabecular thickness, and structure model index (SMI), is based on the binary image that is converted from the original CT image by bone/non-bone segmentation.

The most widely used bone/non-bone segmentation method is based on a global threshold. A single threshold is determined according to the histogram of absolute gray values of all pixels in a single CT image slice or in the whole image stack. A pixel is set as bone (white) if its gray value is greater than global threshold, otherwise it is set as nonbone (black).

In many cases global threshold method does not work well because of the effect of beam hardening (since lower energy X-rays are preferentially absorbed as the X-rays traverse the specimen, the center of the specimen is exposed to more high energy X-rays, which results in darker pixels in the center) and partial volume effects (the gray value of a pixel with both bone material and nonbone material is lower than that of a pixel with all nonbone material, and greater than that of a pixel with all bone material). Local threshold method leads to more precise segmentation result by choosing specific threshold to each pixel according to the information provided by its neighborhood of a selectable size. Waarsing JH et al. (2004) developed a local threshold algorithm by detecting edges of the bone. The gray value of a voxel that is part of the edge sets is used as a local threshold for its neighbors.

Cancellous bone segmentation is used to segment cancellous bone from cortical bone, so the cancellous bone and the cortical bone can be analyzed separately. Due to the complexity of cancellous bone network and a large number of image slices, it is a time-consuming and tedious process to do segmentation manually. It is also difficult to tell where the exact boundary between cancellous bone and cortical bone is if the cortex is very porous because of osteoporosis or other diseases, or if the volume of the interest (ROI) is dominated by cancellous bone. Manual segmentation of images often produces

subjective results that are highly dependent on the knowledge and experience of the operator. Therefore, more efforts have been made recently to do segmentation automatically (Dufresne T, 1998; Helterbrand JD et al., 1997; Elmoutaouskkil A et al., 2002). Since automatic segmentation by computer is a more objective and reproducible process, it allows longitudinal study of the same subject and comparison studies between different subjects with reduced human bias and error. Helterbrand et al (Helterbrand JD et al., 1997) has developed an automatic segmentation method based on the knowledge that generally cortical bone elements are closer to the outer bone surface and have higher intensity than cancellous bone elements. The accuracy of this method decreases when the cortical bone thickness varies a lot in a single image slice. Dufresne (Dufresne T, 1998) proposed Euclidean Distance Map (EDM) in which each voxel of 3D whole bone data set contains its distance information to the nearest surface. The cortical bone is determined by finding the center of the cortical bone and dilating out the center based on its EDM value. This method requires that the holes in cortex are removed before segmentation is carried out, again resulting in a slow manual process and some human errors. Another approach involves use of a dual threshold technique (Buie HR et al, 2007), in which one threshold is used to extract the non-bone region and the other threshold is used to define the marrow cavities. To apply the algorithm, the user must adjust two threshold values to the specific dataset at hand, which impact the final segmentation result. Dilation and erosion operations are then used to reconnect marrow cavities, thus eliminating trabeculae, allowing extraction of a trabecular region mask via a connectivity filter. The extent of the dilation should be as small as possible while satisfying the requirement: the cortical porosity is removed and marrow cavities are reconnected for all datasets.

Unfortunately, this requirement cannot be satisfied for all cases, which leads to bad decision of the pores in the cortex, which further leads to bad cancellous bone segmentation.

In this dissertation, an automatic segmentation method based on the binary image information of bone structure only is introduced. Similar with the method of Buie et al (2007), marrow space is used in the new method to define the cancellous bone. In order to find the marrow space, instead of dilation and erosion operation in Buie's method, the new method takes advantage of 3D structure of the non-bone region, which can define the pores in the cortex objectively and precisely. Though the experience of two years using this method has shown excellent qualitative agreement with manual techniques, the new method was also measured quantitatively. The method was validated by comparing segmented results with manual work and a published method, the Helterbrand method.

The principle advantages of the new method are as follows: 1. It is automatic, precise and accurate; 2. The cancellous bone segmentation is dependent on the bone architecture only, no assumption is needed; 3. The method has the potential to do segmentation even when the ROI has a complex structure and irregular shape; 4. Any pores in the cortex can be distinguished from the marrow space objectively and accurately. The method is validated by comparing segmented data sets with manual method and a previous published segmentation method (Helterbrand method).

2.6 EVALUATION OF BONE COMPETENCE BY MECHANICAL TESTING

Mechanical tests in the form of three-point bending, four-point bending and torsion are the most common methods of measuring bone mechanical properties (Turner

RT et al., 2001). Because these testing are performed at the middle shaft of the diaphysis, they measure cortical bone qualities. Since the bone size of the rat is so small, there have been no reports to my knowledge of attempts to study rat bones using four-point bending testing due to the small size of rat bone sample. Three-point bending is a simple testing due to the easy bone sample preparation and test execution. It is suitable for long bones because the span of the specimen that is loaded must be sufficiently long to guarantee an accurate test. Three-point bending test has been applied to measure the strength of cortical bone (Azuma Y et al., 1998; Yang KH et al, 2007; Trebacz H et al, 2006). As an alternative to bending tests, torsional testing can be used for the evaluation of bone mechanical qualities (Lind PM et al., 2001; Burstein AH et al., 1971; Lepola V et al., 1993). Torsion testing applies the load at the end of the bone sample, which allows the load away from the region of the interest (ROI). Torsional testing requires the mounting of the specimen ends into the testing grips, which increases the time, labor and the cost of testing.

Assessment of trabecular structural characteristics and mechanical qualities may further improve the ability to understand the pathophysiology and progression of osteoporosis and other bone disorders. Compression testing has been performed on trabecular samples which have been machined into cubic subvolumes (Ulrich D et al., 1997). Unfortunately, the rat model is small and its cancellous bone cores do not meet the continuum requirement for compressive tests (Harrigan TP et al., 1988) that the specimens side length span at least five intertrabecular distances. Indentation test is a type of compression test where an indenter is driven into a sectional surface of a bone specimen (An YH et al, 1997). Although the failure mechanisms are more complicated

and less clear than the conventional compression test, indentation testing has been used to measure the biomechanical properties of cancellous bones, such as Young's modulus and strength of cancellous bone (Sumner DR et al., 1994; Aitken GK et al., 1985; Katoh T et al., 1996; An YH et al., 1997; Jamsa T et al., 2002; Khodadadyan-Klostermann C et al., 2004; Hvid I et al., 1985). The indentation testing is very sensitive to the position of the exposed cancellous bone surface. Since it is not easy to get the same exposed cancellous bone surface of different bone samples, previous studies has focused on mapping biomechanical properties of a single bone specimen, instead of comparison between different specimens. In Pradama Study, the new indentation testing method has been developed to evaluate the strength of cancellous bone resulted from different drug treatments of osteoporosis.

The complete understanding of whole bone performance is very useful for the deep understanding of the pathogenesis of the osteoporosis and the evaluation of drug treatments. The mechanical properties of entire bone can be measured by compression testing of vertebrae (Fox J et al., 2006) and cantilever testing of the neck of the femur (Azuma Y et al., 1998; Sogaard CH et al., 1994). These tests more closely approximate the type of failures associated with osteoporotic fractures. A standardized bending and breaking test at the metaphyseal region of tibias of the rat has been developed recently. This three-point breaking test is highly sensitive to evaluate hormones, substances, and even medications with regard to their osteoprotective efficiency, because the osteoporotic fracture plays the key role in osteoporosis (Sturmer EK et al., 2005).

There are other testings to measure bone quality. For example, tensile testing can be applied on cortical bone and/or cancellous bone, which requires that the bone

specimen must be big enough to meet the continuum limitation; Microtensile testing is carried out on individual trabeculae (McNamara LM et al., 2006) to assess the mechanical behavior of trabecular bone tissue.

Mechanical testing can give direct results of bone strength, but it cannot be used clinically because it is destructive. A better understanding between image analysis and mechanical testing is very helpful clinically because nondestructive methods are the only way to check patients and bone competence is the objective of the clinical examination

2.7 RESEARCH TASK

The main purpose of the present study is to evaluate bone quality using image analyses and mechanical test methods. The main objective and the general aim of the study are to: 1) isolate as much cancellous bone as possible to study the drug effect on the rat model, especially for *in vivo* study, 2) develop a novel, automatic, more precise, and more objective cancellous bone image segmentation method, 3) develop a more precise mechanical indentation test to evaluate cancellous bone quality, 4) develop more sensitive methods (compared to more traditional method, such as Archimedes density measurements and three-point bending testing) to show the differences of the bone structure caused by OVX or different drug treatments, 5) Develop a method to evaluate cortex maximum tensile stress based on the information from CT scanning image, and 6) Relate the 3D image analysis to the bone quality from mechanical results and drug treatments.

CHAPTER 3. MATERIAL AND METHODS

3.1 GENERAL DESCRIPTION

All of the methods developed and described in this dissertation were applied to evaluate the bones of rats used in collaboration with Dr. William Pierce. A total of four separate experiences were performed to study various new drugs being developed by his group for the treatment of osteoporosis. The new drugs are not the focus of this dissertation, so those data are not used. The data from control animals and those treated with reference drugs are presented. The first experiment is referred to as the Alendronate Study simply because of the large response observed in the alendronate treated rats in that experiment. The remaining three experiments are referred to as Pradama Experiment 1, Pradama Experiment 2, and Pradama Experiment 3.

The structural analysis was an image analysis based on the information that was provided by CT scanning images. *In vivo* image analysis was used in the Alendronate Study. *Ex vivo* image analysis was used in the Pradama Studies. Table 3-1 describes the structural analysis used in this study.

Table 3-1 Structural analysis description

Structural analysis	<i>In vivo</i>	<i>Ex vivo</i>
Studies	Alendronate study	Exp 1, Exp 2 and Exp 3
Scanning procedure	One rat per scanning	Six bones per scanning
Study objects	Proximal metaphysis of right tibia	Proximal metaphysis of right tibia
Bone/non-bone segmentation method	Global threshold Method	Global threshold method in Exp1; Local global threshold method in Exp2, Exp3
Cancellous bone segmentation method	Helterbrand method that is described in 3.3.4	New method that is described in 3.4
Improvement	1. Isolate as much cancellous bone as possible to study the drug effect on the rat model	
	2. Developed a GUI program by Matlab to separate VOI from other bones that are connected to VOI	2. The new method used for cancellous bone segmentation is totally automatic, more precise and more objective

There were no mechanical tests in the Alendronate Study. Mechanical tests were executed in the Pradama Studies. Table 3-2 describes the mechanical tests used in this study.

Table 3-2 Mechanical test description

Mechanical tests	Torsion	Three point bending	Indentation	Three point breaking
Studies	Pradama Exp1	Pradama Exp 1, Exp 2 and Exp 3	Pradama Exp 1, Exp 2 and Exp 3	Pradama Exp 1, Exp 2 and Exp 3
Scanning procedure		Six bones per scanning	One bone (embedded in Bondo) per scanning	
Study objects	Left femur	Middle shaft of right femur	Proximal metaphysis of left tibia	Proximal metaphysis of Right tibia
Improvement		Make it possible to evaluate cortex maximum tensile stress based on the information from CT scanning image	Develop a new method to trim the top of the bone sample at a precise position to expose the cancellous bone surface	

3.2 STUDY OBJECTS AND DRUG TREATMENTS

The animal-use protocol in the research was approved by the institutional animal care and use committee at the University of Louisville. All rats were ovariectomized (OVX) at the beginning of the experiment except the rats of the Sham group. Sham operations were performed on the Sham group by exposing the ovaries and then closing the incision. Sham procedures are typically performed to isolate the actual surgical intervention as an independent variable. In the Alendronate Study, the rat group name was arranged as TreatmentMethod. For example, SHAM means that all rats of this group were sham-operated. In pradama studies, the rat group name was arranged as TreatmentMethod_SacrificedTime. For example, SHAM_W6 means that all rats of this group were sham-operated and were sacrificed six weeks after surgery; OVX_W5 means all rats of this group were ovariectomized and sacrificed five weeks after surgery; ALEN_W12 means that all rats of this group were ovariectomized then treated by alendronate and were sacrificed twelve weeks after surgery.

3.2.1 Alendronate study

Twenty-four female Sprague-Dawley rats weighing 150g, corresponding to about 7-8 weeks old, were purchased at the beginning of the experiment, in which four rats were sham-operated and thirty rats were ovariectomized by the vendor. All rats were housed in plastic cages (L 430 mm x W 220 mm x H 200 mm), one rat per cage, and subjected to a 12-hour light/dark cycle. All rats were allowed to move freely throughout the experiment period. Tap water and the standard rodent diet were available to all rats ad libitum.

There were 6 groups of rats based on treatment: sham control (SHAM), OVX control (OVX), OVX + Alendronate (ALEN), OVX + 17 β -Estradiol₂ (E2), OVX + Raloxifene (RALOX), and OVX + Teriparatide (PTH) (Table 3-3). At the beginning of the eighth week after surgery, each rat was weighed and injected subcutaneously three times per week (on Monday, Wednesday, and Friday). On the sixteenth week after surgery, the rats were sacrificed using CO₂. The uteri, blood, femur, tails and tibiae were collected and refrigerated. 10% buffered formalin was used to fix the femur, tails and tibiae.

Table 3-3 Treatment Arrangement for Alendronate Study

Group name	SHAM	OVX	ALEN	E2	RALOX	PTH
Rat number	4	4	4	4	4	4
Drug dosage	Vehicle: 5% DMSO in corn oil; 500 μ m per 100g body weight		0.166 mg/kg	0.01 mg/kg	1.0 mg/kg	0.001 mg/kg

3.2.2 Pradama study

All rats (totally 120 rats) were housed in plastic cages (L 430 mm x W 220 mm x H 200 mm), three or four rats per cage, and subjected to a 12-hour light/dark cycle. All rats were allowed to move freely throughout the experiment period. Tap water and the standard rodent diet were available to all rats ad libitum. The rats were asphyxiated using CO₂. The uteri, blood, femur, vertebrae and tibiae were collected. Right femur, left femur, right tibia and left tibia were soaked in saline and frozen immediately after the collection. Vertebrae were soaked in formalin and refrigerated for further study.

3.2.2.1 Pradama study: Experiment 1 (Pradama Exp1)

Thirty-seven female Sprague-Dawley rats, about six-months old, were purchased at the beginning of the experiment, in which eleven rats were sham-operated and twenty rats were ovariectomized by the vendor. There were ten groups of rats based on treatment and the time point of sacrifice (the week of the surgery was set to week zero): sham control (SHAM_W2), sham control (SHAM_W4), sham control (SHAM_W8), OVX control (OVX_W2), OVX control (OVX_W4), OVX control (OVX_W8), OVX + Alendronate (ALEN_W8), OVX + Estradiol (E_W8), OVX + 17-Ethinyl Estradiol (E2_W8), and OVX + Teriparatide (PTH_W8) (Table 3-4). All rats were weighed on the fifth day after surgery. On the thirty fourth day after surgery, drugs were given to rats three times per week (on Monday, Wednesday, and Friday). PTH and Estradiol were injected subcutaneously. 17-Ethinyl estradiol and alendronate were given orally.

Table 3-4 Treatment Arrangement for Pradama Exp1

Group name	SHAM_W2	SHAM_W4	SHAM_W8	OVX_W2	OVX_W4	OVX_W8	ALEN_W8	E_W8	E2_W8	PTH_W8
Rat Num	3	3	5	3	4	3	4	4	4	4
Drug dosage	None		Vehicle: 5% DMSO in corn oil; 500µm per 100g body weight			1.6 mg/kg	0.5 mg/kg	0.5 mg/kg	0.08 mg/kg	

3.2.2.2 Pradama study: Experiment 2 (Pradama Exp2)

Forty-one female Sprague-Dawley rats, 5.5 month old, were purchased at the beginning of the experiment, in which ten rats were sham-operated and thirty-one rats

were ovariectomized by the vendor. There were seven groups of rats based on treatment and the time point of sacrifice: sham control (SHAM_W5), sham control (SHAM_W11), OVX control (OVX_W5), OVX control (OVX_W11), OVX + Alendronate (ALEN_W11), OVX + 17-Ethinyl Estradiol (E2_W11), and OVX + Teriparatide (PTH_W11) (Table 3-5). All rats were weighed on the sixth date after surgery. On the forty second day after surgery, drugs were given to rats three times per week (on Monday, Wednesday, and Friday). PTH was injected subcutaneously. 17-Ethinyl estradiol and alendronate were given orally.

Table 3-5 Treatment Arrangement for Pradama Exp2

Group name	SHAM_W5	SHAM_W11	OVX_W5	OVX_W11	ALEN_W11	E2_W11	PTH_W11
Rat Num	4	6	6	6	6	7	6
Drug dosage	None			Vehicle: 5% DMSO in corn oil; 500µm per 100g body weight	1.6 mg/kg	0.45 mg/kg	0.08 mg/kg

3.2.2.3 Pradama study: Experiment 3 (Prodama Exp 3)

Forty-two female Sprague-Dawley rats, 6 month old, were purchased at the beginning of the experiment, in which eleven rats were sham-operated and thirty-one rats were ovariectomized by the vendor. There were six groups of rats based on treatment and the time point of sacrifice: sham control (SHAM_W6), sham control (SHAM_W12), OVX control (OVX_W6), OVX control (OVX_W12), OVX + Alendronate (ALEN_W12), OVX + 17-Ethinyl Estradiol (E2_W12), and OVX + Teriparatide

(PTH_W12) (Table 3-6). All rats were weighed on the fourth date after surgery. On the forty-fifth day after surgery, drugs were given to rats three times per week (on Monday, Wednesday, and Friday). PTH was injected subcutaneously. 17-Ethinyl estradiol and alendronate were given orally.

Table 3-6 Treatment Arrangement for Pradama Exp3

Group name	SHAM_W6	SHAM_W12	OVX_W6	OVX_W12	ALEN_W12	E2_W12	PTH_W12
Rat Num	5	6	6	7	6	6	6
Drug dosage	None			Vehicle: 5% DMSO in corn oil; 500µm per 100g body weight	1.6 mg/kg	0.43 mg/kg	0.08 mg/kg

3.3 *IN VIVO* STRUCTURAL ANALYSIS

3.3.1 Scanning design

Sixteen-bit CT image data were collected using a customized micro-CT system (ACTIS 150/225 system, BIR Inc., Lincolnshire, IL). The study object was the proximal metaphysis of the right tibia. All the rats were scheduled to be scanned at week 0, week 8, week 12 and week 16 after sham or ovariectomy surgery. Before the scanning, the rat was placed in a plastic chamber. The chamber consisted of two acrylic cylinders and a flange (Figure 3-1). The flange was located on the lower cylinder. The chamber was fixed on the part manipulator by tightening screwing bolts through the holes in the flange and the holes in the part manipulator, which made sure that there was no relative movement between the chamber and the part manipulator. The upper cylinder had 2.75 inch inner

diameter which should provide enough space for a rat and 3 inch outer diameter. The top cover had 3 inch inner diameter and there was a swivel fitting on its top side. The swivel was connected with a tube, through which the gas, 1L/min O₂ with 2-2.5% isoflurane by volume, could enter into the chamber for the purpose of rat's anaesthesia. The lower side of the upper cylinder was connected with the lower cylinder that had 1.25 inch inside diameter. A rough hook of VELCRO was fixed on the lower side of the lower cylinder. The scanning equipment is shown in Figure 3-1.

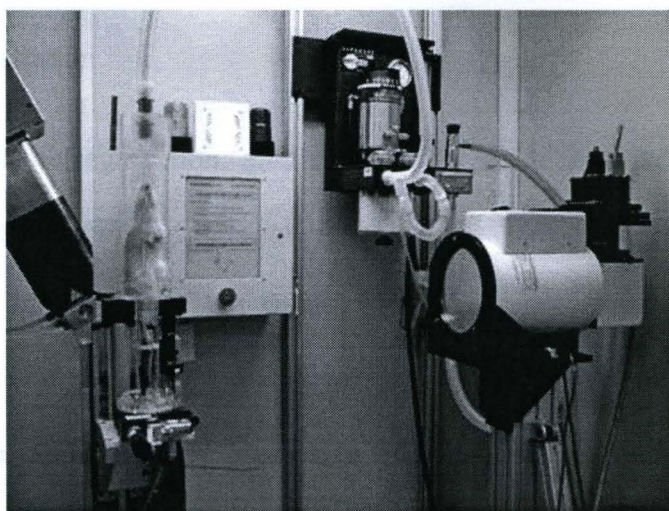


Figure 3-1 It is the description of the CT scanning used in the Orthopaedic Bioengineering Lab. X-ray source is on the left, part manipulator is in the middle and x-ray detector is on the right. X-ray source-detector system is fixed all the time. Before the scanning, a rat is sedated and fixed on the part manipulator. During the scanning the rat is rotates with part manipulator.

Generally, the rat was sedated within 5-10 minutes. Because the rat does not blink when it is under unconscious conditions, ophthalmic ointment (NEO-POLY-BAC, Bausch & Lomb Incorporated, Tampa, FL) was used to maintain proper moisture of the eyes. The tail, the right hint leg of the rat and a soft loop of VELCRO were tied together by tape. The rat was placed in the upper cylinder while the tail and the right hint leg were extended into the lower cylinder. The tail and the right hint leg were fixed by pressing the

soft loop surface to the rough hook surface of Velcro, which made sure that there were no relative movement between the study object (tail and right leg) and the chamber during CT scanning. By pulling down VELCRO soft loop and pressing soft loop surface to VELCRO rough hook surface, the right hind leg remained straight and erect during the scanning. Since the rat cannot support its body in erect position because of its relaxed muscle when it is sedated, the rat was stretched up in a vertical position by hanging its teeth on a loop of string.

3.3.2 Image registration

The aim of the registration: after registration, the image stacks of the VOI (the proximal metaphysis of tibia) of the same rat scanned at four different time points (week 0, week 8, week 12 and week 16) should be in the same orientation and the same position. An exact biological match of two scans made at different time points would be a match in which a bone structure present in one scan falls on top of the same bone structure in the second scan. Because bone grows during the experiment period, the longer the time period between the two scans, the greater the morphological changes in the bone. To make the change between the biological matches at two time points as small as possible, the image stack that was scanned at the middle time point (week 8) of the whole study was chosen as the reference image stack of registration, and the image stacks at week 0, week 12 and week 16 (floating image stacks) were oriented to match it, which resulted in the longest time period between the two time points of a registration to be 8 weeks.

There were four steps to do registration.

Step 1: Display the four image stacks of the same rat scanned at 4 different time points.

An original CT image data set that was obtained directly after CT reconstruction included 749 ~ 1284 image slices and the size of each image slice was 8196 KB. The image shown in Figure 3.3-2 (a) was an example of an original CT image. Since the size of the image stack was very big (6.1 ~ 10.5 GB), it was hard to display even only one image stack on the computer screen because of the computer memory limitation. ImageJ was used to open the image data sets. The following measures were taken to make the displaying fast and successful: 1) the scale of the image was set to 25%, 2) one image every four images was read in one image stack, and 3) the original image was converted to 8-bit grayscale. The required computer memory was decreased dramatically by taking these measures. For example, the size of an image stack of which the original size was 6.1 GB was reduced to 47 MB ($6100 \text{ MB} / 4$ (read one slice every 4 slices) / $(4 * 4)$ (25% image scale) / 2 (converted to 8-bit) = 47 MB), which was only 0.78% of the original size. Although some details of the image data sets were lost by taking these measurements, the reduced images were still good enough because only rough registration was performed in this step.

Step 2: Rotated the floating image stacks manually to such position that the VOI of the floating image stacks had the similar orientation to that of the reference image stack.

To compare the relative orientations, it was also necessary to display the same positions of the four image stacks. Because bone is growing, the structure of the bone is changing. In the analysis, it was assumed that arterial openings in the cortex do not

change, or at least to a much lesser extent than the general shape of the bone. Figure 3-2 (a) and (b) show the images of a floating image stack before orienting and after orienting, respectively.

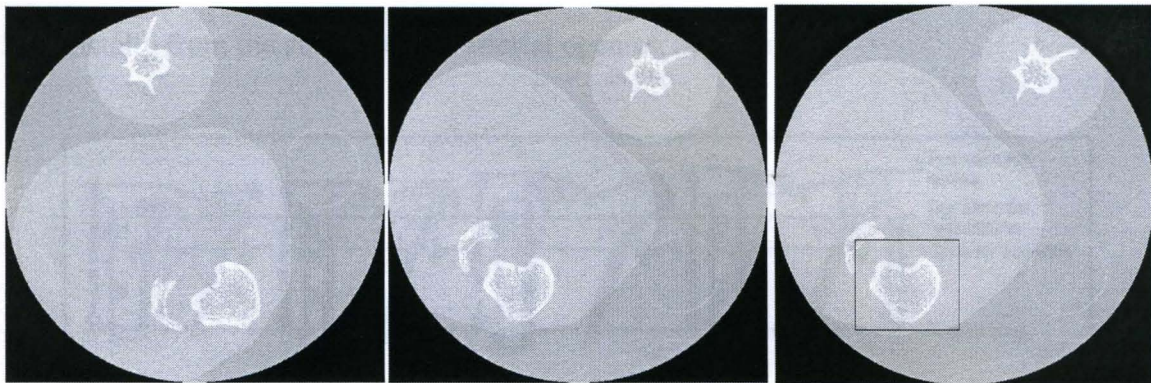


Figure (a)

Figure (b)

Figure (c)

Figure 3-2 It is the orientation process of a floating image stack. Figure (a) shows the image with cortex opening before orientation. Figure (b) shows the orientation result. The VOI was cut from original CT image stack by a rectangular (figure (c)).

Figure 3-3 shows the orientation results, in which Cross-section A-A, B-B, C-C and D-D were the same positions at week 0, week 8, week 12 and week 16, respectively. The opening in these cross-sections should be the same artery opening in cortex at different time points.

Step 3: Choose the volume for registration purpose (VReg) and the volume for reslicing purpose (VRes).

T0, T8, T12 and T16 in Figure 3-3 were distances between the slices with the arterial opening in the cortex and the slices that were just below the growth plate at week 0, week 8, week 12 and week 16, respectively. Since bone is growing, T0 should be the minimum value of T0, T8, T12 and T16. The top slice of each image stack for VReg was at the distance of T0 proximally from the slice with the arterial opening in the cortex.

B0, B8, B12 and B16 in Figure 3-3 were distances between the slices with the arterial opening in the cortex and the slices that were located at the most bottom of the image stack at week 0, week 8, week 12 and week 16, respectively. The bottom slice of each image stack for VReg was at the distance of the minimum value of B0, B8, B12 and B16 distally from the slice with the arterial opening in the cortex.

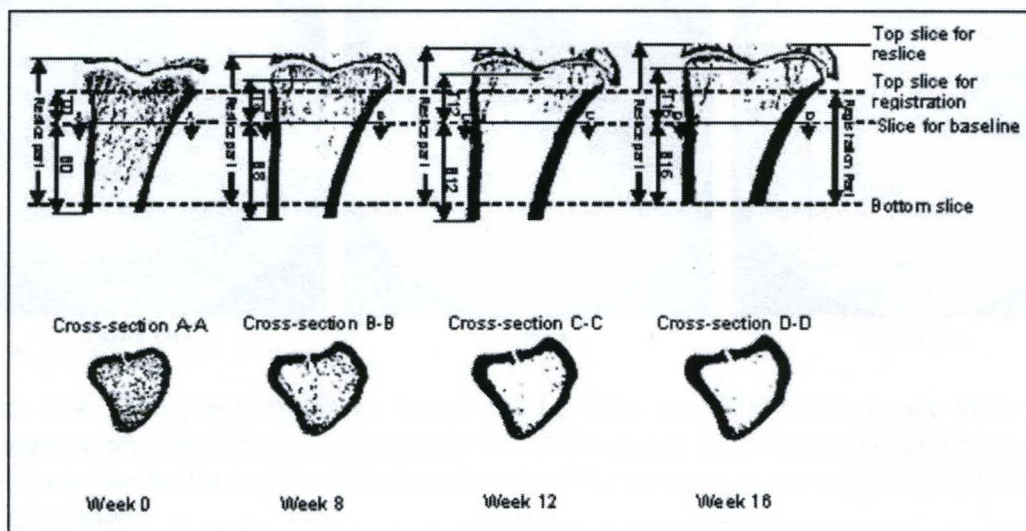


Figure 3-3 Description of the registration parts and the reslice parts

The top slice of VRes part was chosen to make sure that the whole metaphysis at the proximal end of the tibia was included. The bottom slice of VRes was the same as that of VReg.

The VOIRR (Volume of Interest, including both Reslice part (VRes) and Registration part (VReg)) was cut from the original reconstructed image in rectangular shape (Figure 3-4). The rectangle should be big enough that the whole VOIRR was included and also small enough to save computer memory and computing time.

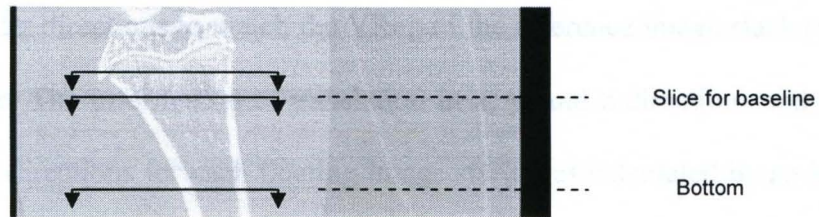


Figure (a)

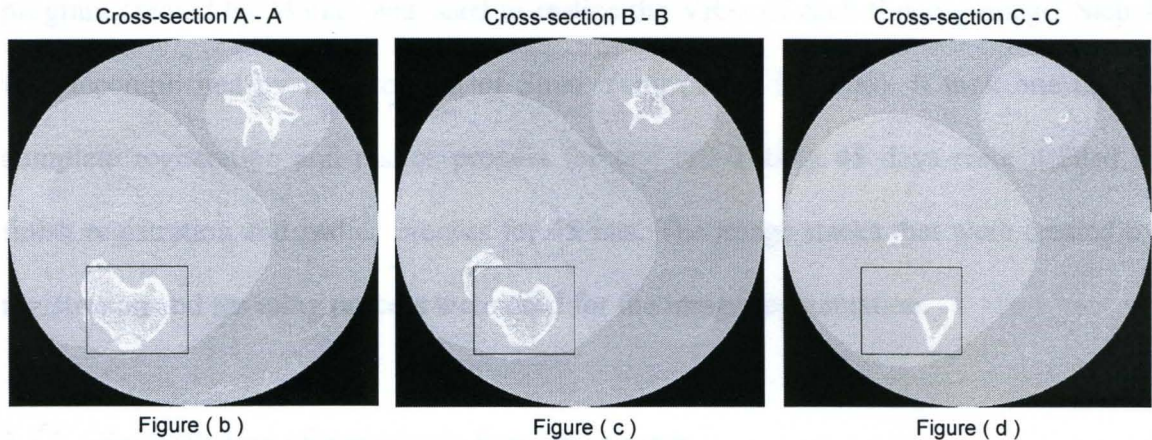


Figure 3-4 The position of the image of the tibia was moved from one side of the rectangle to another side of the rectangle when the image slices were checked from top of the tibia to the bottom of the tibia because the tibia was not in the vertical position when it was scanned.

The following information that was got from observing original image stacks was used as the input for a in-house Matlab (Mathworks, MA) program to do the rough registration: the rotation angle that was used to rotate the original reconstructed data sets to expected orientation, the top and bottom slice number for registration, the top and bottom slice number for reslice, x and y position of the right upper corner and the left lower corner of the rectangle that was used to cut the tibia stack from the original reconstruction image set.

Step 4: Register and reslice image stacks.

After the rough registration, each VReg of the floating image stacks (week 0, week 12 and week 16) should move a little bit in x, y and z directions, and rotate a little

bit around x, y and z directions to match the VReg of the reference image stack (week 8) as well as possible. The information of translation in x, y, and z directions and rotation around x, y, and z directions for each floating image stack was calculated by an in-house Matlab program and used as the input for the reslicing process. An in-house reslicing program created by Matlab was used to reslice the VRes of each floating image. Step 4 was accomplished by the program of Shuo Yang (Yang S, 2006). It took one day to complete registration and reslice process for one rat. Totally 45 days were needed to finish registration and reslice process for 45 rats. The image stacks that were created by registration and reslicing process were used for the image segmentation.

3.3.3 Segmentation of metaphysis from other bones

The study object in the research was the metaphysis of the proximal tibia. The objective of this step was to remove the epiphysis and/or patella from the image stack, so there was only metaphysis left for later analysis.

The volume of interest (VOI) for image segmentation was taken from the image slice that was just below the growth plate of the proximal tibia and progressed distally approximately 3.75 mm (269 slices x 14 microns/slice). This image stack included the VOI (metaphysis) and other bones (such as epiphysis and patella) (Figure 3-4 (b), (c) and (d)). The VOI that was surrounded by the rectangle in Figure 3-4 (b), (c) and (d) might change a little bit after registration and reslice process, but it gave a good picture about what kind of trouble will be in the further segmentation process. If the VOI was connected with other bones, it was difficult to figure which was the VOI automatically by

computer. It resulted in further troubles when the cancellous bone of the VOI was separated from the cortical bone of the VOI.

Figure 3-5 is a description of how whole bone segmentation worked. An in-house GUI program created by Matlab is illustrated in Figure 3-5a. Before whole bone segmentation, two types of the image stack were created: one stack was black-white image style (Figure 3-5a) in which pixels with black color are non-bone elements and pixels with white color are bone elements, and the other stack keeps the information of pixel gray intensity (Figure 3-5b). To create black-white image stack, the global threshold for non-bone and bone tissue (bone/non-bone threshold) was determined slice by slice using the method of Otsu, N. (Otsu, N., 1979), which computed the threshold to minimize the intraclass variance of the black and white pixels. The pixel represented bone element if its gray intensity was greater than bone/non-bone threshold, otherwise, it represented non-bone element.

By selecting 'OpenStack1' button (the left upper button in Figure 3-5a), the image stack with black-white style was opened and displayed on GUI. A polygon mask can be plotted after selecting 'PlotMetMaskLine' button (the left upper button in Figure 3-5a). All metaphysis (VOI) should be inside the mask, and other bones should be outside of the mask. The bone elements that were inside the area of the mask were kept and the bone elements that were outside of the mask were deleted after the whole bone segmentation was carried out by selecting 'Segmentation (from bottom to top)' button (the left lowest button in Figure 3-5a). 'ConfirmMask' button (the left middle button in Figure 3-5a) was used to record the mask shape, the mask position and the number of the slice on which the mask was plotted. For example, the number of the current slice is 239 in Figure 3-5. If

'ConfirmMask' button was clicked, the mask position was recorded and all bone pixels on the slice 239 that were inside the mask were kept and all bone pixels on slice 239 that were outside of the mask were deleted after segmentation. It was not necessary to plot mask for every slice of an image stack because one mask can be valid for several continuous slices. If no mask information of a slice was recorded by selecting 'ConfirmMask' button, the mask of the nearest slice with the lower slice number relative to the current slice was used as the mask for the current slice.

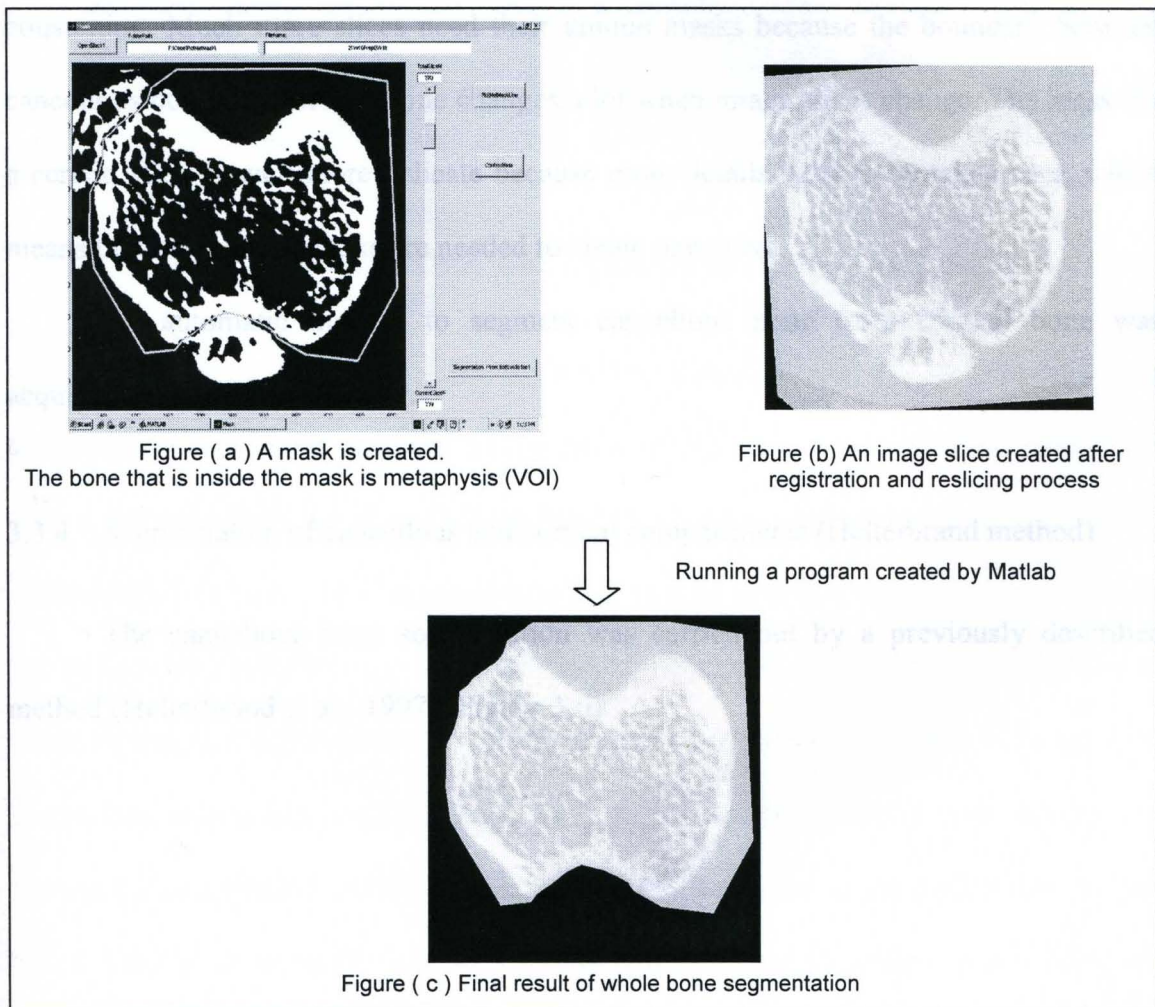


Figure 3-5 Whole bone segmentation

Because the black-white image stack illustrated clearly which parts were bone and which parts were non-bone, which made the boundary clearer between the VOI and other bones, it was used to create whole bone mask. Then the mask was applied on the image stack with the information of pixel gray intensity to create the stack which contained the VOI only (Figure 3-5c).

The same method can be used to separate cancellous bone from cortical bone. It works if appropriate mask for cancellous bone was plotted and only cancellous bone was maintained after selecting 'Segmentation' button. But this method is time and labor consuming. Much more slices need their unique masks because the boundary between cancellous bone and cortical bone changes a lot when image slices change. The mask for a certain slice is such more delicate because more details need to be taken care, which means that much more clicks are needed to create one mask.

An automatic method to segment cancellous bone from cortical bone was acquired to save time and labor.

3.3.4 Segmentation of cancellous and cortical compartments (Helterbrand method)

The cancellous bone segmentation was carried out by a previously described method (Helterbrand et al., 1997) (Figure 3-6).

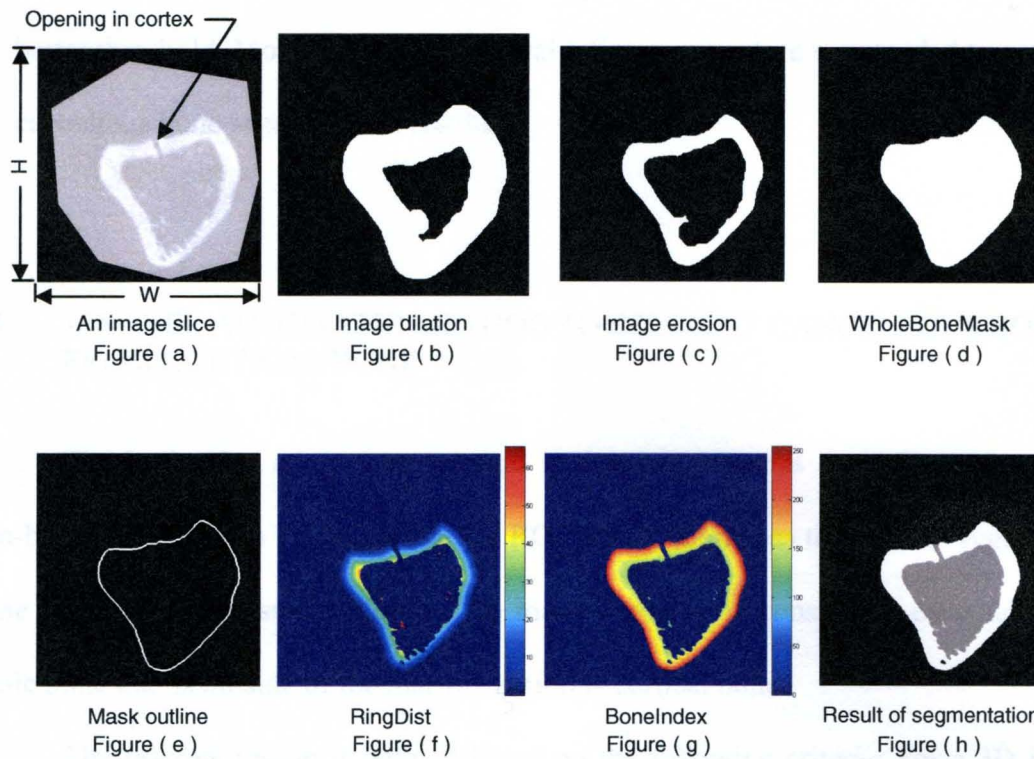


Figure 3-6 Helderbrand method was used to segment cancellous bone from cortical bone

There were two reasons that the refining procedure was needed after applying Helderbrand method: 1) different image slices might have much different shapes of BoneIndex histogram cloud, especially there were inflexions on the histogram curve, and/or there were more than one peak between the first peak and the second peak, which led to bad decision about the value of CortexThresh, and 2) Helderbrand method was based on the knowledge, even though the intensity information was also included, that pixels that represented cortical bone were nearer to mask outline and pixels that represented cancellous bone were located further to mask line. If the thickness of cortex varied greatly in a single image slice, it was unlikely to find a good value of CortexThresh for this slice to segment cancellous bone from cortical bone perfectly.

The Helterbrand method was semi-automatic, requiring several trials to get a better threshold. Most of time, the manual refining procedure was needed to get good cancellous bone segmentation results.

3.4 A NOVEL AUTOMATIC METHOD TO SEGMENT CANCELLOUS BONE FROM CORTICAL BONE

The basic idea of the new method is that a contiguous three-dimensional (3D) non-bone region that is located inside the ROI can be defined as the marrow region. Any bone material that is surrounded by the marrow region is considered cancellous bone while bone that is outside of the marrow region is cortical bone.

The marrow region is defined based on the following criteria: For a 3D ROI, i) Marrow elements are connected to each other and form one and only one continuous marrow cavity; ii) All cavities in the cortex are separated from the marrow cavity; iii) The marrow cavity is the largest cavity among all cavities in ROI.

After 3D marrow region was defined, its 2D image structure was used to create CancellousMask slice by slice. This 2D marrow region was used to create CancellousMask by dilating-filling-eroding process. The perfect CancellousMask should cover and only cover the pixels that represent marrow elements and cancellous bone elements.

Segmentation algorithm

The following sections describe the algorithm steps in detail:

Step 1: Create 3D cavity model of ROI (Figure 3-7).

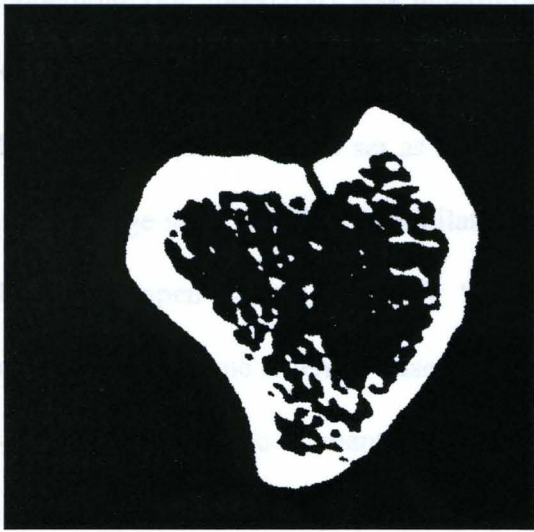


Figure (a) An image slice of binary version

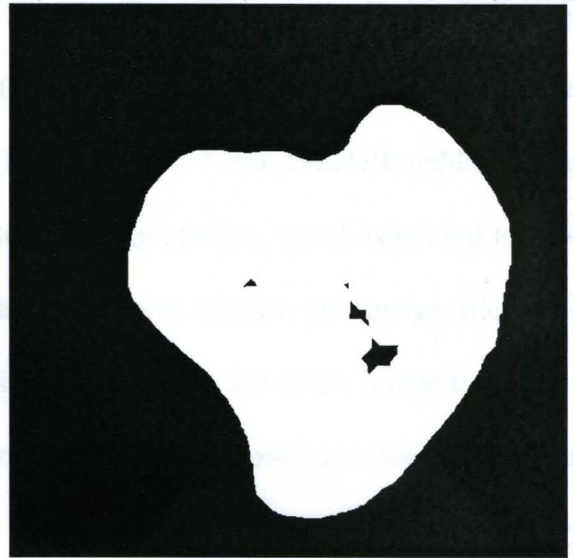


Figure (b) Dilate figure (a) till the cortex opening is closed and enlarge image slice

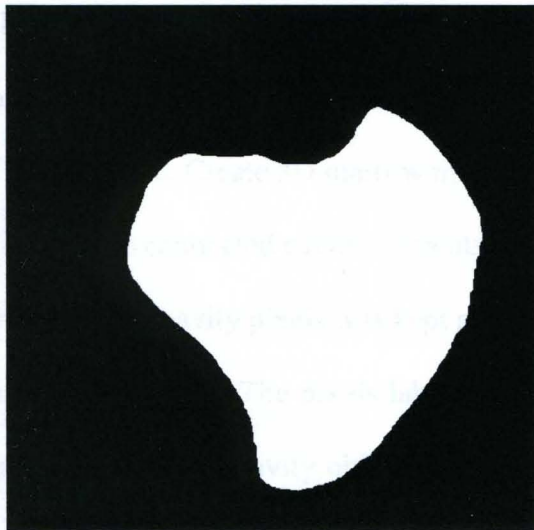


Figure (c) WholeBoneMask (Fill and then erode figure (b) to original size and shrink the image slice to original size) (WholeBoneErodeDilateDiff=0)

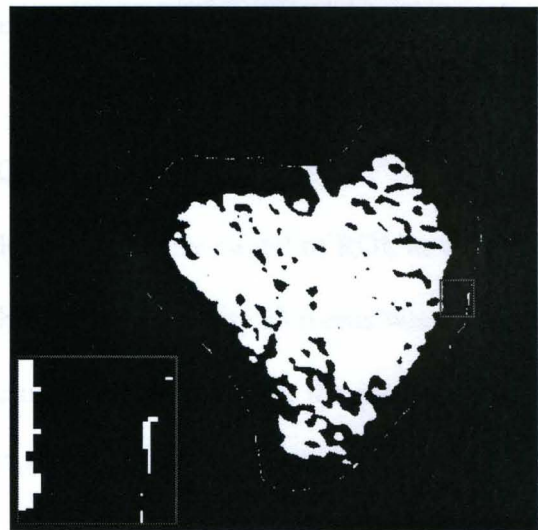


Figure (d) Cavities used to create 3D cavity model of WBROI

Figure 3-7 The dilating-filling-eroding process was used to find WholeBoneMask. The non-bone elements that were covered by WholeBoneMask were treated as cavity elements and were used to create 3D cavity model.

The cavity elements in ROI were marrow elements and other soft tissue elements that were enclosed by cortex. The global threshold for bone and non-bone tissue

(bone/non-bone threshold) was determined slice by slice using the method of Otsu, N (Otsu, N, 1979). The pixel was set as bone (white) if its gray value was greater than the threshold, otherwise it was set as nonbone (black) (Figure 3-7a). WholeBoneMask for a single image slice was found by dilating-filling-eroding process, which was used to fuse the cortex openings (Figure 3-7). When the image was dilated, the image slice was enlarged at the same extent in case that the dilated image flew out of the image slice.

The non-bone elements that were covered by WholeBoneMask were treated as cavity elements. The gray intensity of non-bone pixels that were covered by WholeBoneMask was set to 1 and the gray intensity of all other pixels was set to 0 (Figure 3-7d). 3D cavity model of whole bone was a three dimensional numeric array by overlaying the cavity elements slice by slice.

Step 2: Create 3D marrow model of ROI.

The connected cavity elements re labeled in 3D cavity model of ROI, in which the value of non-cavity pixels was kept at zero. The connected cavity elements were assigned as a single cavity. The pixels labeled 1 made up one cavity object, the pixels labeled 2 made up a second cavity object, and so on. The largest cavity object was defined as the marrow cavity. This method was called as whole matrix method because the largest object was defined in a whole 3D matrix (Figure 3-9). The intensity of marrow elements was set to 1 (white) and the intensity of non-marrow elements was set to zero (black) in 3D marrow model.

Step 3: Find CancellousMask.

CancellousMask should cover all pixels (but only cover the pixels) that represented the marrow elements and the cancellous bone elements. When a single image

slice of marrow region was concerned, it was noticed that cancellous bone was inside or between the marrow region and cortical bone was outside of the marrow region (Figure 3-8b). So CancellousMask could be defined by dilating (Figure 3-8c) and filling this marrow region, then eroding it to its original size (Figure 3-8d) by eroding the dilated image the same extent as that of dilating. The CancellousMask is shown in green and blue color in Figure 3-8e. The green region was the overlapping region of the CancellousMask and the marrow, the blue region was the overlapping region of the CancellousMask and the bone.

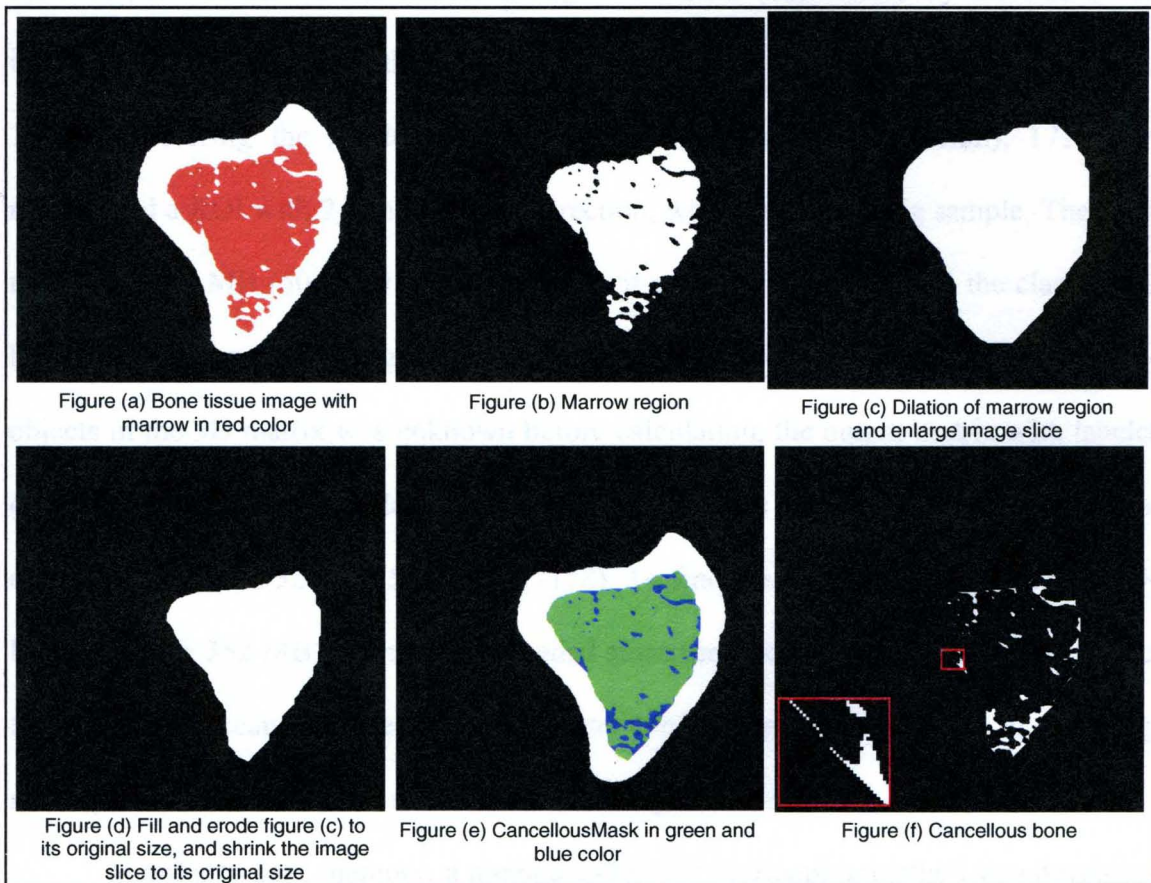


Figure 3-8 CancellousMask was created by eroding the dilated marrow region to its original size.

Step 4: Segment cancellous bone from cortical bone.

The bone pixels that were covered under CancellousMask were treated as cancellous bone (Figure 3-8f). The bone pixels that were not covered by CancellousMask were referred as cortical bone. The cavities that were touching cortical bone region and were not connected to marrow region were referred as cavities in cortex.

Algorithm improvement

1) Efficiency improvement

It worked theoretically to find the largest object by whole matrix method. However, it was difficult to handle a large 3D matrix (determined by the size of the image stack). For example, there was an image stack ($H * W * \text{SliceN} = 505 * 509 * 171$). Considering the resolution of the image (for example 0.014mm), 171 slices represented a ROI with 2.4 mm in axial direction, which was not a big sample. The input matrix was 44 MB ($505*509*171*1$) because it was binary version and the class of the binary version was 8-bit integer (1 byte per element). Since the total number of separated objects in the 3D matrix was unknown before calculation, the output matrix with labeled objects should be of class double, which means 8 bytes per element. The size of the output matrix was 352 MB ($505*509*171*8$). To find the largest object, more than 396 MB (44 MB + 352 MB) memory was needed since the calculation needed other variables and matrixes. Because of the limitation of the computer memory, the size of the image stack was limited, that is, the size of the bone sample was limited.

In order to save memory, a method called the overlapping method was developed to find the largest object for a 3D model. To illustrate it clearly, a 2D matrix was used

here as an example (Figure 3-9). One row in the 2D matrix represented a single slice in a 3D matrix.

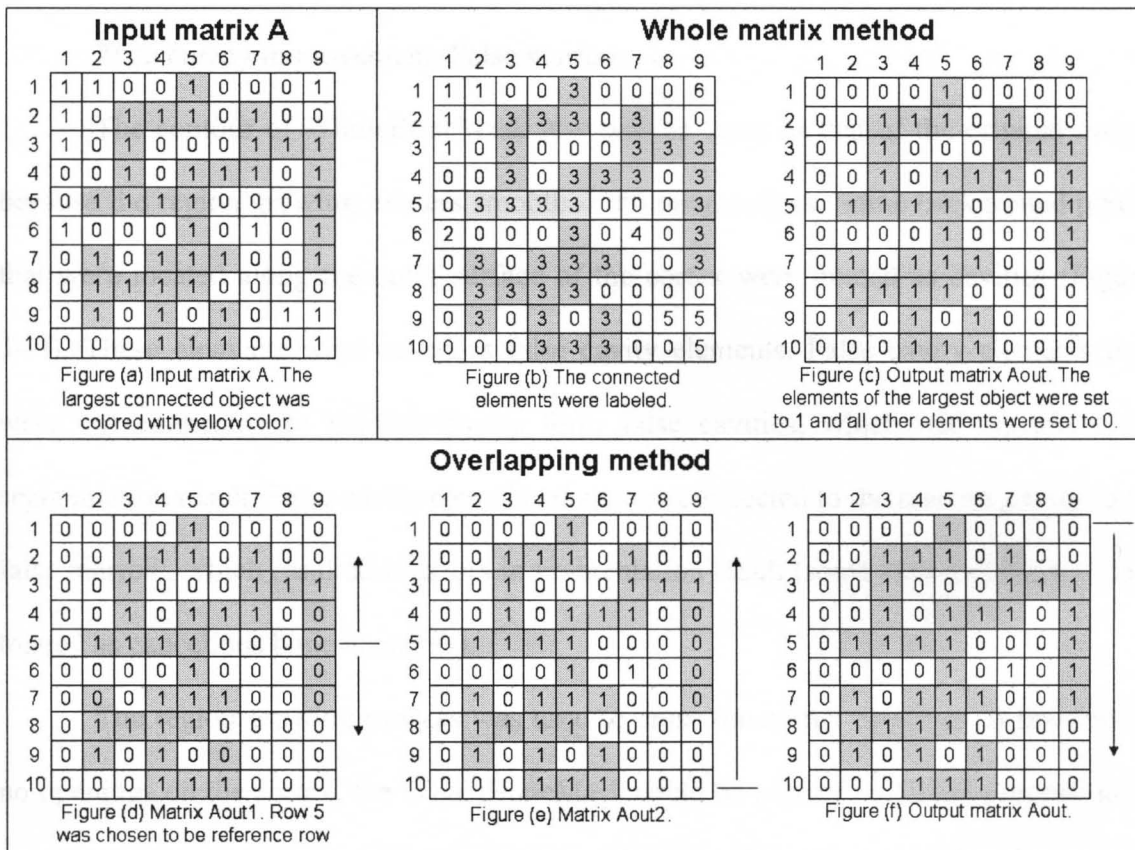


Figure 3-9 Illustration of whole matrix method and overlapping method

To find the largest object, a row was chosen as a start point (reference row). The largest part (LP) in reference row must be part of the largest object of the whole matrix. For example, for a matrix shown in Figure 3-9, row 2, 3, 4, 5, 7, 8 or 10 could be used as the reference row. The elements with value of 1 that were connected to LP were considered as the elements of the largest object of the whole matrix while considering only two rows at a time and moving in two directions through the matrix (Figure 3-9d). One cycle was completed by carrying out the same process from the last row to the first

row (Figure 3-9e), and then from the first slice to the last slice (Figure 3-9f). The whole largest object was identified by continuing the cycling till the result were the same as that from the previous cycle.

2) Accuracy improvement: False marrow

The contour of WholeBoneMask was not the same as that of the original image because the region growing process smoothed the image edges. Some background pixels that were located along the outer surface of the cortex were treated as cavities (Figure 3-7f). These elements were called as false cavity elements. False cavity elements that were not connected to marrow cavity form false cavities, which had no effect on segmentation result. False cavity elements that were connected to the marrow cavity form false marrow, which resulted in errors in segmentation result (some cortex elements were treated as cancellous bone elements).

The region growing process was used to erase the cortex openings. If there were no openings on the cortex, the WholeBoneMask could be created by filling process only, which resulted in the exactly same contour as that of ROI and caused no false cavity elements.

- Check if there are openings on the cortex

The checking of cortex opening was based on the observation that the outer cortex contours of two adjacent image slices should be very similar. The openings of the cortex of one image slice can be detected based on the WholeBoneMask of its adjacent image slice. It was better to start the checking from the end of an image stack with smaller cortex diameter (the first image slice) to the end with larger cortex diameter (the last image slice). The cortex openings of the image slice with the slice number of N (current

image slice) were checked based on the WholeBoneMask of the image slice with the slice number of N-1 (reference image slice).

ElemDiff consisted of the elements that covered by the WholeBoneMask of the reference image slice but not covered by the filled current image (in green color in Figure (f) in Figure 3-10 and Figure 3-11). The Euclidean distance map (EDM) (Figure (g) in Figure 3-10 and Figure 3-11) was a distance transform, in which each element of ElemDiff contained its distance to the nearest outline of WholeBoneMask of the reference image slice.

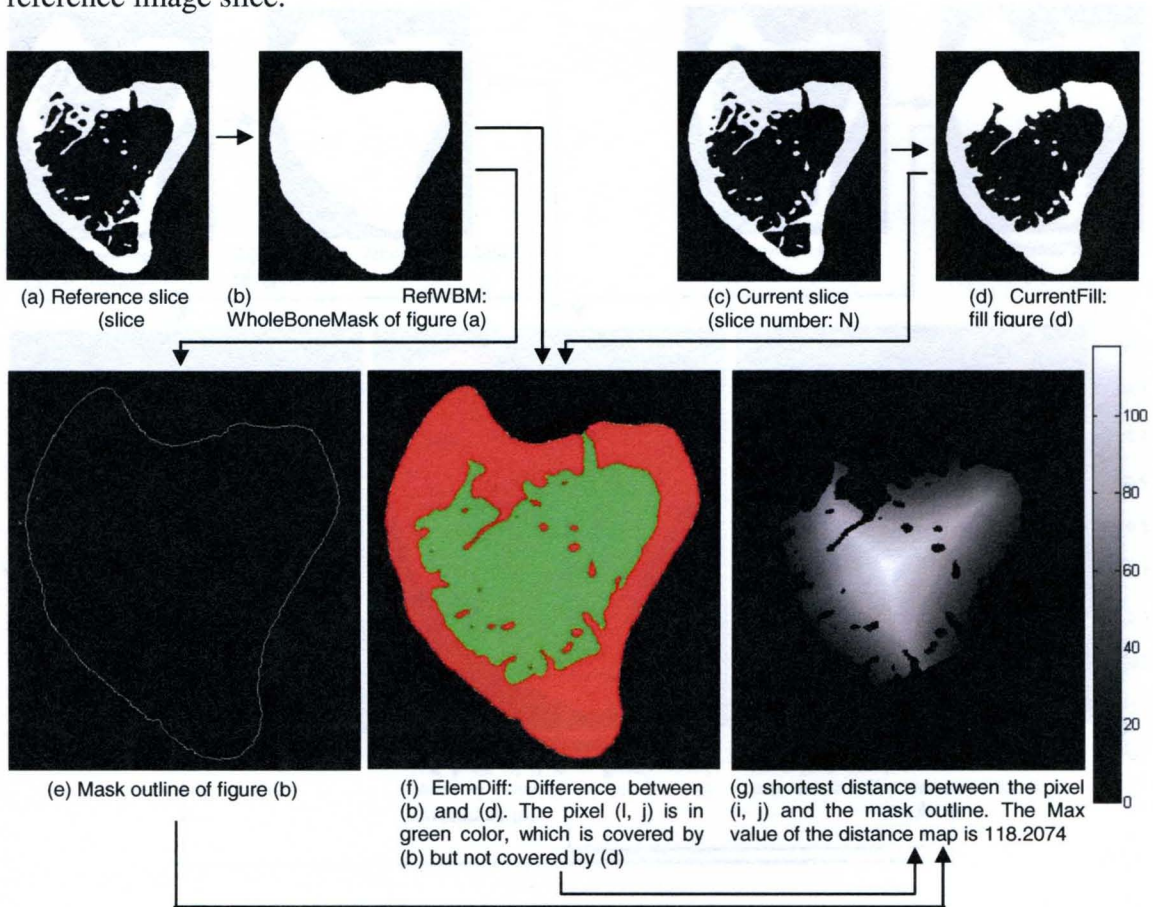


Figure 3-10 An example to check openings on the cortex (There is an opening in the current image slice)

If the maximum value of The Euclidean distance map was greater than a pre-selected value, DistMax, there was at least one opening on the cortex of the current image slice. If the maximum value of EDM was not greater than DistMax, there was no opening. The value of DistMax was decided by the operator according to his experience. DistMax was determined by experience and was set as 20 in the rat tibia model.

The special case was at the very beginning when the openings in the first image slice needed to be checked. In such case, the second slice was used as reference slice.

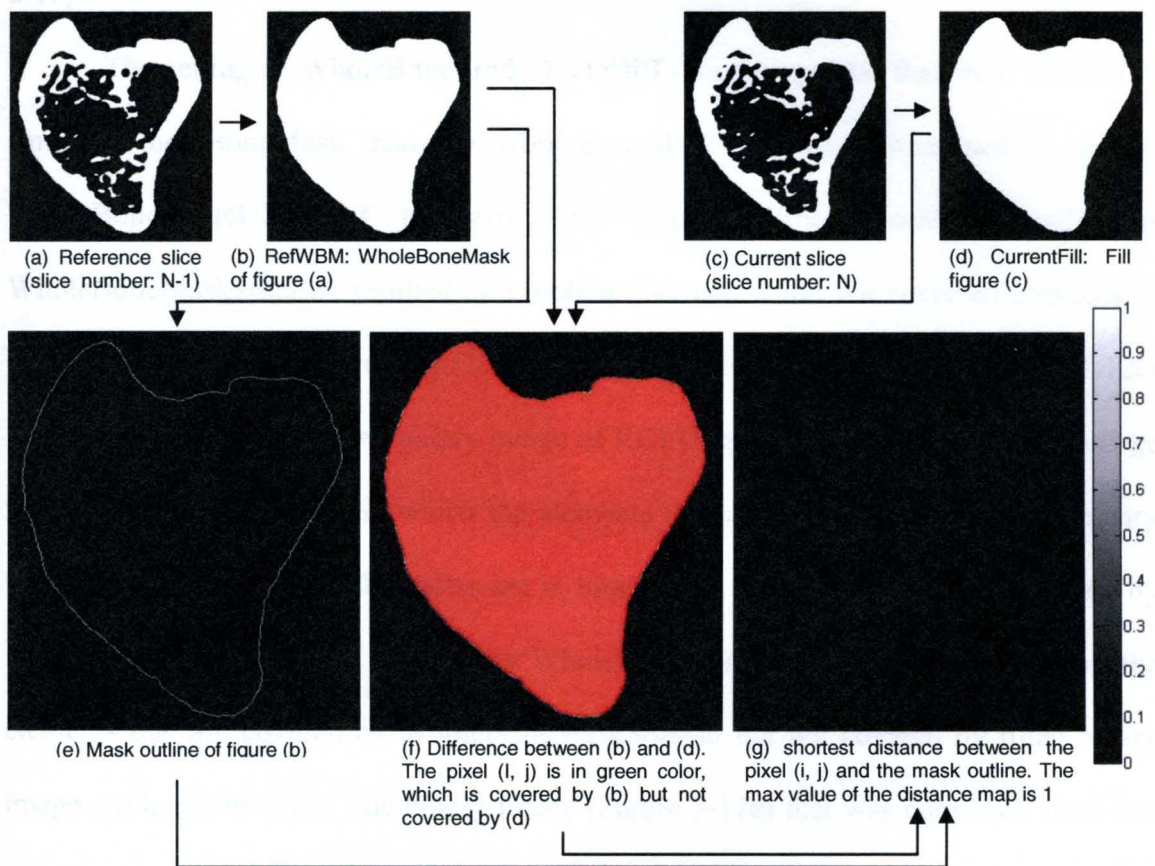


Figure 3-11 An example to check openings on the cortex (There is no opening in the current image slice)

- Illustration of how to decrease false marrow if there are openings on the cortex.

To describe this clearly, a term, WholeBoneErodeDilateDiff, was introduced. If WholeBoneErodeDilateDiff was equal to a number N , it meant that the dilated image of ROI was eroded by N more pixels than the extent of dilating. For example, if the image was dilated by the extent of 20 pixels and WholeBoneErodeDilateDiff was equal to 5, the dilated image was eroded by the extent of 25 pixels. If the image was dilated by the extent of 20 pixels and WholeBoneErodeDilateDiff was equal to 0, the dilated image was eroded by the extent of 20 pixels too, that is, erode the image to its original size (Figure 3-7c).

The setting of WholeBoneErodeDilateDiff that was greater than zero resulted in smaller WholeBoneMask than the WholeBoneMask that was determined by setting WholeBoneErodeDilateDiff to zero. This smaller WholeBoneMask, called as WholeBoneMaskSmaller, resulted in a problem because it did not cover all elements of ROI. To restore the uncovered ROI elements, WholeBoneMaskSmaller (Figure 3-12c) was combined with the filled binary image of ROI (Figure 3-12b). The combined image is shown in Figure 3-12d, in which the elements that are covered by both filled binary image and WholeBoneMaskSmaller are in blue color, the elements that are covered by filled binary image but not covered by WholeBoneMaskSmaller are in white color, the elements that are covered by WholeBoneMaskSmaller but not covered by filled binary image are in green color. The binary image (Figure 3-12e) that was converted from this combined image was the desired WholeBoneMask.

By setting WholeBoneErodeDilateDiff greater than zero, the number of false elements were decreased which resulted in the decreasing of false marrow. Figure 3-7c

and Figure 3-12f showed the different results of WholeBoneMask with different setting of WholeBoneErodeDilateDiff based on same 2DLBO.

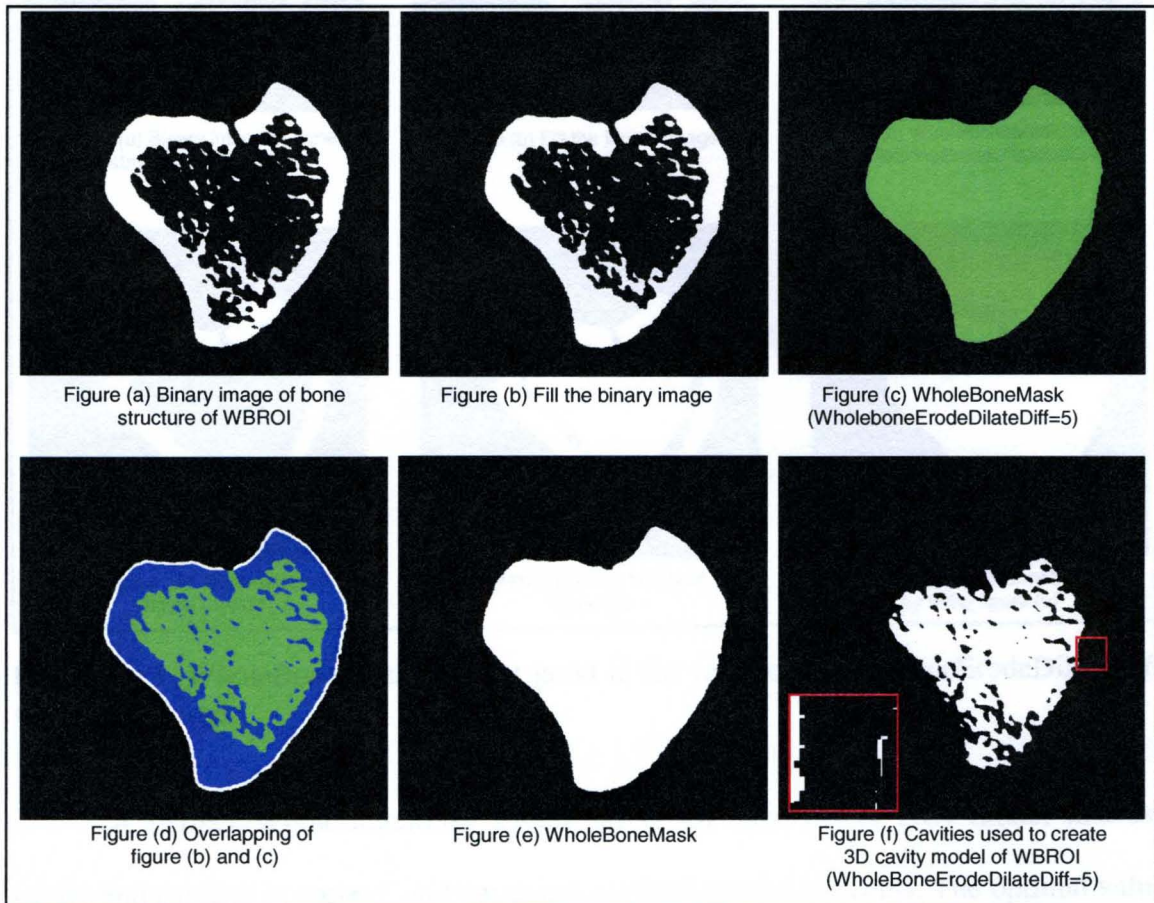


Figure 3-12 Better WholeBoneMask was created. No false elements existed in cavity image (Figure f).

With the increasing value of WholeBoneErodeDilateDiff, the number of false cavities decreased. How about the value of WholeBoneErodeDilateDiff was set too big? There was an example that WholeBoneErodeDilateDiff was set to 40 (Figure 3-13). In this case the WholeBoneMask was not good because some of marrow elements were not covered by WholeBoneMask.

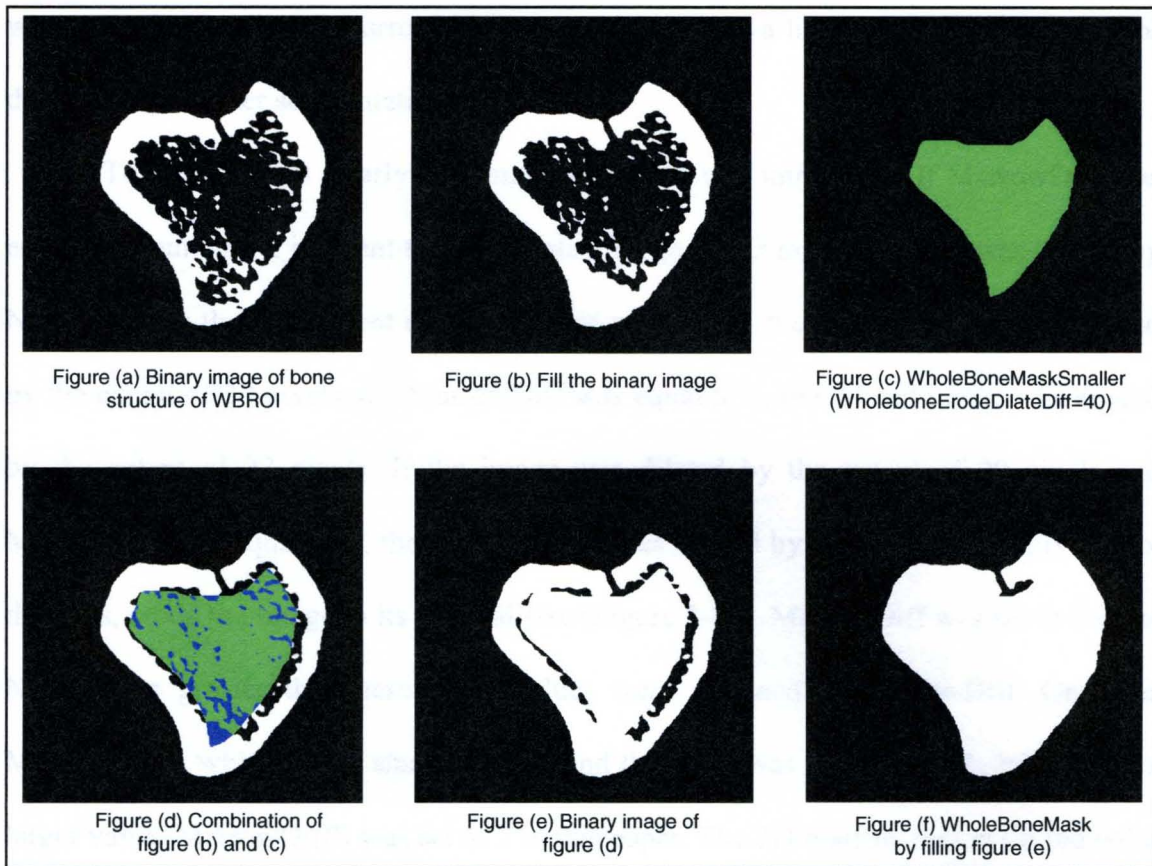


Figure 3-13 WholeBoneMask was not good if the value of WholeBoneErodeDilateDiff was set too large.

A perfect WholeBoneMask should cover all elements of ROI (bone, marrow cavity and cavities in cortex), and not cover any background elements. The optimal value of WholeBoneErodeDilateDiff was such that it rarely resulted in false elements and that it still resulted in a good WholeBoneMask. WholeBoneErodeDilateDiff was set to 5 in this paper.

3) Accuracy improvement: cancellous bone segmentation

A few cortical bone elements that were located near boundary of the inner surface of cortex and marrow region were treated as cancellous bone elements (Figure 3-8e and Figure 3-8f) because of the effect of dilating and eroding process when CancellousMask

was created. The dilated marrow region could be eroded a little more than the extent of dilating to get better segmentation result.

To describe this clearly, a term, MarrowDiff, was introduced. If MarrowDiff was equal to a number N , it meant that the dilated image of 2D marrow region was eroded by N more pixels than the extent of dilating. For example, if the marrow region was dilated by the extent of 20 pixels and MarrowDiff was equal to 2, the dilated image was eroded by the extent of 22 pixels. If the image was dilated by the extent of 20 pixels and MarrowDiff was equal to 0, the dilated image was eroded by the extent of 20 pixels too, that was, erode the image to its original size (Figure 3-8d). MarrowDiff was set to a value N that was greater than zero. Two values were assigned to MarrowDiff. One was MarrowDiffS, which was a smaller value, and the other was MarrowDiffL, which was a larger value. MarrowDiffS was set to 2 in this paper. The 2D marrow region (in red color in Figure 3-14a) was dilated and then eroded by the extent that was 2 more pixels than the extent of dilation. This step resulted in a cancellous mask, CancellousMaskS (in green and blue color in Figure 3-14b). TrabS was the cancellous bone that was covered by CancellousMaskS. MarrowDiffL was set to 6 in this paper. The separated 2D marrow region (in red color in Figure 3-14a) was dilated and then eroded by the extent that was 6 more pixels than the extent of dilating. This step resulted in another cancellous mask, CancellousMaskL (in green and blue color in Figure 3-14c). CancellousMask1 (in green and blue color in Figure 3-14d) was formed by the elements that were covered by CancellousMaskL and/or TrabS. CancellousMask (in green and blue color in Figure 3-14e) was the biggest part of CancellousMask1. This step avoided the resulted in that

some cortical bone elements that were located near the boundary of inner surface of cortex and marrow region were treated as cancellous bone.

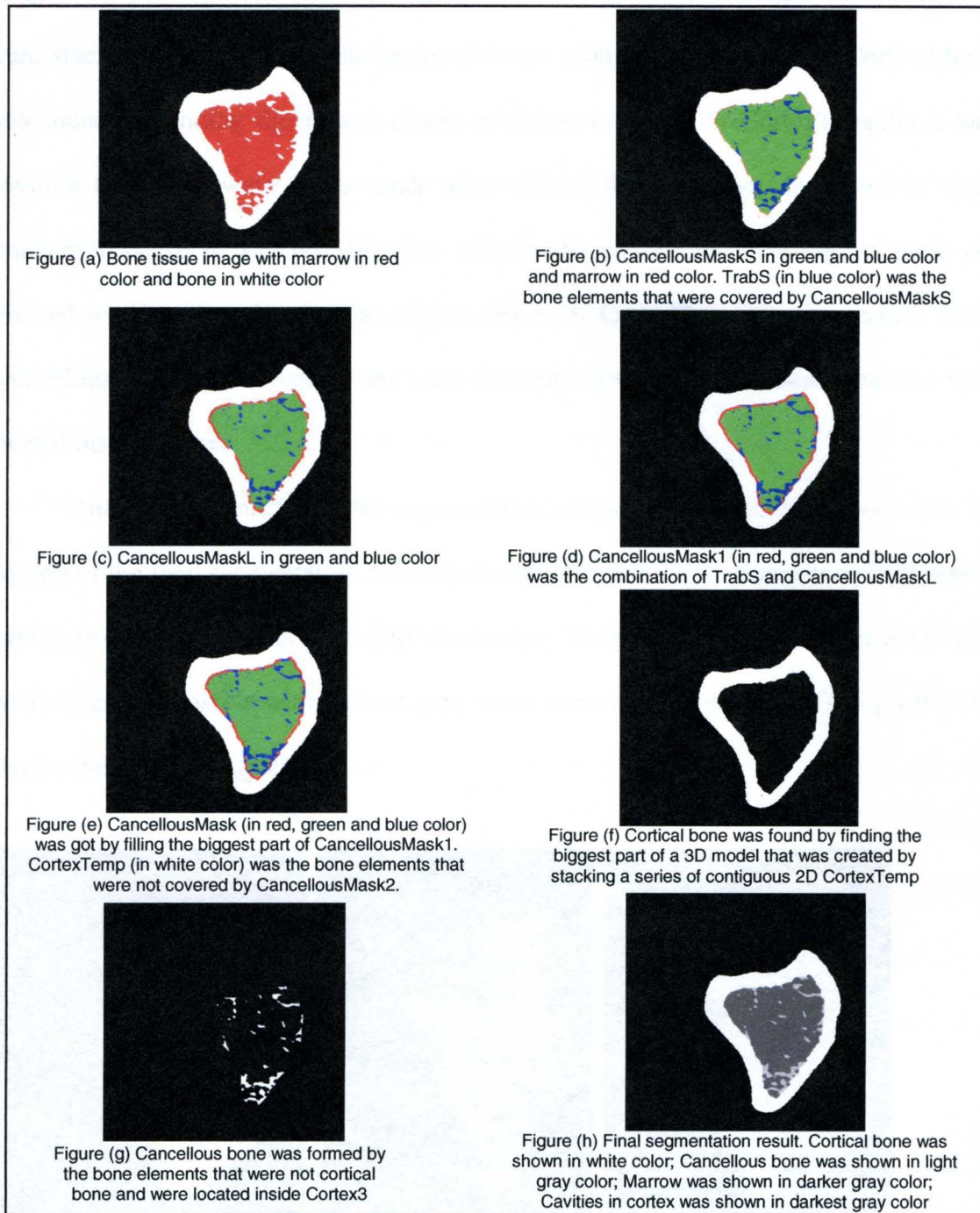


Figure 3-14 CancellousMask and cancellous bone were determined with MarrowDiffS = 2 and MarrowDiffL=6

3.5 CortexTemp (in white color in Figure 3-14e) was formed by the bone elements that were not covered by CancellousMask. Every image slice of the image stack had its unique CortexTemp. The series of contiguous two-dimensional images of CortexTemp were stacked to form a three-dimensional cortex model, CortexTemp3D. Cortical bone was found by finding the largest object of CortexTemp3D. In CortexTemp3D it was possible that there were some small bone objects that were not connected to main structure because it was possible that some small cancellous bone objects were not covered by CancellousMask. The biggest object of CortexTemp3D was cortical bone. Cancellous bone was formed by the bone elements that were not cortical bone and were located inside cortex.

The 3D version of the final segmentation result is shown in Figure 3-15. The 2D version of the final segmentation result is shown in Figure 3-14h. Cancellous bone was in light gray color. Cortical bone was in white color. The pixels with darker gray color were marrow, and the pixels with darkest gray color were cavities in cortex. The pixels with black color were background.

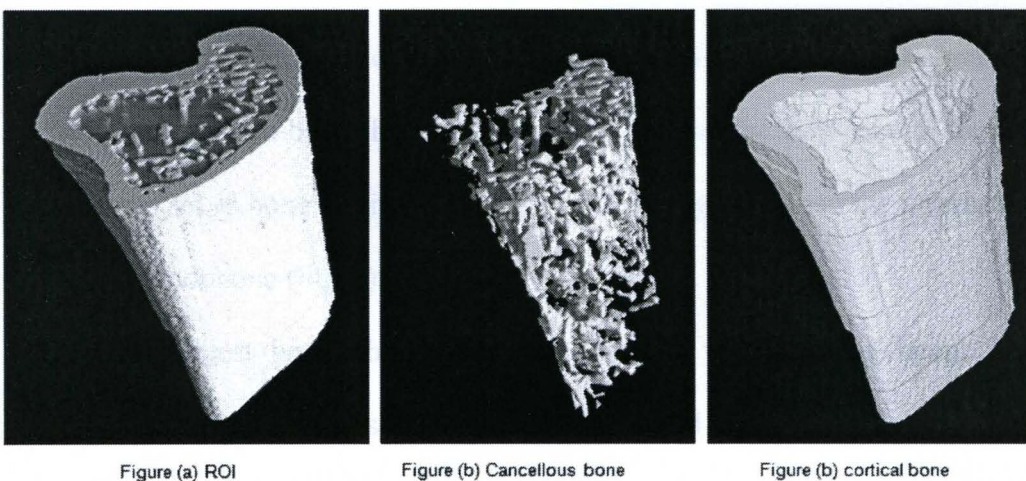


Figure 3-15 3D segmentation result

3.5 AN IMPROVED METHOD OF BONE/NON-BONE SEGMENTATION (LOCAL GLOBAL THRESHOLD)

Generally, cortical bone has higher gray value than cancellous bone because of beam hardening and partial volume effects in the thinner cancellous bone structures. A single global threshold results in the loss of some cancellous bone. Two global thresholds were used in the research. One was cortical bone threshold, which was used for cortical bone identification. It was a single threshold that was determined according to the histogram of absolute gray values of all pixels that were covered by WholeBoneMask. The other was cancellous bone threshold, which was used for cancellous bone identification. It was a single threshold that was determined according to the histogram of absolute gray values of all pixels that were covered by CancellousMask.

The following sections described the algorithm steps in detail:

Step 1: Create a WholeBoneMask that was used to determine cortical bone threshold.

A global threshold for bone and non-bone tissue (bone/non-bone threshold) was determined slice by slice using the method of Otsu (Otsu N, 1979). Instead of concerning all pixels of a single slice, only the pixels with non-zero gray values were used in the decision of bone/non-bone threshold, which eliminated the influence of the black pixels. A pixel was set as bone (white) if its gray value was greater than the threshold, otherwise it was set as nonbone (black).

The largest bone object was found in the whole binary image stack by the overlapping method that was described in Chapter 3.4. This largest bone object should be part of the ROI. Since the global threshold method did not work well, some trabeculae were not connected to the largest bone object. The loss of some trabeculae did not effect

the creation of WholeBoneMask. The WholeBoneMask was created slice by slice using dilating-filling-eroding method.

Step 2: Determine cortical bone threshold.

The cortical bone threshold was determined slice by slice using the method of Otsu according to the histogram of absolute gray values of the pixels that were covered by the WholeBoneMask. Every image slice had its own cortical bone threshold. The cortical bone threshold was applied on its corresponding image slice. All pixels of the whole image slice were set as bone or nonbone based on cortical bone threshold. A pixel was set as bone if its gray value was greater than the threshold, otherwise it was set as nonbone. The binary image created in step 2 had good cortical bone identification. Because the relatively higher value of cortical bone threshold, some cancellous bone pixels were set as nonbone.

Step 3: Determine cancellous bone threshold.

The CancellousMask was created by dilating-filling-eroding the marrow region identified according to the binary image created in step 2. The Ccancellous bone threshold was determined slice by slice using the method of Otsu according to the histogram of absolute gray values of the pixels that were covered by the CancellousMask. The cancellous bone threshold was applied on its corresponding image slice. All pixels that were covered by CancellousMask were set as bone or nonbone based on cancellous bone threshold.

Step 4: Create binary image.

The final binary image was created by the combination of the Figure 3-16e and the Figure 3-16i. Figure 3-17 shows the bone/non-bone segmentation results from the

local global threshold method and from the single global threshold method. Better segmentation result was created by the local global threshold method.

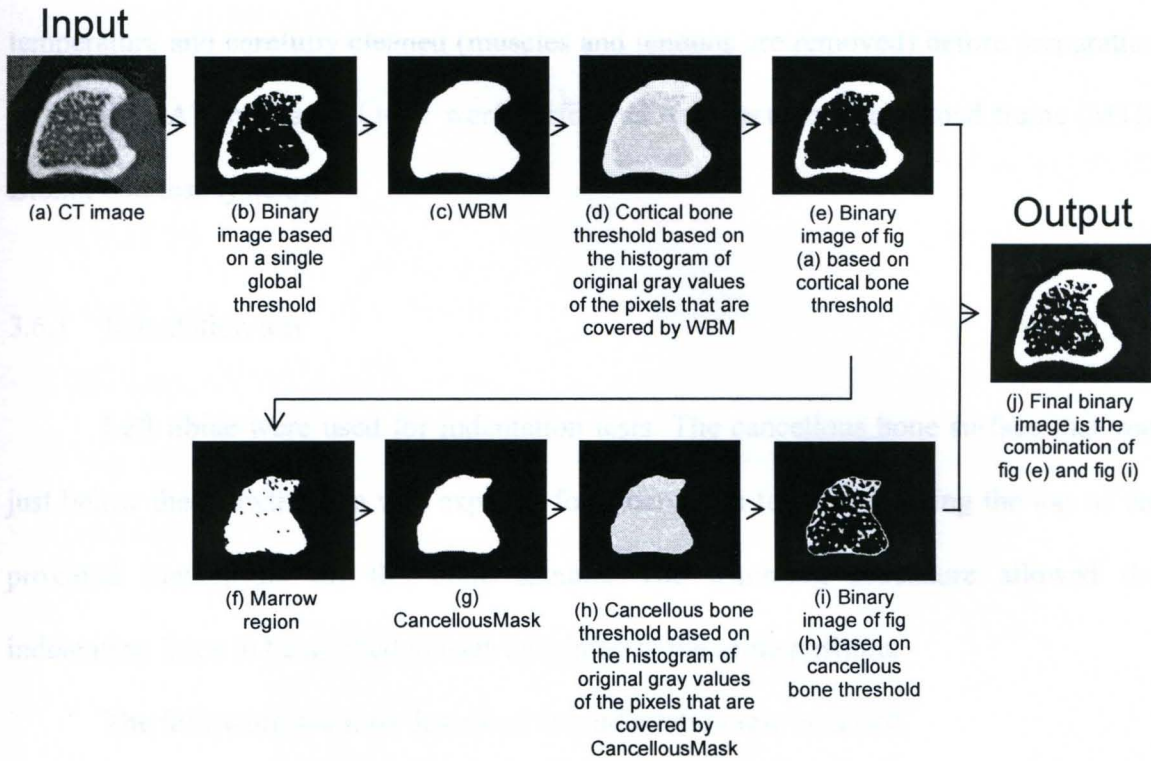


Figure 3-16 The illustration of the local global threshold method

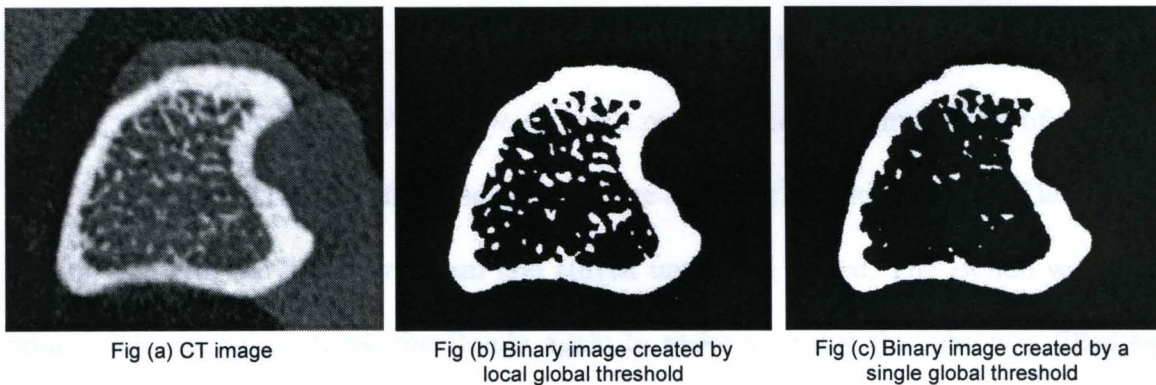


Figure 3-17 The comparison of the bone/non-bone segmentation results from the local global threshold method and from the single global threshold method

3.6 MECHANICAL PROPERTY ANALYSIS

The description of study objects that were used for mechanical property analysis is illustrated in Table 3-1. Bone samples were fresh frozen in saline, thawed at room temperature and carefully cleaned (muscles and tendons are removed) before preparation and testing. All mechanical tests were performed on a servohydraulic load frame (MTS, Bionix 858 test system).

3.6.1 Indentation test

Left tibiae were used for indentation tests. The cancellous bone surface that was just below the growth plate was exposed for indentation test by trimming the top of the proximal metaphysis off the bone sample. The trimming procedure allowed the indentation force to be applied to each specimen at the same position.

The following sections described the indentation test in detail:

Step 1: Embed left tibia.

A container for epoxy resin (Bondo, Dynatron Corp, Atlanta) was combined by a PVC ½ inch cap (inner diameter was 22.3mm) and a plastic tube (outer diameter was 22.3mm, inner diameter was 17.7mm, length was 30mm). Before inserting the tube into the cap, a small amount of WD-40 was placed on the inner bottom surface of the cap, which made it easier to pull the tube off from the cap after Bondo hardened. The Bondo was mixed with the hardener cream and stirred until well mixed. The Bondo was then poured into the tube, stirred the Bondo again to make sure that the tube was filled by Bondo and there were no air bubbles in the tube. The distal end of the tibia was placed into the Bondo. The bone position was adjusted until it was perpendicular to the bottom

surface of the cap. It was better to embed every bone in Bondo compound with the same posture, so after trimming, the bone had similar exposed bone surface. After the Bondo set, the tube was removed from the cap. The exposed portion of the tibia was kept moist in saline soaked gauze until the bone was scanned.

Step 2: Scan the proximal metaphysis (Figure 3-18).

After embedding, the bone sample was scanned. The first CT slice was at the position of the top point of the proximal tibia. Above and below growth plate, images were made every 0.002 inch (0.0508mm). After scanning, the CT images were checked and the image that represented the plane just below the growth plate was identified as the trimming surface. The distance from the top of the proximal tibia to the trimming surface was recorded.

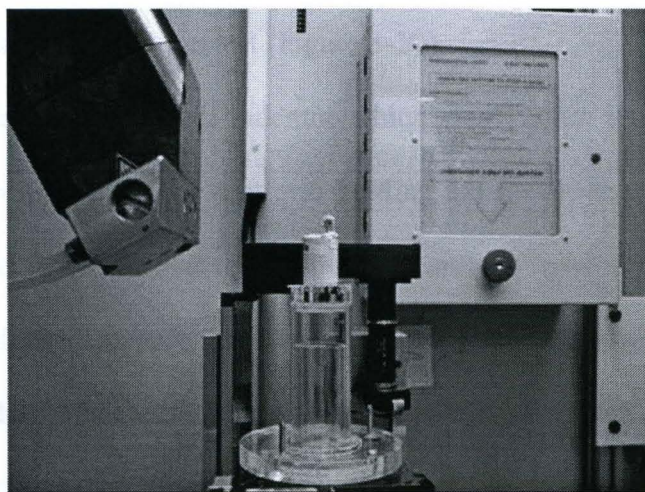


Figure 3-18 The bone sample was embedded in Bondo and was CT scanned

Step 3: Trim the top part of the proximal metaphysis (Figure 3-19).

A low speed diamond saw (Isomet, Buehler, Lake Bluff, Illinois) was used to cut the bone. First, the tube containing the bone was fixed into the pivoting mounting arm of

the saw. With the blade turning, the top end of the bone was advanced toward the blade until a noise was heard, indicating first contact with the blade. A cut was then made after adjustment to set the position to the distance determined in step 2.



Figure 3-19 The top part of the proximal metaphysis was trimmed by the diamond saw

Step 4: Perform indentation test (Figure 3-20).

A cylindrical stainless steel indenter which was 1.5mm in diameter with a flat bone-contacting tip was used. The platform holding the specimen was leveled to ensure that the loading was perpendicular to the specimen surface to be tested. The sample was positioned on the platform in such position that the indenter was driven into the middle of the exposed cancellous bone surface. The indenter position was also carefully adjusted so the indenter surface was very close to the bone surface but not touching the bone surface. Then the indenter, descending at a rate of 2mm/min, compressed the exposed cancellous bone surface until the cancellous bone failed. The actual compression force was recorded every 0.001 second during the lowering of the top part of the fixture.

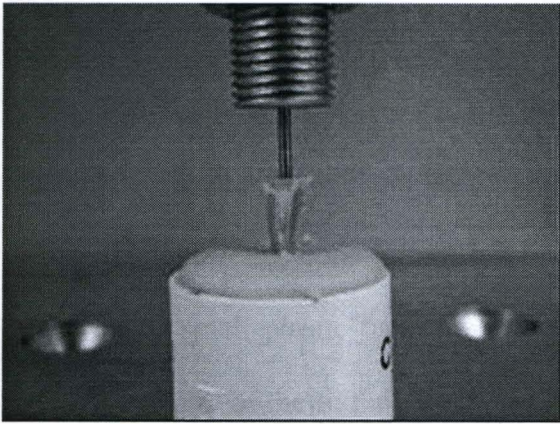


Figure (a) indentation test

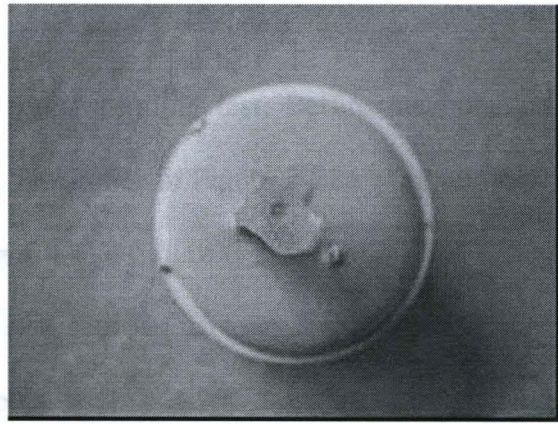


Figure (b) Failure of indentation test

Figure 3-20 Description of indentation test

The typical curve of compression load is shown in Figure 3-21. The indentation force was the maximum compressive force that was recorded from the lowest point of the force-displacement curve.

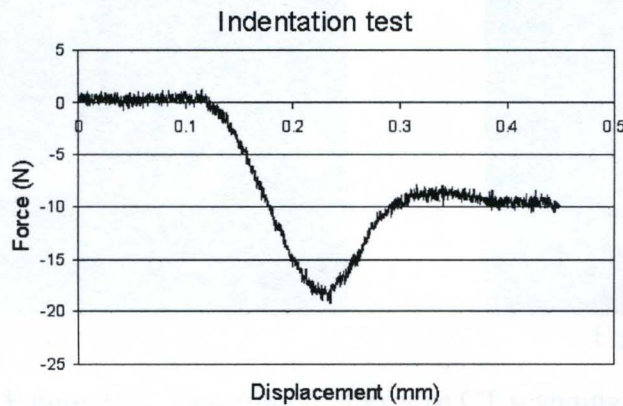


Figure 3-21 Typical curve of the indentation result (Exp2, I_Red)

3.6.2 Three-point bending test

The right femur was used for three-point bending test.

The following sections described the three point bending test in detail:

Step 1: Scan right femur.

The right femur was used for three point bending test. Before the bone was scanned, it was thawed at room temperature. The bones in Figure 3-22a were numbered as bone 1, bone 2, ..., bone 6 from left to right. . The fixture (Figure 3-22a) had 6 slots. There was 1 small plastic tube attached in slot 1 of the fixture, 3 small plastic tubes attached in slot 3 of the fixture, and 5 small plastic tubes attached in slot 5 of the fixture. Bone 1 was put in slot 1, bone 2 was put in slot 2, ..., bone 6 was put in slot 6. All these 6 bones were held on the fixture by rubber band and scanned together. It made scanning more efficient to scan 6 bones at one time than scanning bones separately.



Figure (a)

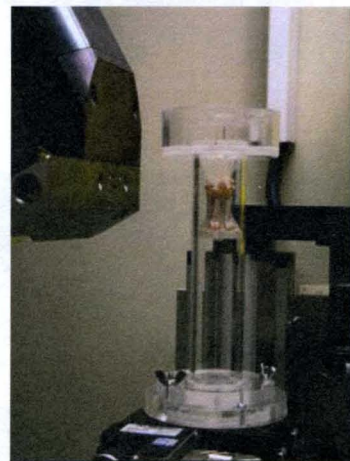


Figure (b)

Figure 3-22 Description of *ex vivo* CT scanning

Because the grey scale of the rubber band was similar with that of the bone material, the rubber band should be placed away from the middle part of the bone. The middle of the right femur shaft was CT scanned by one rotation encompassing 107 slices using a cone-beam scanning mode. The CT image of the middle of the shaft (image with

number 54) was used to calculate the bone area, moment of inertia and maximum tensile stress.

Step 2: Calculate cross-sectional area and area moment of inertia of the bone sample.

Bone area was calculated by counting bone pixels. The line OO' shown in Figure 3-23c was the axis for calculation of the moment of inertia I_x , which was also the axis of the bending. This was assumed to be the axis for the bending based on the geometry of the test and the orientation of the femur. The point O was the centroid of the bone area. The point O' was picked up by observing the image that was opened by ImageJ. I_x was calculated according to the formula: $I_x = \int y^2 dA$, where dA is an elemental area, y is the perpendicular distance from the axis x to the element dA .

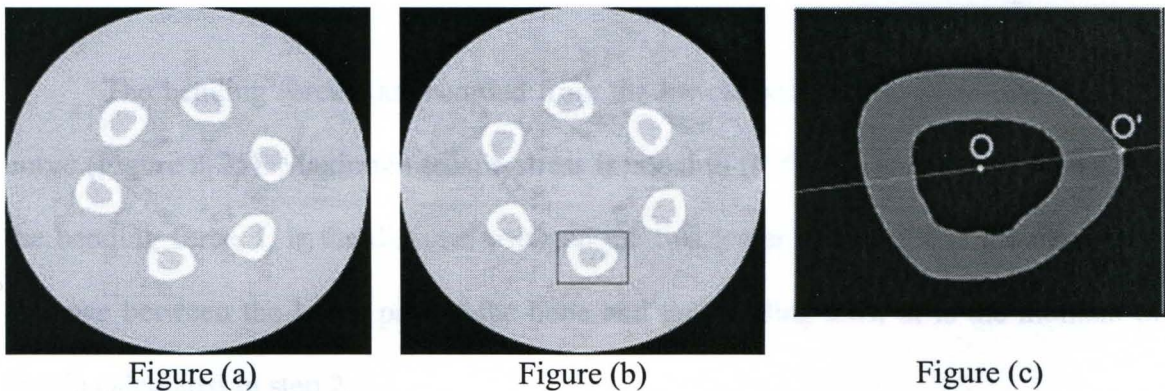


Figure 3-23 Illustration of Bone area and moment inertia calculation

Step 3: Perform three-point bending test (Figure 3-24).

The right femur was positioned on a fixture with the anterior side toward the loader. Load was applied on the midpoint between two supports that were 12 mm apart. The top part of the fixture was also carefully adjusted so the surface of the top part of the

fixture was very close to the bone surface but not touching the bone surface. Then the top part of the fixture, descending at a rate of 1mm/min, compressed the mid-shaft of the bone until the bone failed. The actual compression force was recorded every 0.01 second during the lowering of the top part of the fixture. The force applied on the bone was continually recorded until complete fracture occurred.

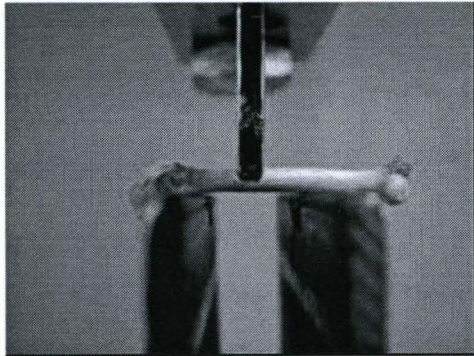


Figure (a)

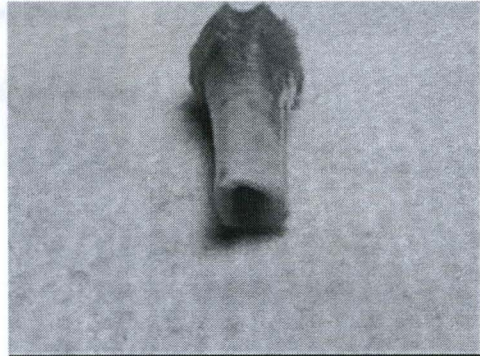


Figure (b)

Figure 3-24 Three point bending test and the typical curve of the test result

The bending force was recorded from the lowest point of the force-displacement curve (Figure 3-25). Maximum tensile stress is equal to $(F * L * c) / (4 * I_x)$, where F is the bending force, L is the distance between the two lower supports, c is the maximum distance between the lower part of the bone and the bending axis, I_x is the moment of inertia calculated in step 2.

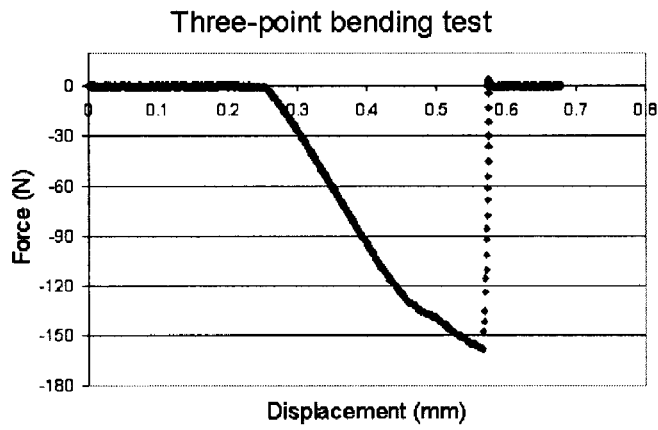


Figure 3-25 Force-displacement Curve (Exp2, C_Green2)

3.6.3 Torsion test

Left femur was used for torsion test. The middle of the femur shaft was CT scanned before the test. Torsion test is described in Figure 3-26.

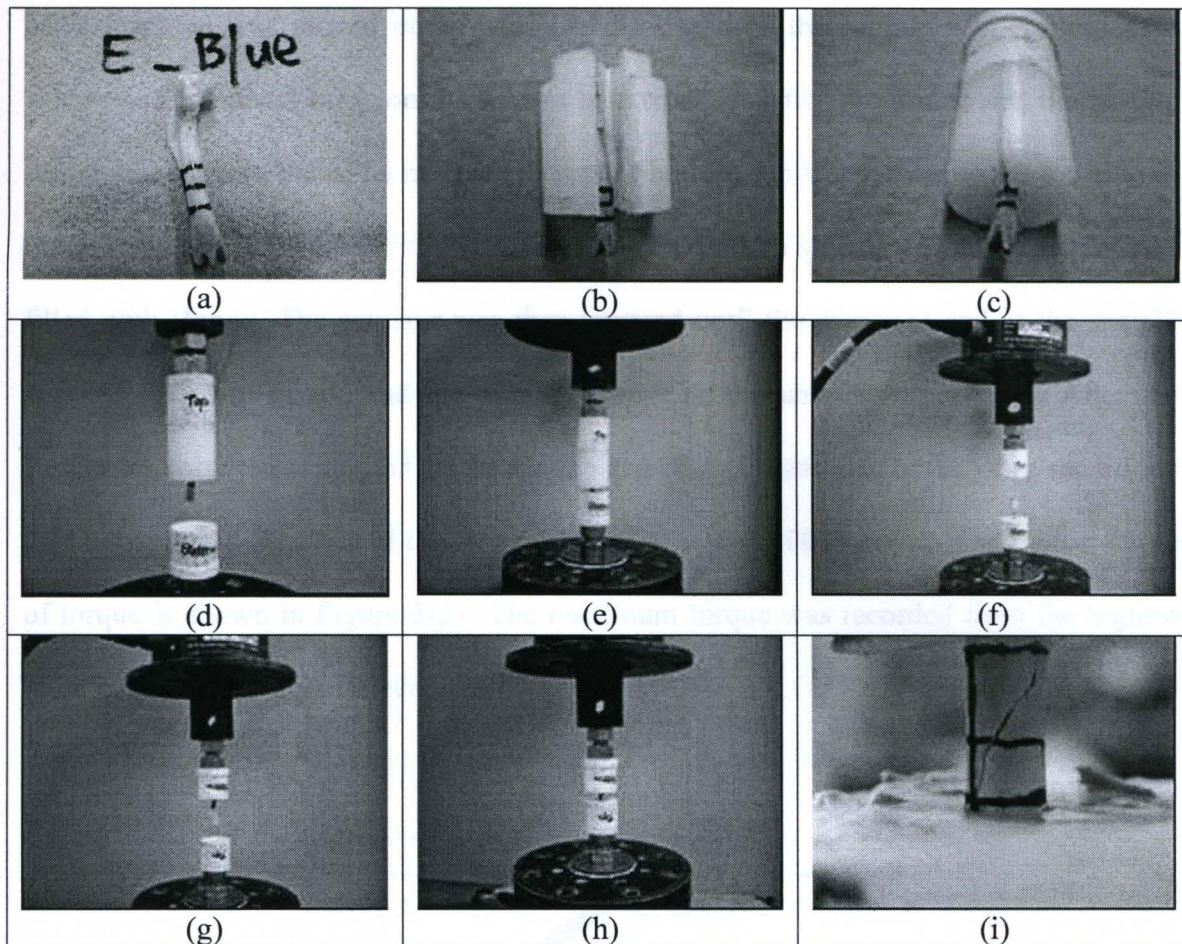


Figure 3-26 Torsion test

The distal and proximal marks were made on the femur, which decided how deep to embed the distal and proximal ends of the femur into Bondo. Two PVC ½ inch caps were needed for each bone sample. One was the bottom cap which was used to hold the distal end of the femur. The other was the top cap which was used to hold the proximal end of the femur. The distal end of the femur was embedded in Bondo first. To make sure that the bone sample remained aligned while the Bondo was hardened, the bottom cap with Bondo was fixed on the bottom of MTS machine, and the middle shaft of the sample was held by a plastic holder which was fixed to the top of the MTS machine. The plastic holder was made in to keep the sample aligned during embedding. The actuator of the

MTS machine was moved down until the distal end of the sample was embedded in Bondo and the distal mark on the sample was reached. After the Bondo set, the sample was removed from the MTS machine. Next the bottom cap was moved to the top side of the MTS machine. The other cap was placed on the bottom side of the MTS machine and filled with Bondo. The actuator was then lowered until the proximal end of the sample was embedded in Bondo and the proximal mark on the sample was reached. After the Bondo set, torque was applied on the sample at a displacement rate of 0.25 deg/sec till the failure happened. The actual torque was recorded every 0.001 second. The typical curve of torque is shown in Figure 3-27. The maximum torque was recorded from the highest point of the torque-angle curve.

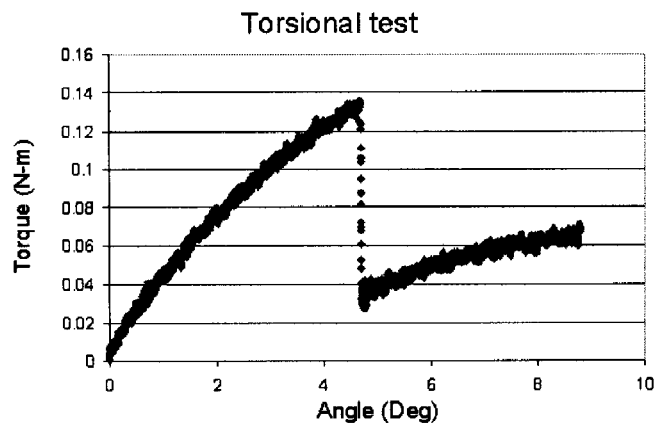


Figure 3-27 The typical curve of the test result (Exp1, A_BlK)

3.6.4 Three-point breaking test

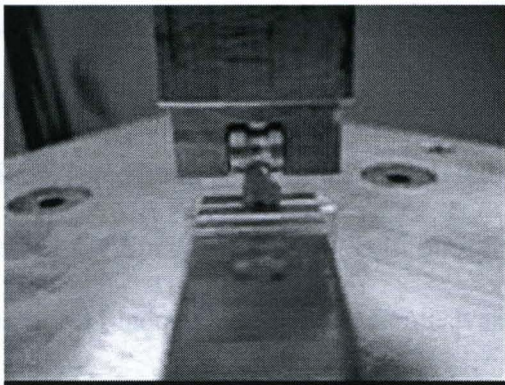
The right tibia was used for three-point breaking test. The testing was done blinded with regard to the test groups. In Prodama Study, some details were different from the test procedure that was described in Sturmer's paper (Sturmer EK et al., 2005).

A few hours before the testing, the right tibiae were completely thawed at room temperature. The soft tissues were carefully removed prior to the testing. The fibula was separated from tibia at the synostosis. The proximal tibia epiphysis was removed to avoid the movement of the proximal growth plate during the test. The tibia was placed on the base stamp (Figure 3-28). There were three rounded edge-free notches (1mm deep; 2, 3, or 4 mm in diameter) on the top of the base stamp. The proximal end of the tibia was put in one of the notches. The roller stamp consisted of an aluminum roller and a U-shaped support. The roller axle was fixed in the support and the support was connected to the MTS machine. The roller was adjusted until it was close to the bone surface but not touching the bone surface. The distance between the front surface of the support and the center of the roller was 3 mm. A plate with flat plane was placed on the front surface so the front surface of the support and the flat plane of the plate attached to each other tightly. The position of the base stamp was adjusted till the end of the proximal tibia touched the flat plane of the plate, which guaranteed that the distance between the end of the proximal tibia and the center of the roller stamp was exactly 3 mm.

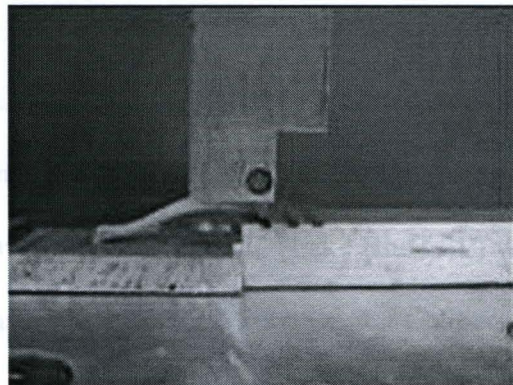
After a final visual check of the correct tibia position, the roller was lowered slowly and carefully until an initial force of 1N was reached. When the testing was started, the roller moved down at the speed of 5mm/s (In Sturmer's paper, the speed of the feed motion was 50mm/s). The trial was automatically ended by a displacement change of 1 mm (In Sturmer's paper, the trial was automatically ended by a drop in strength of >20N or a linear displacement of >2 mm).

A typical force-displacement curve for the tibia breaking test is shown in Figure 3-28e. Three parameters were analyzed: breaking force, breaking yield force, and

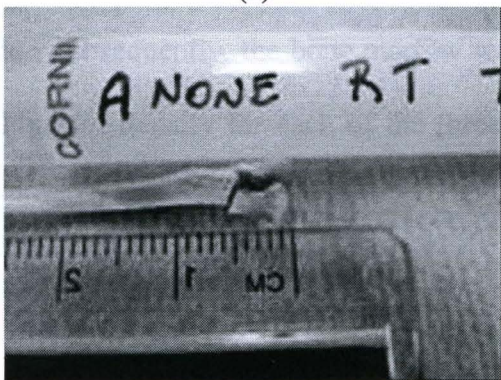
breaking energy. The breaking force was determined from the top of the curve. The compression force corresponding to 50% of maximum slope was determined as the breaking yield force. The breaking energy was equal to the area under the force curve up to the failure load. The failure load was found at the point where the curve started to drop abruptly (almost vertical), which corresponded to the complete failure of the bone sample.



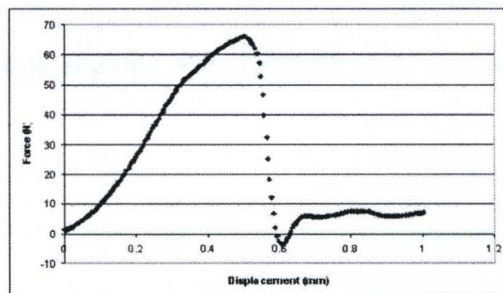
(a)



(b)



(d)



(e)

Figure 3-28 Three-point breaking test and the typical curve of the test result (Exp2, G_Green)

3.6.5 Femoral density via Archimedes' principle

Right femurs were submerged in distilled water and fully hydrated under a vacuum for 1 hr. Subsequently, the mass of each hydrated femur was obtained in air and

when submerged in water. Densities were determined using Archimedes' Principle according to the following formula: density = [mass of hydrated femur / (mass of hydrated femur - mass of hydrated femur submerged in water)] x density of distilled water at a given temperature (Keenan MJ, et al., 1997).

The proximal and distal ends of the femur were comprised primarily of cancellous bone, whereas the femoral diaphysis contained primarily cortical bone. Evaluation of the density of each of these femoral regions may thereby increase the understanding of the effect of a drug on each of these types of bone. The left femurs were separated into three regions (proximal left femur, distal left femur, and left femoral diaphysis) using an Isomet Low Speed Precision Sectioning Saw from Buehler Limited (Lake Bluff, IL) with a diamond blade. Briefly, each femur was measured with a Cen-Tech Digital Caliper and a cut was made from each end at 20% of the length of the femur plus half the width of the blade. Subsequently, the bone marrow was washed out of the femoral diaphysis and the Archimedes density for each of the three femoral regions was determined as described above.

3.7 *EX VIVO* STRUCTURAL ANALYSIS

Ex vivo micro-CT based structural analysis was used for Pradama Exp1, Pradama Exp2 and Pradama Exp 3.

3.7.1 Scanning design

The right tibia was used for *ex vivo* structural analysis in this study. Before the bone was scanned, it was thawed at room temperature. For all bone samples of Exp1, Exp

2 and some bone samples of Exp 3, the fibula, epiphysis and patella were removed manually from the metaphysis, so the CT image contained metaphysis only. The other bone samples of Exp 3 had intact epiphyses. They were just cleaned. The reason for the difference in Exp3 was that it was found there was more damage to the metaphysis top surface during the process of removing the epiphysis.

Six right tibiae were fixed to the fixture and scanned together, which was same to what is shown in Figure 3-22. The proximal end of the tibiae should position at the bottom of the fixture, which insured that VOIs of all six bone samples were scanned in fewer rotations. Five rotations, 107 slices per rotation, were taken from the top of the proximal metaphysis into the tibial shaft.

3.7.2 Image segmentation process

The new segmentation method that was described in chapter 3.4 was applied here. The VOI was chosen from the position that was 0.98mm (70 slices x 0.014mm) below the lower end of the growth plate and extending 4.2 mm (300 slices x 0.014mm) distally for Pradama Exp1 and Exp2. When the images were checked down into the distal part of the right tibia from the proximal top of metaphysis, the lateral part of the cortex was becoming separated from the main part. For Pradama Exp 3, the VOI was chosen from the position where the lateral part was just separated from the main part and extending 200 slices distally.

The method was totally automatic if one criterion was met: there were no other bones connected to the VOI. For the bone samples of which the epiphysis and patella were removed from metaphysis before they were scanned, there were no other bones in

the CT original scanning images. For the bone samples that did not go through the epiphyseal removal procedure, such as in Exp3, the VOI was chosen distally enough to make sure that there were no other bones connected to the VOI in the CT original scanning images. No pre-step was needed to separate metaphysis from other bones before Cancellous and cortical bone segmentation. The whole image segmentation process was totally automatic.

3.8 RESULTS ANALYSIS METHODS

3.8.1 Validation of cancellous bone segmentation method

1) The new method is objective

For a given image stack, the segmentation results will be same no matter how many times the program is run. It is obvious that the new method is objective because the segmentation is performed automatically by computer. By contrast, a manual method can differ between trials and between different operators.

2) The new method is more accurate, precise and repeatable

Two right tibiae (one sham, one OVX) were collected from 37-week-old Sprague Dawley female rats. The epiphyses were removed before scanning (Micro CT, ACTIS 150/225 system, BIR Inc., Lincolnshire, IL). Six image stacks were obtained by loading and scanning the proximal metaphyses of each bone sample three times. Nominal isotropic resolution was 14 μ m. Three operators segmented cancellous bone from cortical bone manually. Each operator segmented one sham image stack and one OVX image stack. The segmentation results from manual work were used as a “gold standard”. The

new method was used to segment the six image stacks. The Helterbrand method was used to segment the six image stacks.

1) Accuracy validation: The mean values of the cancellous bone volume measured by three different methods were compared by Tukey multiple comparison, 2) Precision validation: The coefficient of variation (CV) of each method was calculated as $CV=100*(\text{Standard deviation})/(\text{mean value of set})$. The smaller the value of the CV, the more precise the method is, and 3) Repeatability validation: The variances of each method were compared by F-test to determine whether the repeatability of the new method was better than the manual method.

3.8.2 Data analysis of Alendronate study

Alendronate study was analyzed by P-value of statistical analysis that was ANOVA followed by Post-hoc t-test (Tukey multiple comparisons). The drug effect was evaluated by comparing the results at week 12 and week 16 with its own baseline at week 8. The drug effects were also compared with OVX group at the same time point (at week 12 and week 16).

3.8.3 Data analysis of the Pradama Study in engineering perspective

Two groups were analyzed: Sham group and OVX group.

1) Sensitivity analyses

The new methods (volume fraction, indentation testing, three-pt breaking testing) were compared to the old methods (Archimedes and 3-pt bending testing). The new methods were expected to be more sensitive to detect the differences between OVX and

Sham. By focusing on only two groups at the same time points (11 weeks or 12 weeks), simple t-tests (two-sample assuming unequal variances) was used to compare the mean values for the various measurements and calculate p-values for each. Statistical power and % difference were calculated if there is significant difference between sham and OVX. % difference = $((\text{Sham} - \text{OVX}) / \text{Sham}) * 100$.

The p-values of the followings parameters were picked up by one tail t-test: BV/TV from 3D image analysis, density from Archimedes method, Indentation force, breaking force, and breaking yield force. The p-values of the followings parameters were picked up by two tail t-test: Breaking energy, bending force, moment of inertia, area, and maximum tensile stress.

The comparisons of new methods versus old methods were: 1) Volume fraction vs. Archimedes, 2) Indentation testing vs. Archimedes, 3) Three-pt breaking testing vs. Archimedes, 4) Volume fraction vs. three-pt bending testing, 5) Indentation testing vs. three-pt bending testing, and 6) Three-pt breaking testing vs. three-pt bending testing.

2) Linear regression analyses

Finally, as another evaluation of the newly described bone quality measurements developed in this dissertation work, the image processing method was correlated to the mechanical test methods. In this way, the most significant linear correlations, if good enough, could allow the transition from mechanical testing as the gold standard of bone quality measurement to image analysis as a standard method. This would permit the use of *in vivo* analysis and more powerful longitudinal studies.

It was expected that there were better relationship between indentation results and cancellous bone volume fraction instead of whole bone volume fraction and cortical bone

volume fraction, because indentation testing evaluated the mechanical competence of cancellous bone directly.

It was expected that there was a better relationship between 3-pt breaking results and whole bone volume fraction instead of cancellous bone volume fraction and cortical bone volume fraction, because 3-pt breaking testing evaluated the mechanical competence of whole bone as a composite of cancellous and cortical bone at the metaphysis.

3.8.4 Data analysis of Pradama Study (drug effect)

Drug effects on osteoporosis were shown by P-value of statistical analysis as ANOVA followed by post-hoc t-test (Tukey multiple comparisons) for individual image analysis and mechanical testing. It was not the focus of this dissertation

3.8.5 Description of P-value of statistical analysis

ANOVA, Post-hoc t-test (Tukey multiple comparisons), F-test, and regression analysis were used in the research. A P value < 0.05 was considered to be statistically significant. The P value less than 0.05 were in bold. A P value greater than 0.05 and less than 0.1 was followed by *.

CHAPTER 4. RESULT

4.1 CANCELLOUS BONE SEGMENTATION

Table 4-1 and Figure 4-1 are the cancellous bone volumes (mm^3) of the sham sample and the OVX sample.

Table 4-1 Cancellous bone volume (mm^3) calculated from different segmentation methods

Sham (n=3)			OVX (n=3)		
Manual	New	Helterbrand	Manual	New	Helterbrand
2.08	2.07	2.47	1.14	1.15	1.47
2.37	2.12	2.51	1.27	1.17	1.80
2.15	2.10	2.57	1.20	1.18	1.65

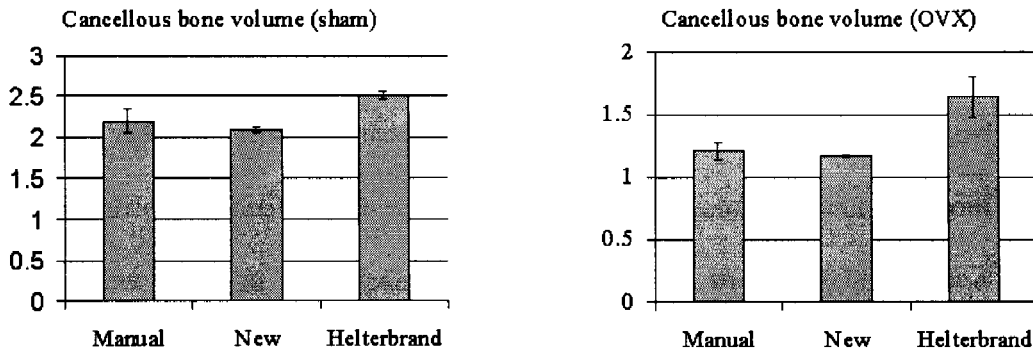


Figure 4-1 The results of cancellous bone volume (mm^3) from different segmentation methods

The P-values in Table 4-2 were calculated based on the results of the sham sample. The cancellous bone volume calculated from Helterbrand method was significantly different from the cancellous bone volume calculated from manual method

and also significantly different from the cancellous bone volume calculated from the new method. There was no significant difference between the cancellous bone volume calculated from manual method and that from the new method.

Table 4-2 the comparison of the means (cancellous bone volume of the sham sample) between different segmentation methods

	New	Helterbrand
Manual	0.3901	0.0125
Helterbrand	0.0031	

The new method resulted in the smallest coefficient of variation (CV). The CVs were around 1% for the new method, pointing to a good precision of the method (Table 4-3).

Table 4-3 The coefficient of variation (CV) of each method (%)

sham			OVX		
Manual	New	Helterbrand	Manual	New	Helterbrand
6.7	1.1	1.9	5.6	0.9	10.1

The P-values in Table 4-4 were calculated based on the results of the OVX sample. The cancellous bone volume calculated from Helterbrand method was significantly different from the cancellous bone volume calculated from manual method and also significantly different from the cancellous bone volume calculated from the new method. There was no significant difference between the cancellous bone volume calculated from manual method and that from the new method.

Table 4-4 the comparison of the means (cancellous bone volume of the OVX sample) between different segmentation methods

	New	Helterbrand
Manual	0.9016	0.0050
Helterbrand	0.0033	

Both the sham sample and the OVX sample showed that the new method resulted in statistically smaller variance than the manual method (Table 4-5).

Table 4-5 The comparison of the variances between manual segmentation method and the new method

Sham	OVX
0.0490	0.0490

4.2 ALENDRONATE STUDY

All images and data were referenced to week 8. Alendronate Study was designed for the drug recovery experiment, that is, the bone needed to be lost first, then the drugs were given to see if the bone mass was increased. Week 8 was the time point on which the large bone loss was observed. The bone volume fractions of the different group are shown in Figure 4-2.

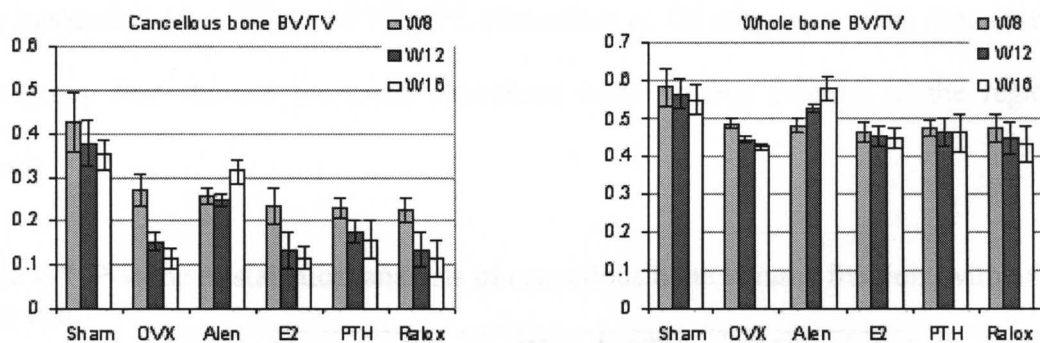


Figure 4-2 Bone volume fraction results of Alendronate study

All OVX rats, including the four treatment groups, were significantly different from Sham at all time points ($P < 0.05$), with the exception of Alen_W16 (0.31 ± 0.027) (P value is 0.9914) (Table 4-6).

Table 4-6 P-value of statistical analysis of cancellous bone volume fraction (with sham data)

	Alen_ W12	Alen_ W16	E2_ W12	E2_ W16	PTH_ W12	PTH_ W16	Ralox_ W12	Ralox_ W16
Alen_W8	1.0000	0.9108						
E2_W8			0.0798	0.0200				
PTH_W8					0.9111	0.5685		
Ralox_W8							0.2128	0.0381
OVX_W12	0.0910*		1.0000		1.0000		1.0000	
OVX_W16		0.0001		1.0000		0.9738		1.0000
Sham_W12	0.0017		0.0001		0.0001		0.0001	
Sham_W16		0.9914		0.0001		0.0001		0.0001

Comparing the cancellous bone volume fractions without considering the Sham group, the E2 group and the Ralox group showed the significant decrease of the cancellous bone volume fraction at week 12 and week 16 when they compared with their own references at week 8 (E2_W8 and Ralox_W8, respectively), with the exception of Relox_W12 (P value was 0.0706) (Table 4-7). The cancellous bone volume fraction of Alen_W12, Alen_W16, PTH_W12 and PTH_W16 were not significantly different from their baselines (Alen_W8 and PTH_W8, respectively). Of all groups, Alen group was the only group that showed increased cancellous bone volume fraction in the region of interest.

Table 4-7 P-value of statistical analysis of cancellous bone volume fraction (without sham data)

	Alen_ W12	Alen_ W16	E2_ W12	E2_ W16	PTH_ W12	PTH_ W16	Ralox_ W12	Ralox_ W16
Alen_W8	1.0000	0.7179						
E2_W8			0.0200	0.0038				
PTH_W8					0.7185	0.2926		
Ralox_W8							0.0706*	0.0082
OVX_W12	0.0236		0.9996		0.9999		0.9999	
OVX_W16		0.0000		1.0000		0.8741		1.0000

All OVX rats, including the four treatment groups, were significantly different from Sham at all time points ($P < 0.05$), with the exception of Alen_W12 (0.53 ± 0.010) (P value was 0.9790), Alen_W16 (0.58 ± 0.029) (P value was 0.9978) and PTH_W16 (0.46 ± 0.049) (P value was 0.0666) (Table 4-8).

Table 4-8 P-value of statistical analysis of whole bone volume fraction (with sham data)

	Alen_W12	Alen_W16	E2_W12	E2_W16	PTH_W12	PTH_W16	Ralox_W12	Ralox_W16
Alen_W8	0.9482	0.0357						
E2_W8			1.0000	1.0000				
PTH_W8					1.0000	1.0000		
Ralox_W8							0.9998	0.9844
OVX_W12	0.1053		1.0000		1.0000		1.0000	
OVX_W16		0.0001		1.0000		0.9687		1.0000
Sham_W12	0.9790		0.0034		0.0136		0.0016	
Sham_W16		0.9978		0.0086		0.0666*		0.0021

Comparing the whole bone volume fraction without considering the Sham group, the Alen group, E2 group, PTH group and Ralox group at week 12 and week 16 were not significantly different from their own references (Alen_W8, E2_W8, PTH_W8 and Ralox_W8, respectively), with the exception of Alen group at 16 weeks ($P=0.0133$) (Table 4-9).

Table 4-9 P-value of statistical analysis of whole bone volume fraction (without sham data)

	Alen_W12	Alen_W16	E2_W12	E2_W16	PTH_W12	PTH_W16	Ralox_W12	Ralox_W16
Alen_W8	0.8486	0.0133						
E2_W8			1.0000	1.0000				
PTH_W8					1.0000	1.0000		
Ralox_W8							0.9981	0.9368
OVX_W12	0.0449		1.0000		0.9999		1.0000	
OVX_W16		0.0000		0.9995		0.8949		1.0000

4.3 SENSITIVITY ANALYSES

4.3.1 Pradama Exp1 (Week 11)

Table 4-10 is the summary of the sensitivity study results of Pradama Exp1. There were not significant differences detected in cancellous bone volume fraction, cortical bone volume fraction, whole bone volume fraction, breaking energy, bending force, moment of inertia, maximum tensile stress, torsional force, and whole bone density by Archimedes's method (Keenan MJ et al, 1997). There were statistically significant differences between OVX and sham in indentation force, breaking force, breaking yield force, and cross-sectional area. Comparing the OVX group with the Sham group, the difference of cross-sectional area was 5.2%, while the differences were 73.2% in indentation force, 41.6% in breaking force and 52.3% in breaking yield force.

Table 4-10 Pradama Exp1 outcomes

	Sham (n=5)	OVX (n=3)	P value	Power	% difference
Cc BV/TV (%)	8.80 ± 3.62	4.88 ± 0.50	0.0761*		
Ct BV/TV (%)	46.76 ± 2.15	46.41 ± 4.42	0.9050		
W BV/TV (%)	51.45 ± 2.50	49.02 ± 4.39	0.4434		
In F (N)	39.98 ± 11.32	10.71 ± 1.77	0.0048	0.8179	73.2
Bk F (N)	116.98 ± 10.89	68.29 ± 7.80	0.0003	0.9907	41.6
Bk YF (N)	112.34 ± 11.48	53.54 ± 3.31	0.0001	0.9996	52.3
Bk E (N*mm)	28.49 ± 5.54	23.28 ± 2.07	0.1166		
Bd F (N)	148.29 ± 11.60	160.15 ± 6.61	0.1149		
MOI (mm ⁴)	5.38 ± 0.20	5.78 ± 0.48	0.7279		
Area (mm ²)	5.61 ± 0.11	5.91 ± 0.02	0.0041	0.8473	-5.2
MTS (MPa)	138.55 ± 6.49	137.50 ± 3.82	0.7819		
Ts F (N)	0.32 ± 0.13	0.25 ± 0.16	0.5783		
W D (g/cm ³)	1.43 ± 0.02	1.41 ± 0.01	0.3214		

Note: All values are expressed as mean ± SD. Cc: cancellous bone; Ct: cortical bone; W: whole bone sample; In: indentation testing; F: Force; Bk: 3-pt breaking testing; YF: yield force; E: energy; Bd: 3-pt bending testing; MOI: Moment of Inertia; MTS: Maximum tensile stress; Ts: torsion testing; D: Density.

Estrogen deficiency did not result in significant changes in the bone volume fractions (Figure 4-3).

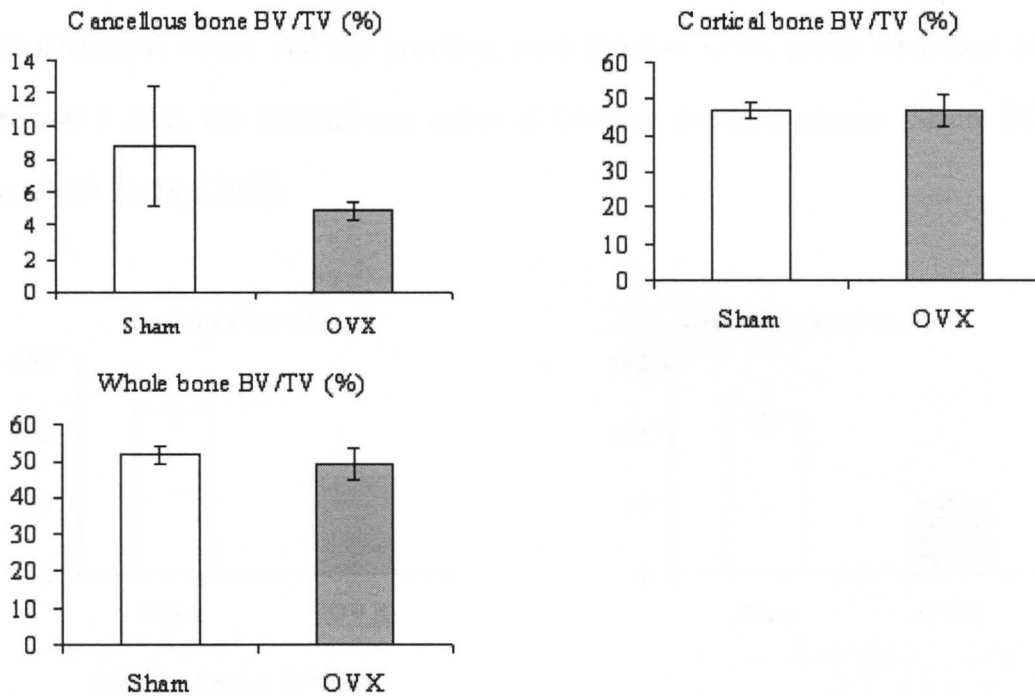


Figure 4-3 Bone fraction results of Exp 1 from 3D image analysis.

Figure 4-4 shows the mechanical bone strength of the cancellous bone of the left tibia. The indentation force for the OVX group (10.71 ± 1.77) was significantly lower than that of the Sham group (39.98 ± 11.32) ($P < 0.01$). There was a substantial decrease in the indentation force by 73.2% in the OVX animals.

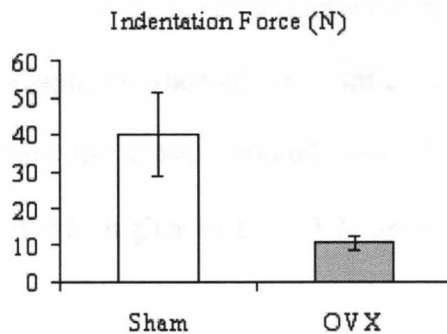


Figure 4-4 Indentation testing results of Exp 1.

OVX operation significantly decreased the breaking force (116.983 ± 10.889 for sham and 68.29 ± 7.80 for OVX) ($P < 0.001$) and breaking yield force (112.34 ± 11.48 for sham and 53.54 ± 3.31 for OVX) ($P = 0.001$) (Figure 4-5). The breaking force of OVX group decreased 41.6% and the breaking yield force of OVX group decreased 52.3%. There was a mild, but insignificant effect of OVX on breaking energy (Sham: 28.49 ± 5.54 ; OVX: 23.28 ± 2.07).

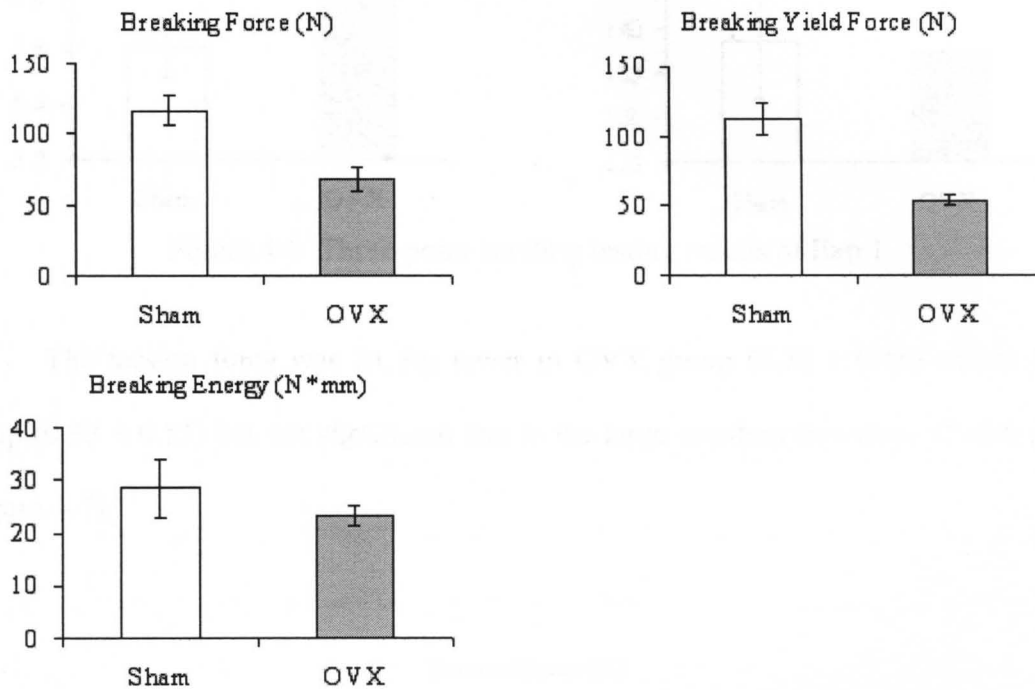


Figure 4-5 Three-point breaking testing results of Exp 1.

The bending force, moment of inertia and maximum tensile stress of the cortical bone in the femoral mid-diaphysis showed very little changes because of estrogen deficiency (Figure 4-6). Only the cross-sectional area of femoral mid-diaphysis was significantly different and it was higher in the OVX group versus the Sham group by 5.2%.

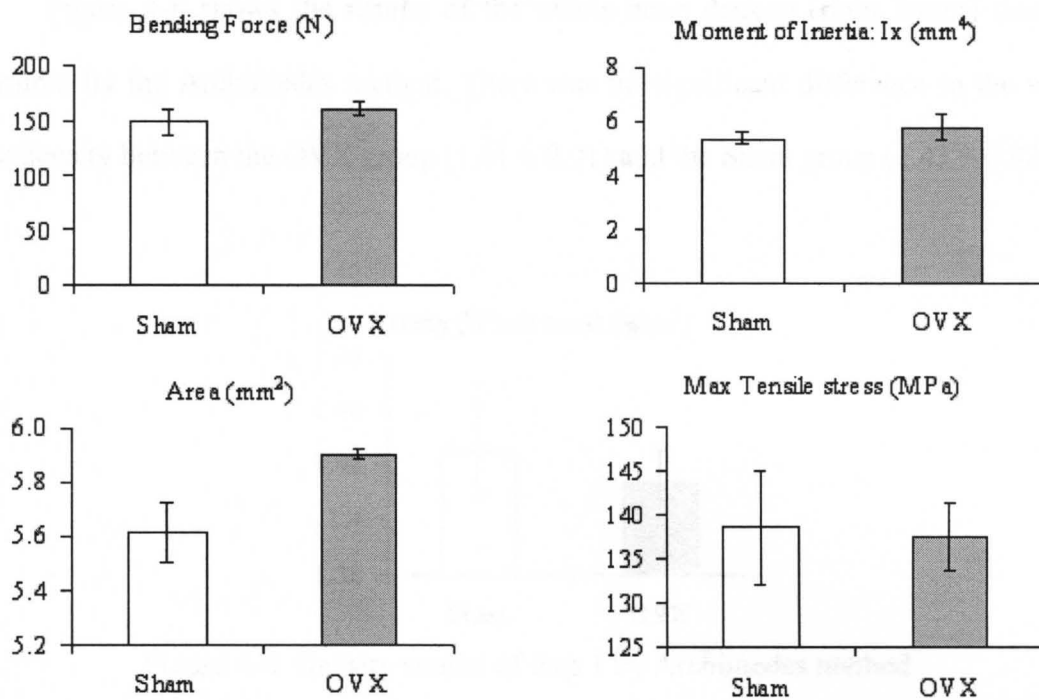


Figure 4-6 Three-point bending testing results of Exp 1

The torsion force was 21.5% lower in OVX group (0.25 ± 0.16) versus Sham group (0.32 ± 0.13) but not significant due to the large standard deviation of each group (Figure 4-7).

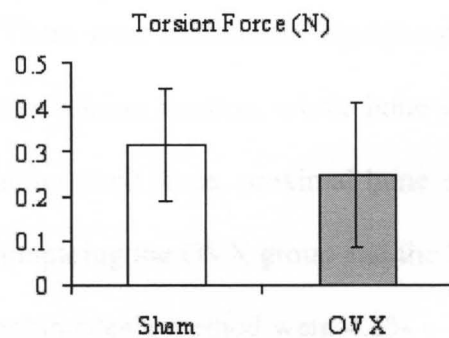


Figure 4-7 Torsion testing results of Exp 1

Figure 4-8 shows the results of the whole bone density (right femur) that was measured by the Archimedes method. There was no significant difference in the whole bone density between the OVX group (1.41 ± 0.01) and the Sham group (1.43 ± 0.02).

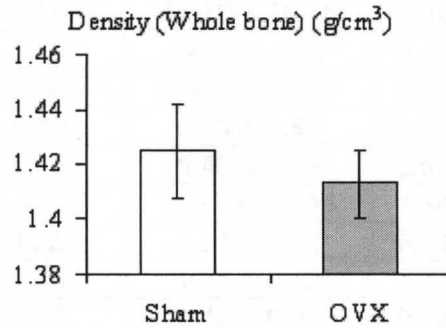


Figure 4-8 Density results of Exp 1 by Archimedes method

4.3.2 Pradama Exp2 (Week 11)

Table 4-11 is the summary of the sensitivity study results of Pradama Exp2. There were not significant differences detected in cortical bone volume fraction, breaking energy, bending force, moment of inertia, cross-sectional area, maximum tensile stress and middle bone density. There were statistically significant differences between OVX and sham in cancellous bone volume fraction, whole bone volume fraction, indentation force, breaking force, breaking yield force, proximal bone density, distal bone density, and whole bone density. Comparing the OVX group and the Sham group, the differences of densities detected by Archimedes's method were 4.2% ~ 4.9%, while the differences were 72.5% in cancellous bone volume fraction, 73.0% in indentation force, 31.4% in breaking force and 42.3% in breaking yield force.

Table 4-11 Pradama Exp2 outcomes

	Sham (n=6)	OVX (n=6)	P value	Power	% difference
Cc BV/TV (%)	26.34 ± 5.98	7.24 ± 2.85	0.0002	0.99999	72.5
Ct BV/TV (%)	46.64 ± 3.18	45.99 ± 3.31	0.7359		
W BV/TV (%)	62.24 ± 6.46	49.88 ± 3.80	0.0037	0.9527	19.9
In F (N)	40.32 ± 6.35	10.90 ± 3.68	0.00001	1.0000	73.0
Bk F (N)	102.64 ± 15.33	70.45 ± 17.85	0.0073	0.8548	31.4
Bk YF (N)	88.64 ± 17.68	51.10 ± 10.16	0.0020	0.9815	42.3
Bk E (N*mm)	29.10 ± 10.02	24.19 ± 5.47	0.3206		
Bd F (N)	180.90 ± 16.38	194.52 ± 19.67	0.2218		
MOI (mm ⁴)	6.09 ± 0.80	6.05 ± 0.83	0.9301		
Area (mm ²)	6.49 ± 0.35	6.40 ± 0.26	0.6234		
MTS (MPa)	145.92 ± 13.37	159.78 ± 7.54	0.058		
Pro D (g/cm ³)	1.61 ± 0.02	1.54 ± 0.02	0.0001	0.999969	4.5
Mid D (g/cm ³)	1.81 ± 1.13	1.75 ± 0.12	0.4278		
Dis D (g/cm ³)	1.47 ± 0.02	1.40 ± 0.03	0.0004	0.9970	4.9
W D (g/cm ³)	1.59 ± 0.04	1.53 ± 0.02	0.0037	0.9367	4.2

Note: All values are expressed as mean ± SD. Cc: cancellous bone; Ct: cortical bone; W: whole bone sample; In: indentation testing; F: Force; Bk: 3-pt breaking testing; YF: yield force; E: energy; Bd: 3-pt bending testing; MOI: Moment of Inertia; MTS: Maximum tensile stress; Pro: Proximal bone part; D: Density; Dis: Distal part.

The bone volume fractions are shown in Figure 4-9. There was a dramatic reduction of the cancellous bone volume fraction for the OVX group (7.24 ± 2.85) compared with the Sham group (26.34 ± 5.98) ($P=0.0001$), which is also shown clearly in Figure 4-10. The cancellous bone volume fraction was diminished by 72.5% as a result of the estrogen deficiency. The volume fraction of whole bone of OVX group (49.88 ± 3.80) was significantly lower than that of Sham group (62.24 ± 6.46) by 19.9%. There was not significant difference in the volume fraction of cortical bone between the two groups (46.64 ± 3.18 for sham and 45.99 ± 3.31 for OVX).

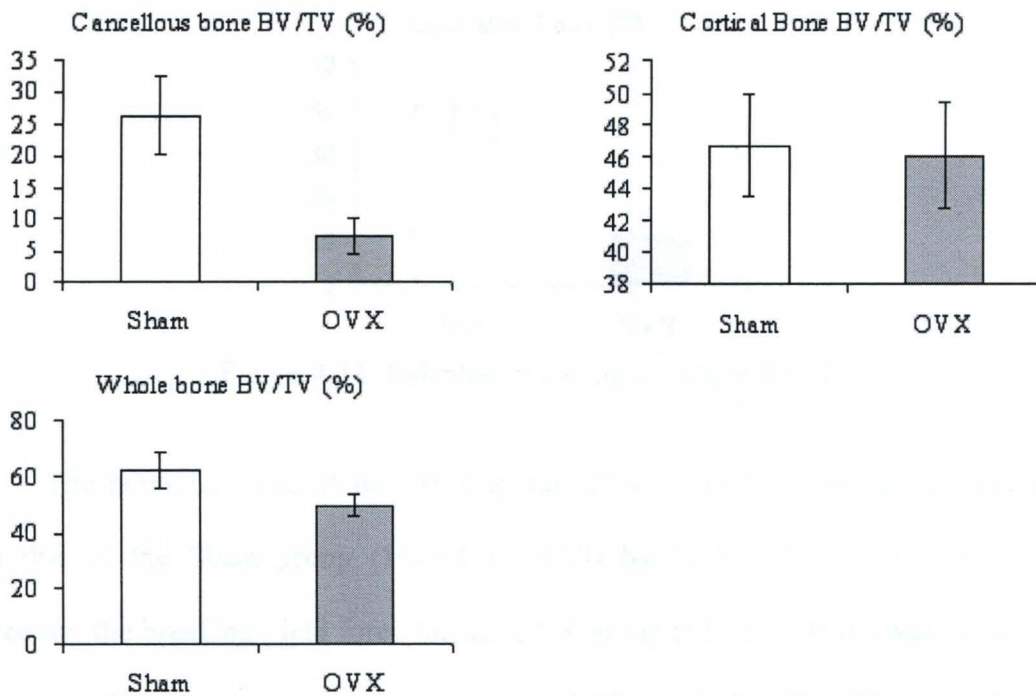


Figure 4-9 Bone fraction of Exp 2 from 3D image analysis

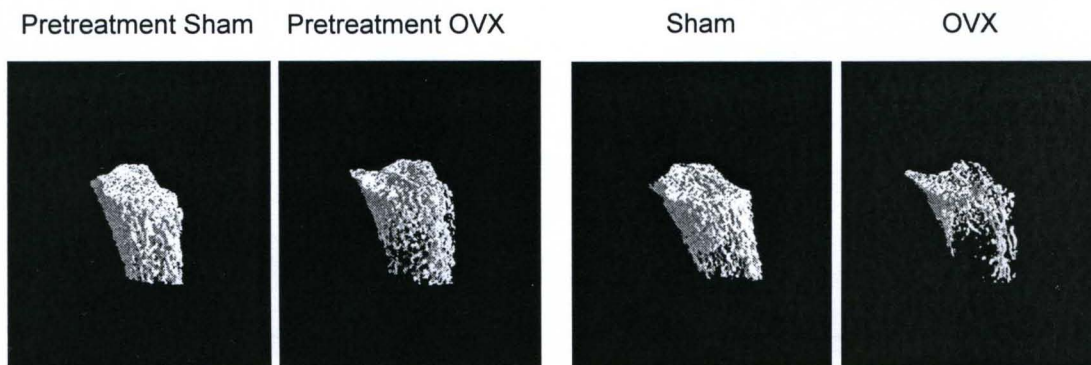


Figure 4-10 Three-dimensional images (Exp2) of the tibial metaphysis of an OVX and sham-operated animal (mean from each group) at the time of week 0 and week 11 after operation: all images are aligned manually using VGStudio MAX to illustrate the internal cancellous bone structure.

The indentation force by testing cancellous bone revealed a dramatic reduction for the OVX group (10.90 ± 3.68) compared with the Sham group (40.32 ± 6.35) ($P=0.00001$) (Figure 4-11). The cancellous bone strength was diminished by 73.0% as a result of the estrogen deficiency.

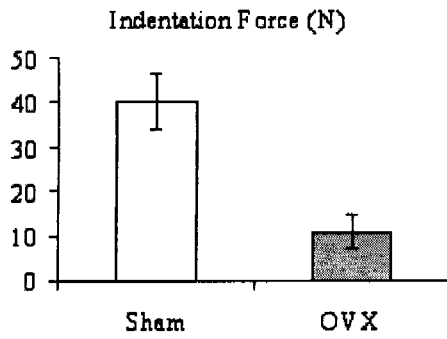


Figure 4-11 Indentation testing results of Exp 2

The breaking force of the OVX group (70.45 ± 17.85) was significantly lower than that of the Sham group (102.64 ± 15.33) by 31.4% ($P < 0.001$) (Figure 4-12). Moreover, the breaking yield force for the OVX group (51.10 ± 10.16) was significantly lower than that of the Sham group (88.64 ± 17.68) by 42.3% ($P = 0.001$). The breaking energy of OVX was slightly lower than that of Sham group but not significant different.

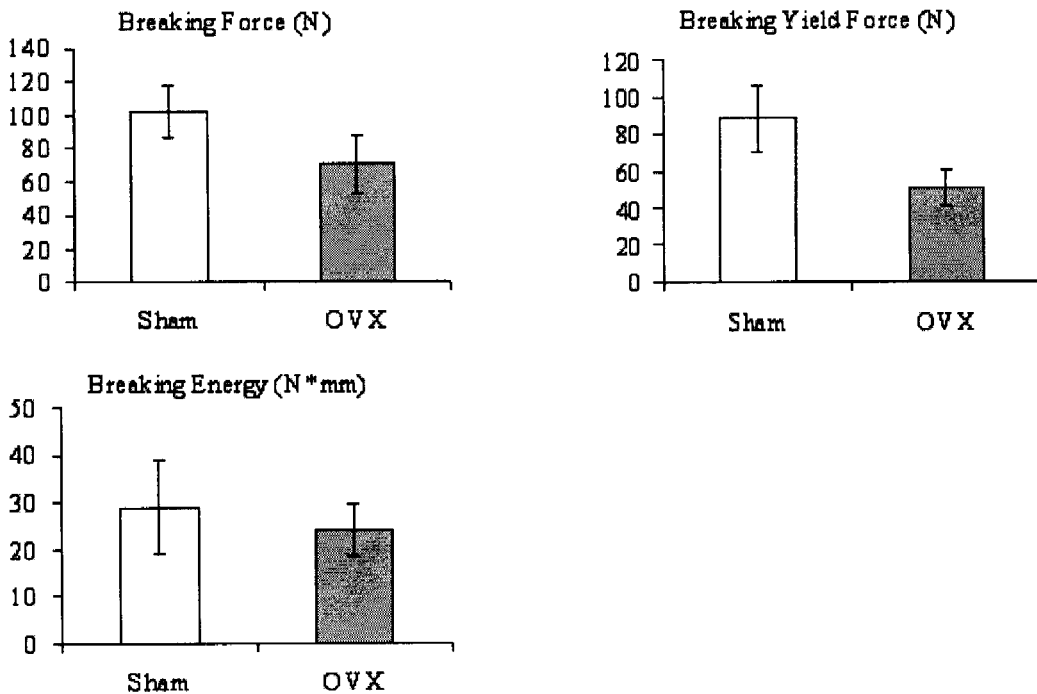


Figure 4-12 Three-point breaking testing results of Exp 2

All measured parameters (bending force, moment of inertia, area, and maximum tensile stress) of the cortical bone in the femoral mid-diaphysis were not significantly different between the OVX group and Sham group (Figure 4-13).

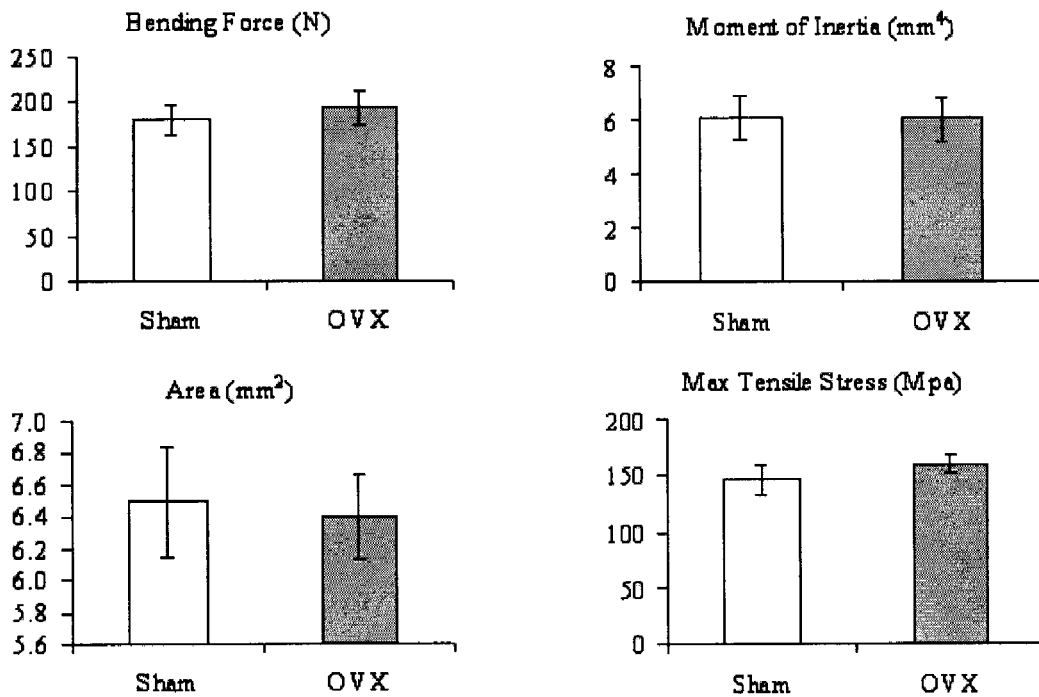


Figure 4-13 Three-point bending testing results of Exp 2

Figure 4-14 reveals the reduction for the OVX group compared with the Sham group. The densities were all significantly lower in OVX group versus Sham group except the density of middle bone part. Due to the estrogen deficiency, the density of whole bone decreased by 4.2%, the density of proximal bone part decreased by 4.5% and the density of distal bone part decreased by 4.9%.

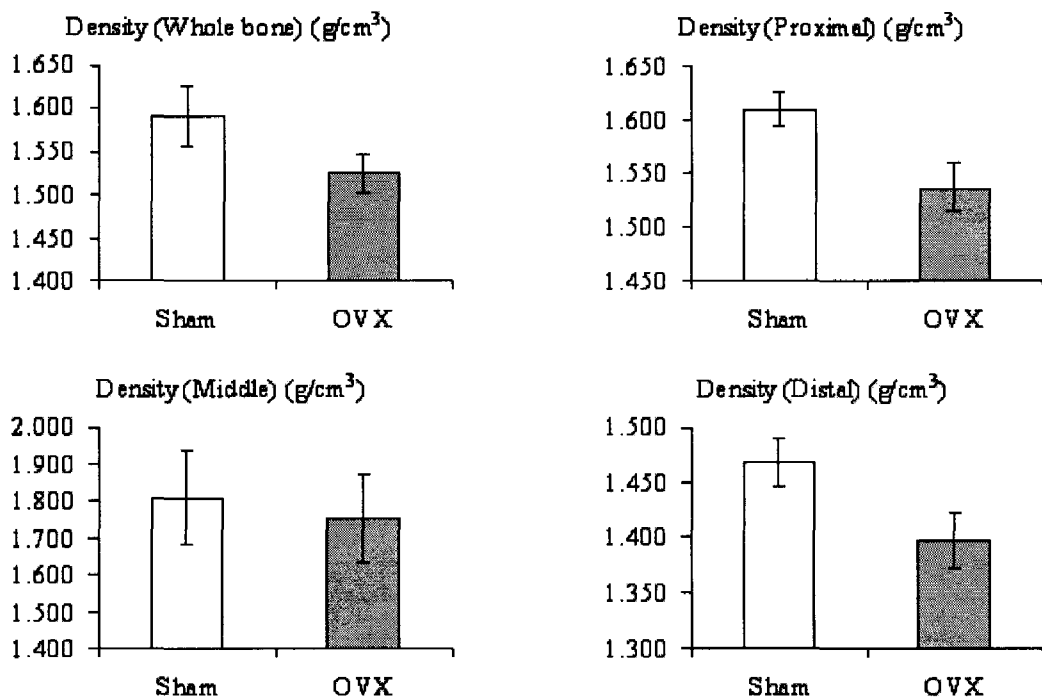


Figure 4-14 Density results of Exp 2 by Archimedes method

4.3.3 Pradama Exp3 (Week 12)

Table 4-12 is the summary of the sensitivity study results of Pradama Exp3. There were statistically significant differences between OVX and sham in cancellous bone volume fraction, whole bone volume fraction, indentation force, breaking force, breaking yield force, breaking energy, and whole bone density. There were not significant differences in cortical bone volume fraction, bending force, moment of inertia, cross-sectional area, maximum tensile stress, proximal bone density, middle bone density and distal bone density. Comparing the OVX group and the Sham group, the greatest difference of the densities detected by Archimedes's method was 3.1%, while the differences were 55.8% in cancellous bone volume fraction, 86.4% in indentation force, 36.3% in breaking force and 47.5% in breaking yield force.

Table 4-12 Pradama Exp3 outcomes

	Sham (n=6)	OVX (n=7)	P value	Power	% difference
Cc BV/TV(%)	26.84 ± 3.05	11.86 ± 3.29	0.000004	1.0000	55.8
Ct BV/TV(%)	42.23 ± 3.29	43.31 ± 2.39	0.5230		
W BV/TV(%)	57.79 ± 1.93	50.08 ± 1.34	0.00002	1.0000	13.3
In F (N)	37.94 ± 13.30	5.16 ± 1.59	0.0018	0.999865	86.4
Bk F (N)	101.38 ± 16.86	64.59 ± 5.38	0.0022	0.997262	36.3
Bk YF (N)	89.60 ± 18.14	47.08 ± 6.81	0.0016	0.99874	47.5
Bk E (N*mm)	25.29 ± 4.08	19.63 ± 5.06	0.047	0.4797	22.4
Bd F (N)	189.32 ± 16.31	200.31 ± 17.95	0.2721		
MOI (mm ⁴)	5.34 ± 0.41	5.72 ± 0.79	0.2886		
Area (mm ²)	6.18 ± 0.23	6.34 ± 0.30	0.3108		
MTS (MPa)	169.30 ± 8.04	173.51 ± 11.98	0.4690		
Pro D (g/cm ³)	1.55 ± 0.04	1.53 ± 0.02	0.3272		
Mid D (g/cm ³)	1.66 ± 0.05	1.63 ± 0.02	0.227		
Dis D (g/cm ³)	1.42 ± 0.03	1.39 ± 0.04	0.2270		
W D (g/cm ³)	1.60 ± 0.02	1.55 ± 0.01	0.0026	0.9863	3.1

Note: All values are expressed as mean ± SD. Cc: cancellous bone; Ct: cortical bone; W: whole bone sample; In: indentation testing; F: Force; Bk: 3-pt breaking testing; YF: yield force; E: energy; Bd: 3-pt bending testing; MOI: Moment of Inertia; MTS: Maximum tensile stress; Pro: Proximal bone part; D: Density; Mid: Middle bone part; Dis: Distal bone part.

The 3D structures of the cancellous bone are shown in Figure 4-15.

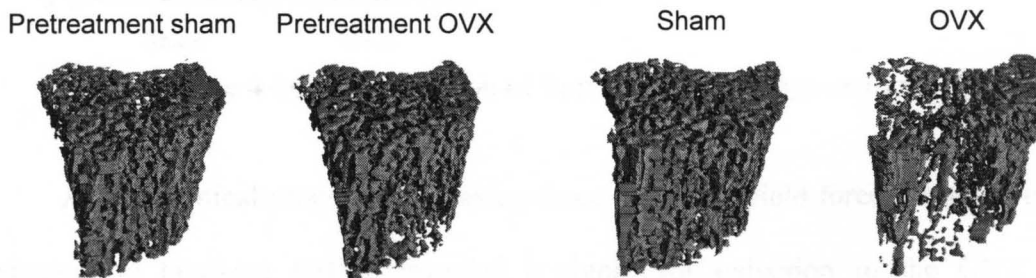


Figure 4-15 Three-dimensional images (Exp3) of the tibial metaphysis of an OVX and sham-operated animal (mean from each group) at the time of week 12 after operation: all images were aligned manually using VGStudio MAX to illustrate the internal cancellous bone structure.

The differences of the volume fractions between the OVX group and the Sham group in Exp3 were similar to those in Exp2, but the magnitudes of the differences in Exp

3 were less than those in Exp 2. The cancellous bone volume fraction of the OVX group was significantly lower than that of the Sham group by 55.8% in Exp 3 instead of by 72.5% in Exp2. In both Exp 2 and Exp 3, the cortical bone volume fraction showed no significant difference between the OVX group and the Sham group.

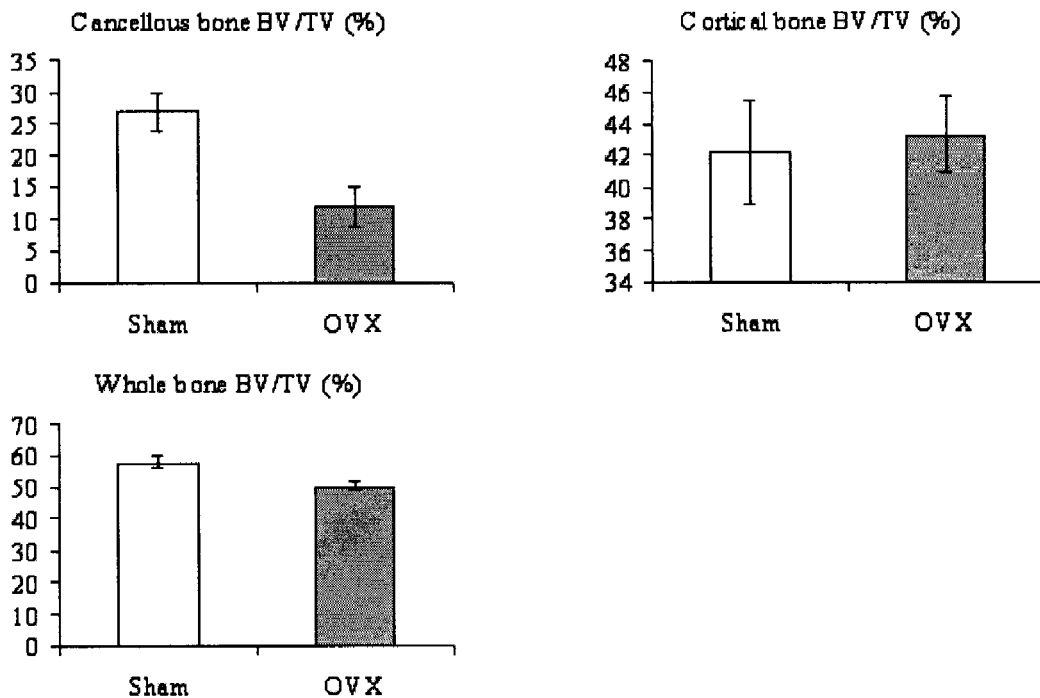


Figure 4-16 Bone fraction of Exp 3 from 3D image analysis

All mechanical properties (breaking force, breaking yield force, breaking energy) evaluated by breaking testing revealed a significant reduction in the OVX group compared with the Sham group. The decreases of breaking force, breaking yield force and breaking energy were 36.3%, 47.5% and 22.4%, respectively, as the result of estrogen deficiency.

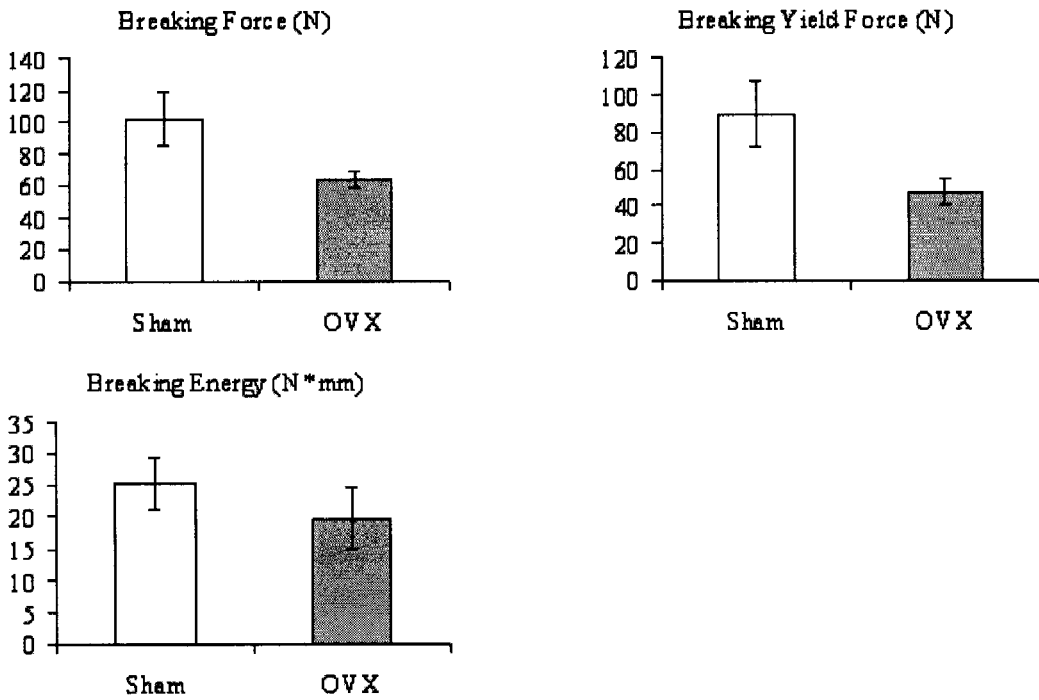


Figure 4-17 Three-point breaking testing results of Exp 3

Figure 4-18 shows the mechanical strength of cancellous bone assessed by indentation testing. The bone strength for the OVX group (5.16 ± 1.59) was significantly lower than that of the Sham group (37.94 ± 13.30) by 86.4% ($P < 0.001$).

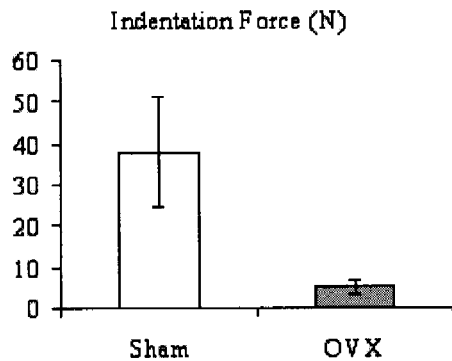


Figure 4-18 Indentation testing results of Exp 3

The measured properties of cortical bone showed no significant changes because of estrogen deficiency (Figure 4-19). The cross-section area showed a mild increase in the OVX group versus that in Sham group by 2.6%, but not significant.

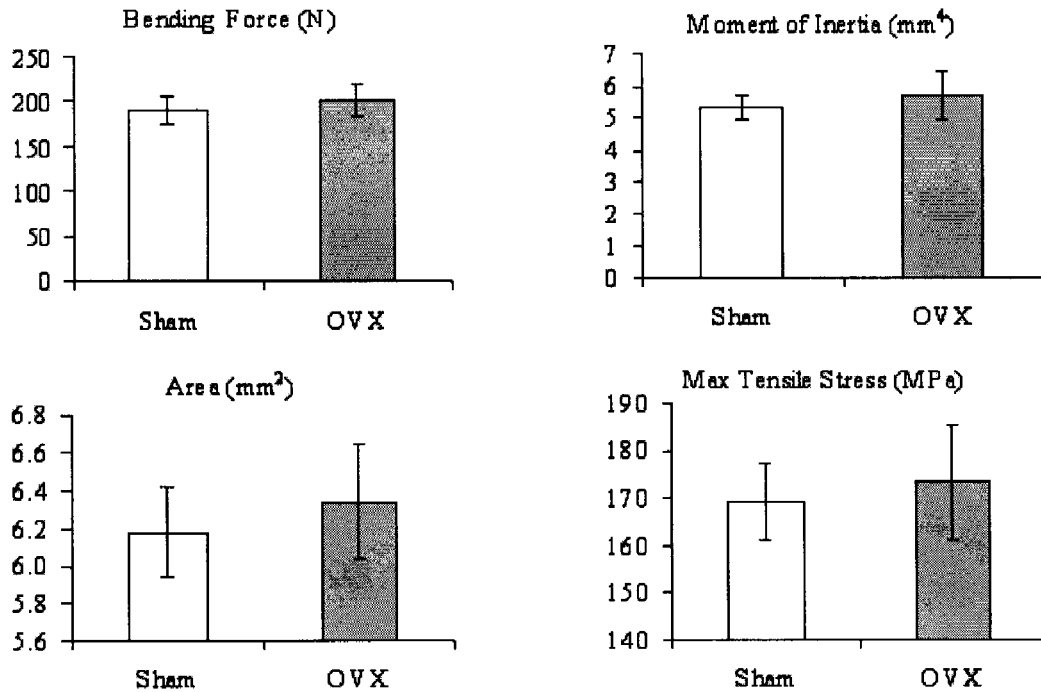


Figure 4-19 Three-point bending testing results of Exp 3

Although all densities of different bone parts showed the decrease due to the estrogen deficiency, there were not significant differences in densities of regional bone parts (Proximal, middle and distal) (Figure 4-20). Only the density of whole bone revealed the significant decrease in the OVX group versus Sham group by 3.1%.

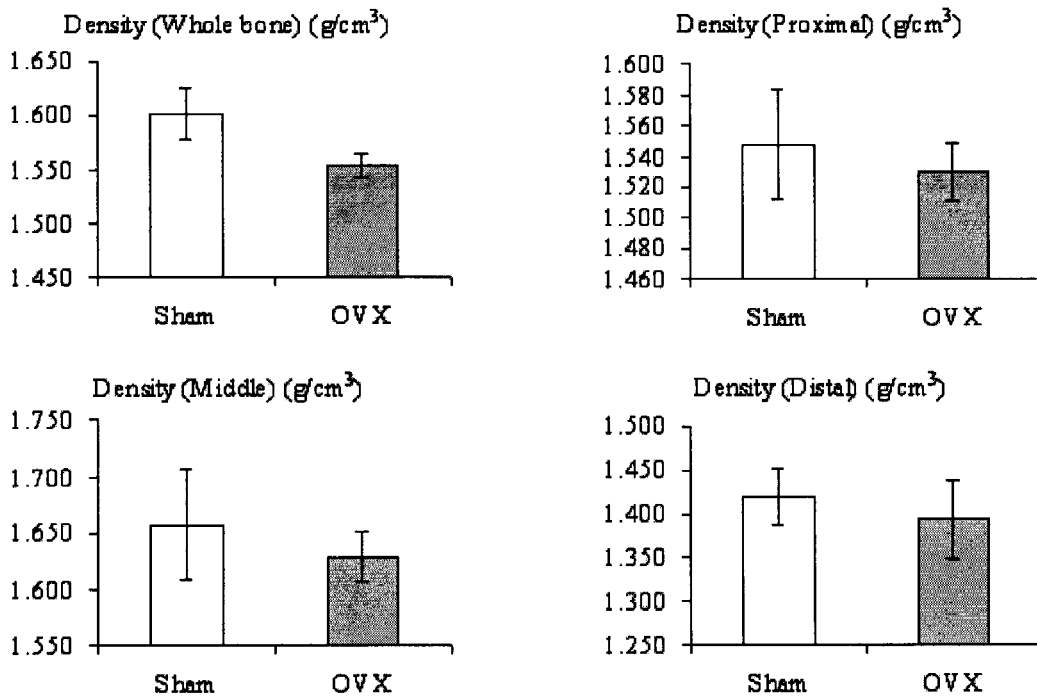


Figure 4-20 Density results of Exp 3 by Archimedes method

4.4 LINEAR REGRESSION ANALYSES

For Exp2, there were 6 data points for BV/TV parameters in group E2_W11 instead of 7 data points because one right tibia in group E2_W11 was destroyed before CT imaging.

4.4.1 Indentation testing vs. volume fraction

In Exp 2, indentation force was highly correlated with cancellous bone volume fraction ($R^2 = 0.569$, $P = 0.000$) and whole bone volume fraction ($R^2 = 0.503$, $P = 0.000$) (Figure 4-21). The R^2 of the correlation between indentation force and cortical bone volume fraction was only 0.245. There was a little fewer statistically significant

correlation between indentation force and whole bone volume fraction than was found between indentation force and cancellous volume fraction.

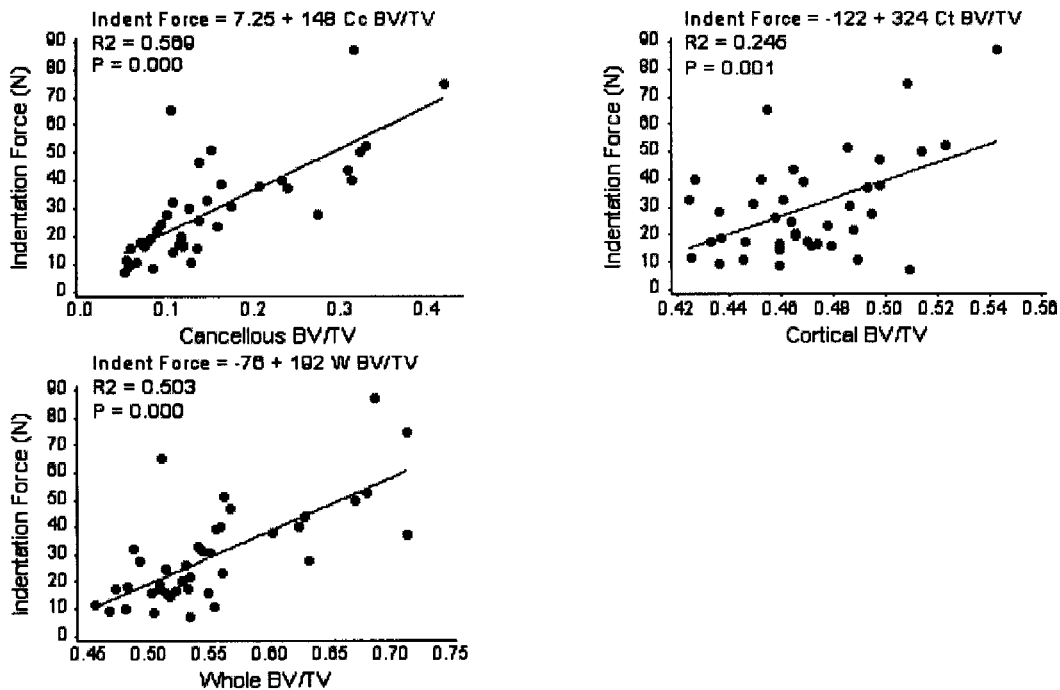


Figure 4-21 Regression analysis of Exp2: Indentation force vs. BV/TV

In Exp 3, indentation force was highly correlated with cancellous bone volume fraction ($R^2 = 0.542$, $P = 0.000$) and whole bone volume fraction ($R^2 = 0.588$, $P = 0.000$) (Figure 4-22). There was not significant correlation between indentation force and cortical bone volume fraction. There was a little fewer statistically significant correlation between indentation force and cancellous bone volume fraction than was found between indentation force and whole bone volume fraction.

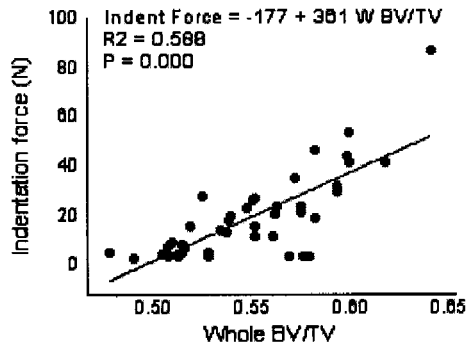
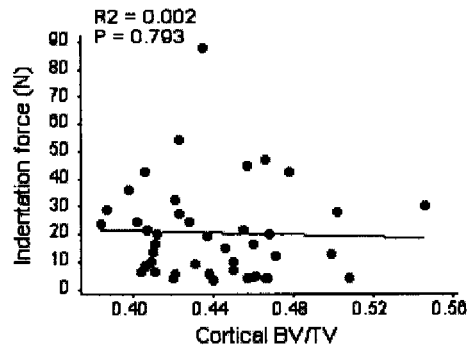
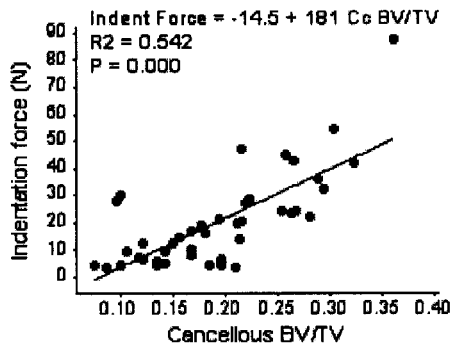


Figure 4-22 Regression analysis of Exp3: Indentation force vs. BV/TV

The R^2 of the correlation between cancellous bone volume fraction and cortical bone volume fraction was only 0.245 in Exp2 (Figure 4-23). Cancellous bone volume fraction was highly correlated with whole bone volume fraction ($R^2 = 0.852$, $P = 0.000$).

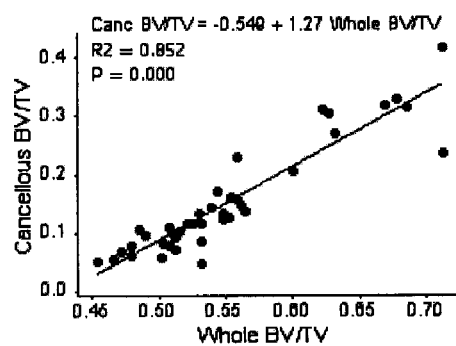
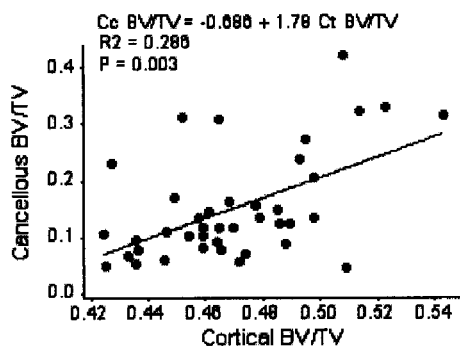


Figure 4-23 Regression analysis of volume fractions (Exp2)

The R^2 of the correlation between cancellous bone volume fraction and cortical bone volume fraction was only 0.218 in Exp3 (Figure 4-24). Cancellous bone volume fraction was highly correlated with whole bone volume fraction ($R^2 = 0.503$, $P = 0.000$)

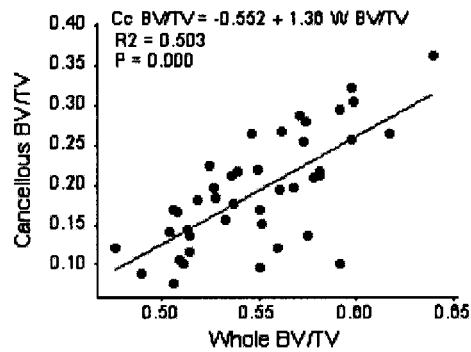
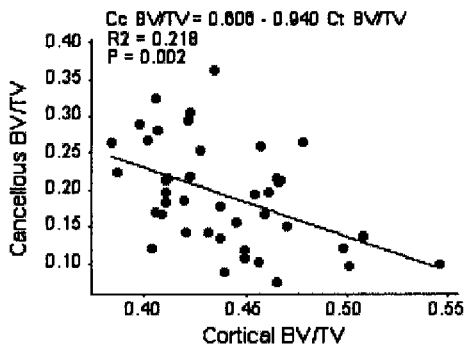


Figure 4-24 Regression analysis of volume fractions (Exp3)

4.4.2 Three-pt breaking testing vs. volume fraction

In Exp2, The R^2 of the correlation between the breaking force and cancellous bone volume fraction was only 0.293 (Figure 4-25). The R^2 of the correlation between the breaking force and whole bone volume fraction was 0.377. The R^2 of the correlation between the breaking force and whole bone volume fraction was 0.424.

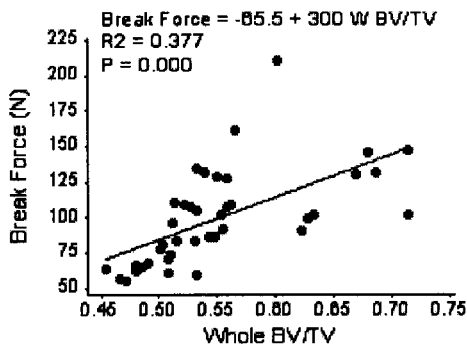
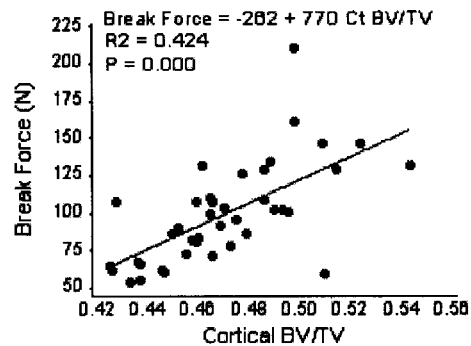
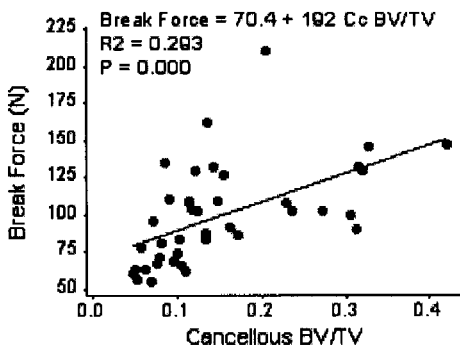


Figure 4-25 Regression analysis of Exp2: Breaking force vs. BV/TV

Figure 4-26 demonstrates a significantly positive correlation between the breaking force and cancellous bone volume fraction ($R^2 = 0.504$, $P = 0.000$) in Exp3. A significantly positive correlation was also demonstrated between the breaking force and whole bone volume fraction ($R^2 = 0.552$, $P = 0.000$). No significant correlation between the breaking force and cortical bone volume fraction was found ($R^2 = 0.001$, $P = 0.877$).

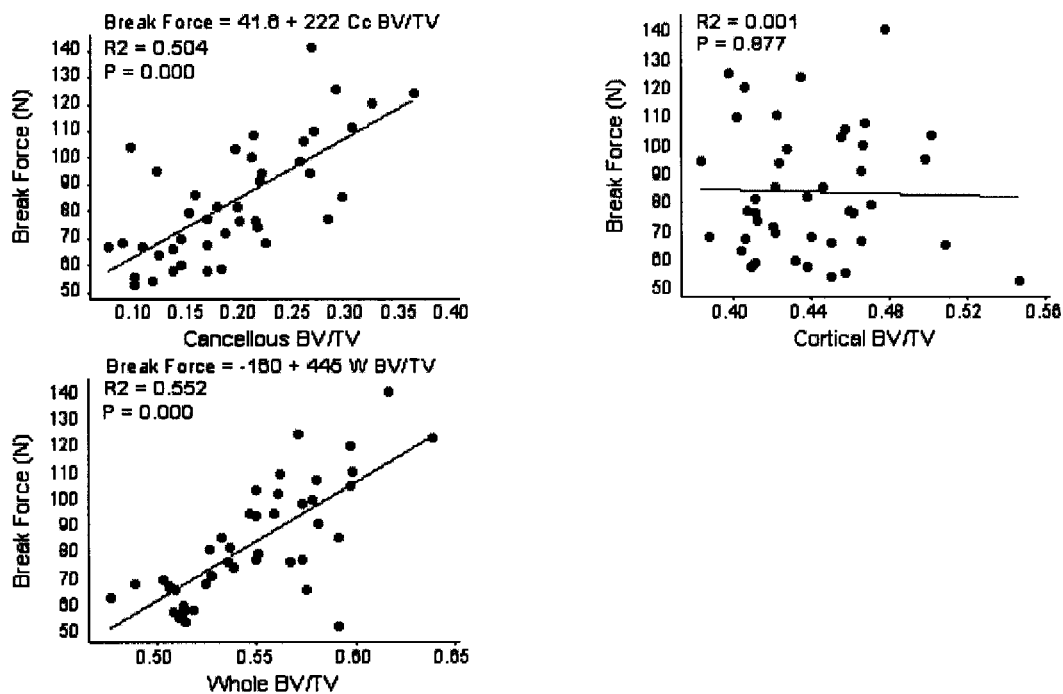


Figure 4-26 Regression analysis of Exp3: Breaking force vs. BV/TV

In Exp2, the R^2 of the correlation between the breaking yield force and cancellous bone volume fraction was 0.306 (Figure 4-27). The R^2 of the correlation between the breaking yield force and whole bone volume fraction was 0.356. The R^2 of the correlation between the breaking yield force and cortical bone volume fraction was 0.347.

In Exp3, the correlation between the breaking yield force and cancellous bone volume fraction was significant ($R^2 = 0.542$, $P = 0.000$) (Figure 4-28). The correlation between the breaking yield force and whole bone volume fraction was also significant

($R^2 = 0.552$, $P = 0.000$). No significant difference was found for the correlation among breaking yield force and cortical bone volume fraction.

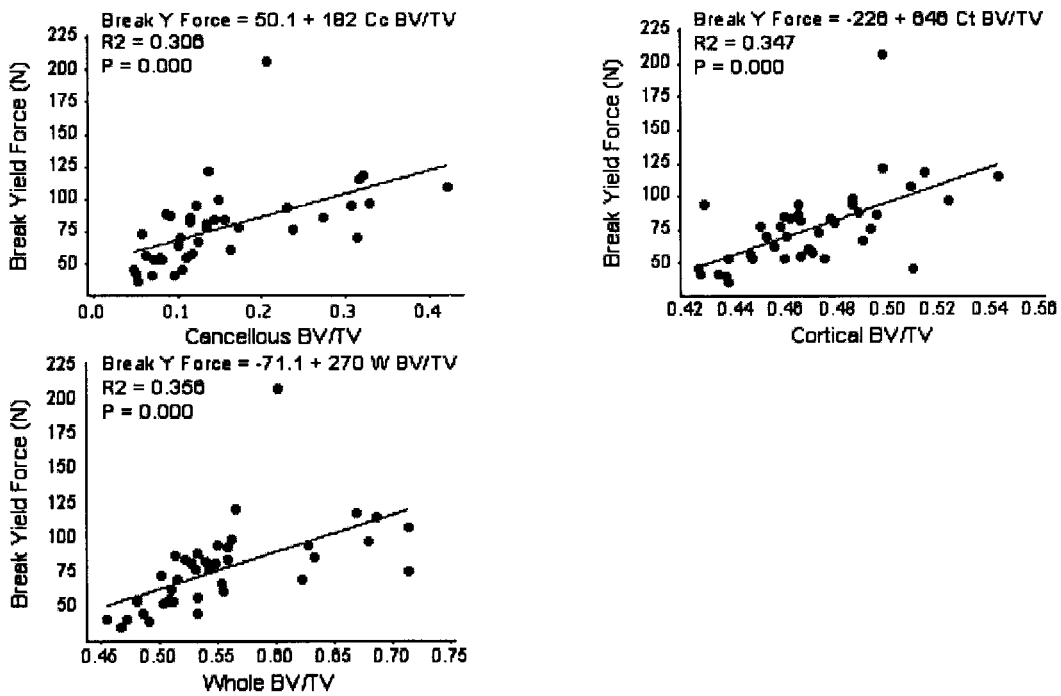


Figure 4-27 Regression analysis of Exp2: Breaking yield force vs. BV/TV

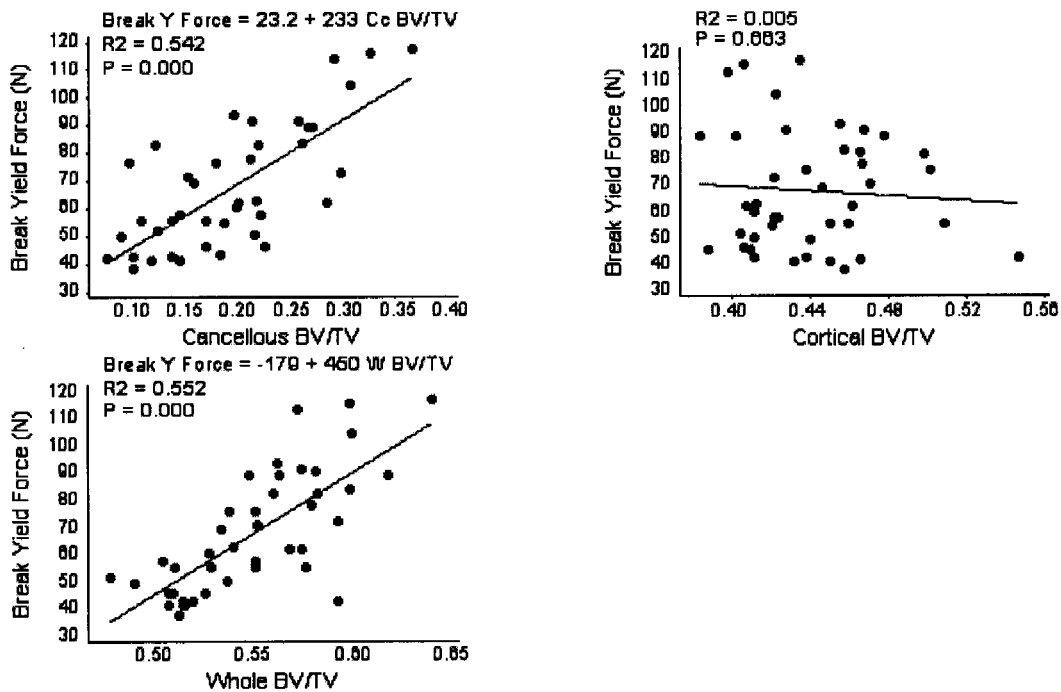


Figure 4-28 Regression analysis of Exp3: Breaking yield force vs. BV/TV

In Exp2, the R^2 of the correlation between the breaking energy and cancellous bone volume fraction was only 0.142 (Figure 4-29). The R^2 of the correlation between the breaking energy and whole bone volume fraction was 0.286. The R^2 of the correlation between the breaking energy and cortical bone volume fraction was 0.206.

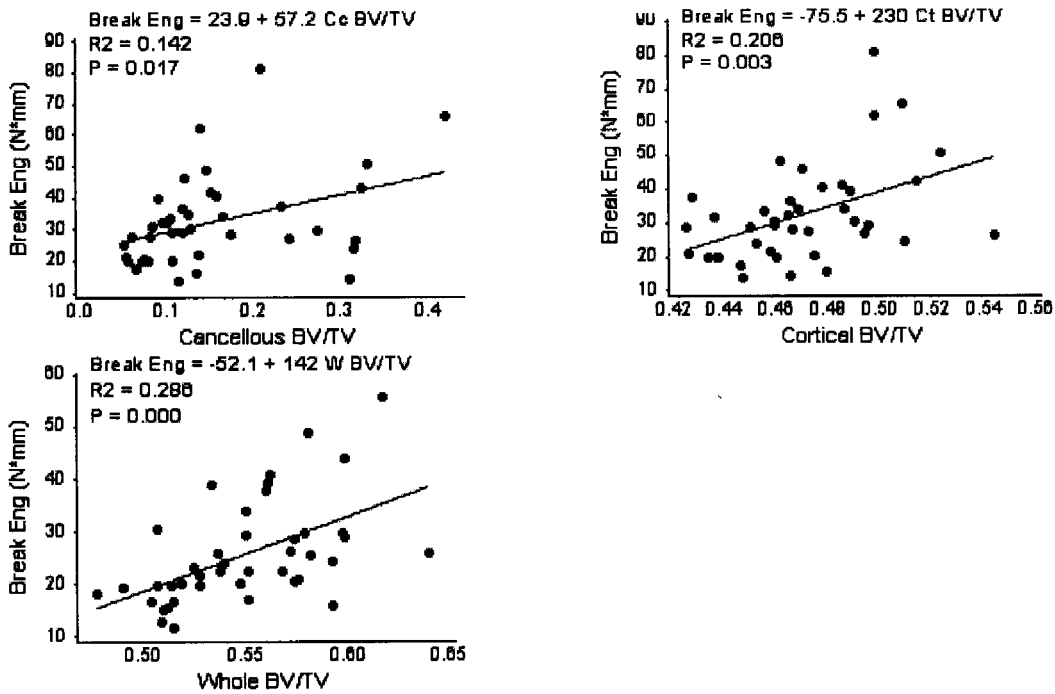


Figure 4-29 Regression analysis of Exp2: Breaking Energy vs. BV/TV

In Exp3, the R^2 of the correlation between the breaking energy and cancellous bone volume fraction was only 0.179 (Figure 4-30). The R^2 of the correlation between the breaking energy and whole bone volume fraction was 0.286. There was no significant correlation between breaking energy and cortical bone volume fraction.

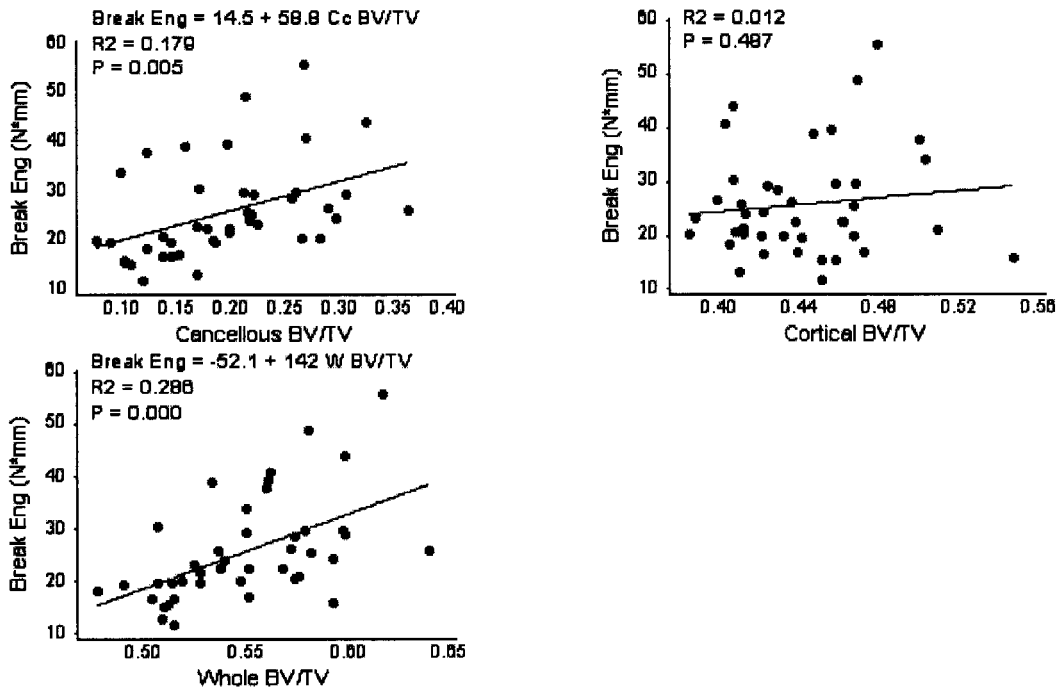


Figure 4-30 Regression analysis of Exp3: Breaking Energy vs. BV/TV

4.5 PRADAMA DATA ANALYSIS (DRUG EFFECT)

The results from Exp3 were used here to illustrate the drug effects on OVX rat models. One right femur from OVX_W6 was destroyed before three-point bending testing, so there were 5 bending force data and 5 maximum tensile stress data instead of 6 data. Table 4-13 is the P-value of statistical analysis results of the drug effect by ANOVA.

Table 4-13 Drug effect P-value of statistical analysis results by ANOVA (Exp 3)

	P value (with sham data)	P value (Without sham data)
BV/TV (Cancellous) (%)	0.000	0.035
BV/TV (Cortical) (%)	0.068*	0.063*
BV/TV (Whole) (%)	0.000	0.000
Indentation Force (N)	0.000	0.010
Breaking Force (N)	0.000	0.000
Breaking Yield Force (N)	0.000	0.000
Breaking Energy (N*mm)	0.000	0.000
Bending Force (N)	0.010	0.009
Moment of Inertia (mm ⁴)	0.039	0.036
Area (mm ²)	0.019	0.020
Max Tensile Stress (MPa)	0.003	0.001

Figure 4-31 shows the charts of the bone volume fractions calculated by image analysis method. The 3D structure of cancellous bone is shown in Figure 4-32.

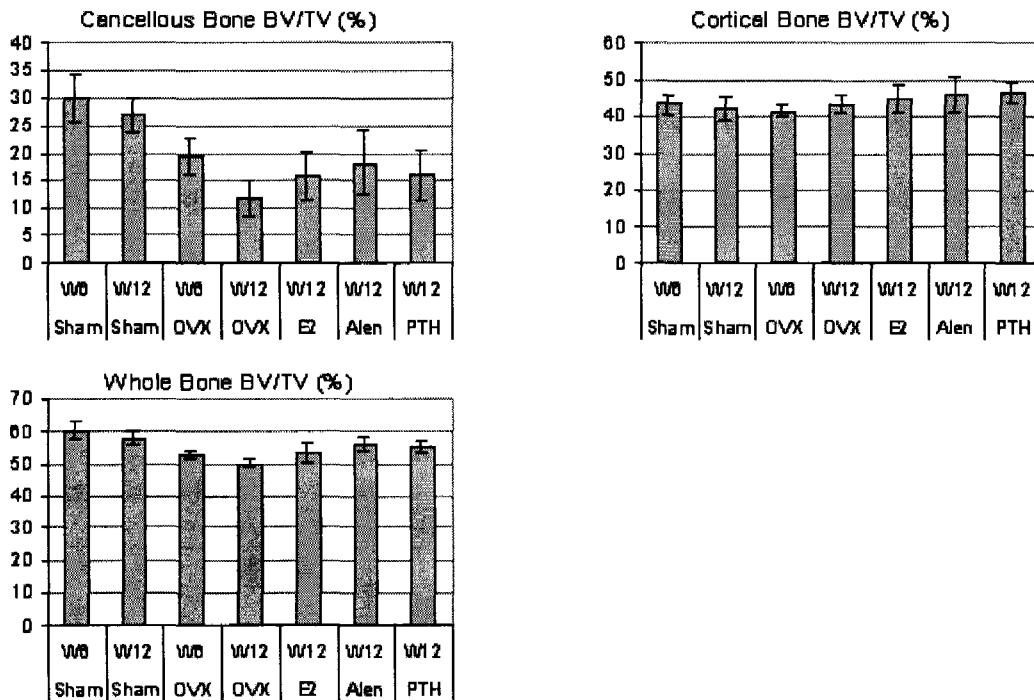


Figure 4-31 Bone fraction of Exp 3 from 3D image analysis

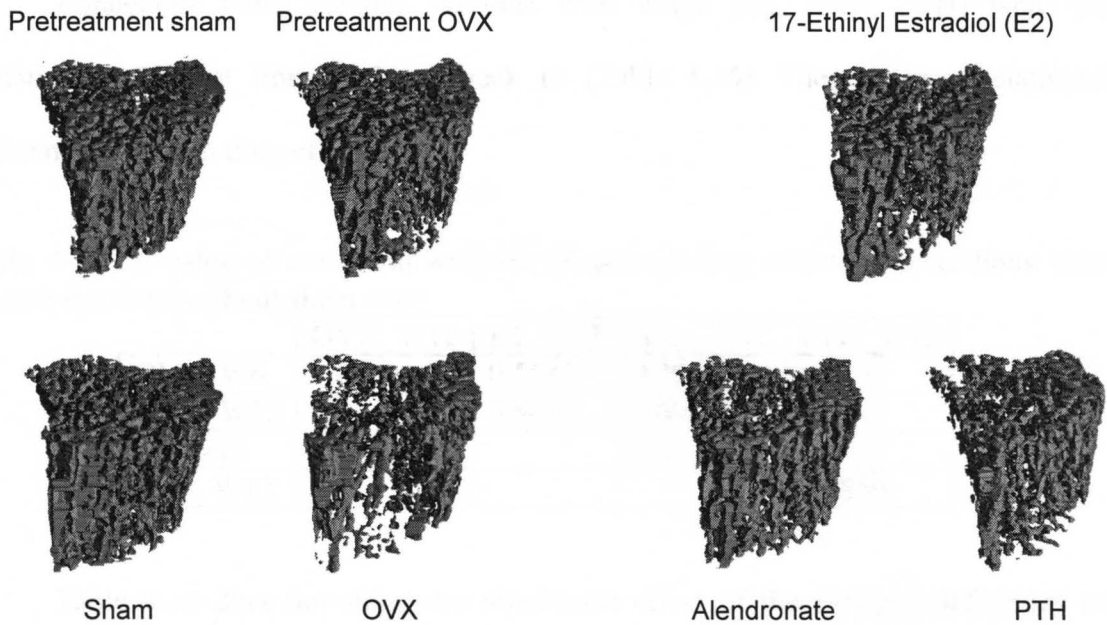


Figure 4-32 Three-dimensional images (Exp3) of the tibial metaphysis of an OVX and sham-operated animal (mean from each group) at the time of week 12 after operation: all images were aligned manually using VGStudio MAX to illustrate the internal cancellous bone structure.

The cancellous bone volume fraction of all OVX rats, regardless of treatment, were significantly different from those of sham at week 12. Estrogen deficiency caused significantly decrease in cancellous bone volume fraction at week 6 and week 12 (Table 4-14).

Table 4-14 P-value of statistical analysis (Exp3) of drug effect on cancellous bone volume fraction (with sham data)

	OVX_W6	OVX_W12	E2_W12	Alen_W12	PTH_W12
Sham_W6	0.0026				
Sham_W12		0.0000	0.0007	0.0137	0.0010
OVX_W6		0.0327	0.6949	0.9985	0.7657
OVX_W12			0.6445	0.1112	0.5647
E2_W12				0.9337	1.0000
Alen_W12					0.9621

Cancellous bone volume fractions with drugs (E2, Alen, PTH) were not statistically different from OVX at week 12 (Table 4-15). There were no statistical differences between drug effects.

Table 4-15 P-value of statistical analysis (Exp3) of drug effect on cancellous bone volume fraction (without sham data)

	OVX_W12	E2_W12	Alen_W12	PTH_W12
OVX_W6	0.0271	0.5519	0.9868	0.6239
OVX_W12		0.5039	0.0841*	0.4325
E2_W12			0.8375	1.0000
Alen_W12				0.8880

Table 4-16 does not show any significant effect of the estrogen deficiency on cortical bone volume fraction.

Table 4-16 P-value of statistical analysis (Exp3) of drug effect on cortical bone volume fraction (with sham data)

	OVX_W6	OVX_W12	E2_W12	Alen_W12	PTH_W12
Sham_W6	0.9494				
Sham_W12		0.9965	0.8012	0.4465	0.2191
OVX_W6		0.9336	0.527	0.2168	0.0881*
OVX_W12			0.9775	0.7686	0.482
E2_W12				0.9969	0.9433
Alen_W12					0.9993

Cortical bone volume fractions with drugs (E2, Alen, PTH) were not statistically different from OVX at week 12 (Table 4-17). There was no statistically different between drug effects.

Table 4-17 P-value of statistical analysis (Exp3) of drug effect on cortical bone volume fraction (without sham data)

	OVX_W12	E2_W12	Alen_W12	PTH_W12
OVX_W6	0.8316	0.3891	0.1522	0.0631*
OVX_W12		0.9179	0.6171	0.352
E2_W12			0.9781	0.8485
Alen_W12				0.9919

Estrogen deficiency caused significant decrease in whole bone volume fraction at week 6 and week 12 (Table 4-18).

Table 4-18 P-value of statistical analysis (Exp3) of drug effect on whole bone volume fraction (with sham data)

	OVX_W6	OVX_W12	E2_W12	Alen_W12	PTH_W12
Sham_W6	0.0000				
Sham_W12		0.0000	0.0175	0.7391	0.4007
OVX_W6			0.9953	0.1352	0.3601
OVX_W12			0.0677*	0.0002	0.0011
E2_W12				0.4072	0.7455
Alen_W12					0.9978

Whole bone volume fractions with drugs (E2, Alen, PTH) were statistically different from OVX at week 12 (Table 4-19). There were not statistical differences between drug effects.

Table 4-19 P-value of statistical analysis (Exp3) of drug effect on whole bone volume fraction (without sham data)

	OVX_W12	E2_W12	Alen_W12	PTH_W12
OVX_W6	0.1470	0.9656	0.0742*	0.2180
OVX_W12		0.0363	0.0002	0.0007
E2_W12			0.2518	0.5506
Alen_W12				0.9794

Figure 4-33 shows the mechanical strength of cancellous bone assessed by indentation testing. Estrogen deficiency caused significant decrease in indentation force at week 6 and week 12 (Table 4-20). At week 12, the bone strength for the OVX group (5.159 ± 1.594) was significantly lower than that of the Sham group (37.936 ± 13.303) by 86.4% ($P < 0.05$).

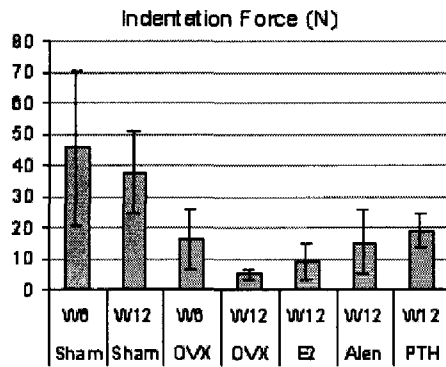


Figure 4-33 Indentation testing results of Exp 3

Table 4-20 P-value of statistical analysis (Exp3) of drug effect on indentation force (with sham data)

	OVX_W6	OVX_W12	E2_W12	Alen_W12	PTH_W12
Sham_W6	0.0030				
Sham_W12		0.0002	0.0022	0.0274	0.1015
OVX_W6			0.9252	1.0000	0.9996
OVX_W12			0.9953	0.6801	0.3269
E2_W12				0.9631	0.7412
Alen_W12					0.9975

The indentation forces with drugs (E2, Alen, PTH) were not statistically different from OVX_W12, with the exception of PTH_W12 (Table 4-21). There were no statistical differences between drug effects.

Table 4-21 P-value of statistical analysis (Exp3) of drug effect on indentation force (without sham data)

	OVX_W12	E2_W12	Alen_W12	PTH_W12
OVX_W6	0.0622*	0.4207	0.9991	0.9647
OVX_W12		0.8497	0.1061	0.0133
E2_W12			0.5686	0.1456
Alen_W12				0.8939

Figure 4-34 shows the mechanical strength of whole bone assessed by three-point breaking testing.

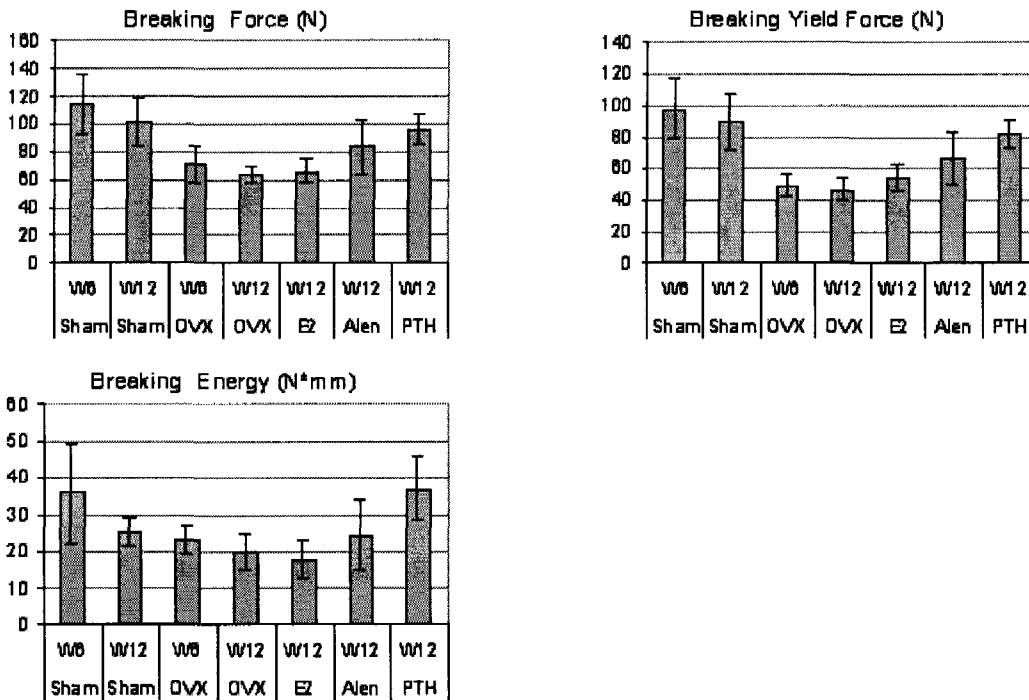


Figure 4-34 Three-point breaking testing results of Exp 3

Estrogen deficiency caused significant decreases in the breaking force at week 6 and week 12 (Table 4-22).

Table 4-22 P-value of statistical analysis (Exp3) of drug effect on breaking force (with sham data)

	OVX_W6	OVX_W12	E2_W12	Alen_W12	PTH_W12
Sham_W6	0.0005				
Sham_W12		0.0010	0.0029	0.3763	0.9974
OVX_W6			0.9931	0.7727	0.0705*
OVX_W12			1.0000	0.2228	0.0052
E2_W12				0.3619	0.0134
Alen_W12					0.7253

PTH treatment resulted in a significant increase of the breaking force reaching values above the OVX_W12, and E2_W12 groups (Table 4-23). E2 and Alendronate treatments did not show significant effect on breaking force.

Table 4-23 P-value of statistical analysis (Exp3) of drug effect on breaking force (without sham data)

	OVX_W12	E2_W12	Alen_W12	PTH_W12
OVX_W6	0.8201	0.9305	0.4537	0.0138
OVX_W12		0.9991	0.0619*	0.0007
E2_W12			0.1244	0.0019
Alen_W12				0.3988

Estrogen deficiency caused significant decreases in the breaking yield force at week 6 and week 12 (Table 4-24).

Table 4-24 P-value of statistical analysis (Exp3) of drug effect on breaking yield force (with sham data)

	OVX_W6	OVX_W12	E2_W12	Alen_W12	PTH_W12
Sham_W6	0.0000				
Sham_W12		0.0000	0.0006	0.0510*	0.9399
OVX_W6			0.9928	0.2672	0.0018
OVX_W12			0.9518	0.1320	0.0005
E2_W12				0.6648	0.0118
Alen_W12					0.3896

PTH treatment resulted in a significant increase of the breaking yield force reaching values above the OVX_W12, and E2_W12 group (Table 4-25). Alendronate also significantly increased the breaking yield force. In contrast, E2 treatment did not show significant effect on breaking yield force.

Table 4-25 P-value of statistical analysis (Exp3) of drug effect on breaking yield force (without sham data)

	OVX_W12	E2_W12	Alen_W12	PTH_W12
OVX_W6	0.9960	0.9079	0.0506*	0.0001
OVX_W12		0.7180	0.0172	0.0000
E2_W12			0.2668	0.0007
Alen_W12				0.0952*

Estrogen deficiency caused insignificant decreases in whole bone volume fraction at week 6 and week 12 (Table 4-26).

Table 4-26 P-value of statistical analysis (Exp3) of drug effect on breaking Eng (with sham data)

	OVX_W6	OVX_W12	E2_W12	Alen_W12	PTH_W12
Sham_W6	0.1062				
Sham_W12		0.8255	0.6290	1.0000	0.1328
OVX_W6			0.9011	0.9998	0.0418
OVX_W12			0.9996	0.8955	0.0037
E2_W12				0.7251	0.0019
Alen_W12					0.0956*

At week 12, PTH was the only treatment that resulted in a significant increase of the breaking energy compared to the OVX (Table 4-27).

Table 4-27 P-value of statistical analysis (Exp3) of drug effect on breaking Eng (without sham data)

	OVX_W12	E2_W12	Alen_W12	PTH_W12
OVX_W6	0.8909	0.6852	0.9939	0.0105
OVX_W12		0.9907	0.6747	0.0008
E2_W12			0.4391	0.0004
Alen_W12				0.0276

Figure 4-35 shows the mechanical strength of cortical bone assessed by three-point bending testing.

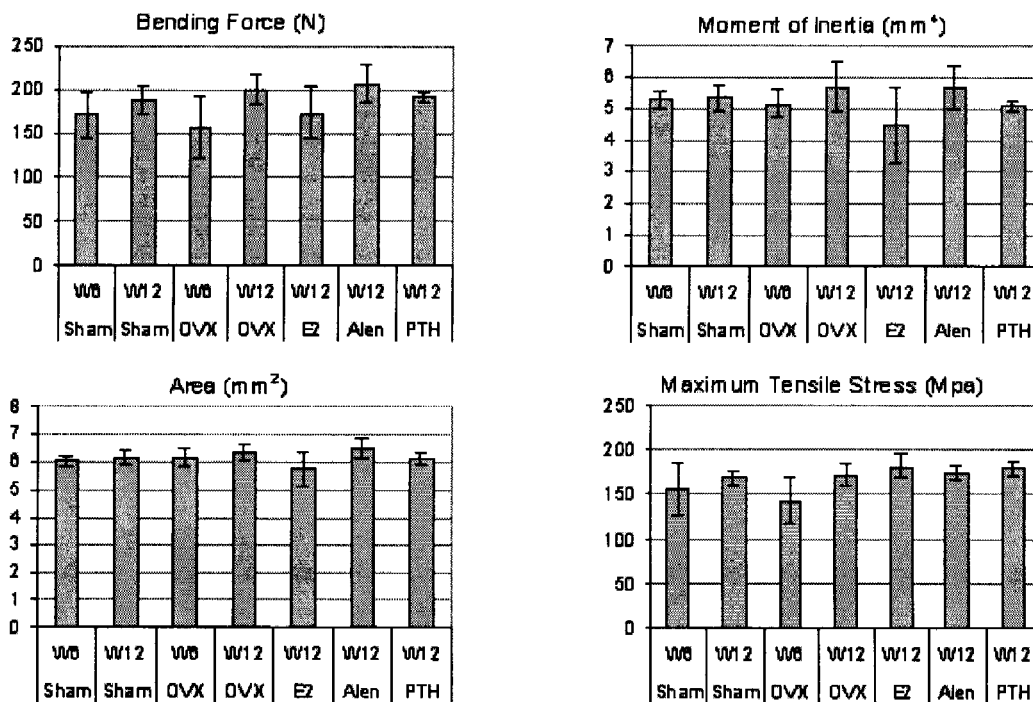


Figure 4-35 Three-point bending testing results of Exp 3

Estrogen deficiency caused insignificant decreases in the bending force at week 6 and week 12 (Table 4-28).

Table 4-28 P-value of statistical analysis (Exp3) of drug effect on bending force (with sham data)

	OVX_W6	OVX_W12	E2_W12	Alen_W12	PTH_W12
Sham_W6	0.9527				
Sham_W12		0.9762	0.9072	0.8099	1.0000
OVX_W6			0.8800	0.0144	0.1741
OVX_W12			0.4019	0.9973	0.9960
E2_W12				0.1815	0.8031
Alen_W12					0.9118

At the same time point, no drug increased the bending force compared with OVX group (Table 4-29).

Table 4-29 P-value of statistical analysis (Exp3) of drug effect on bending force (without sham data)

	OVX_W12	E2_W12	Alen_W12	PTH_W12
OVX_W6	0.0315	0.7532	0.0122	0.1244
OVX_W12		0.2914	0.9800	0.9742
E2_W12			0.1296	0.6580
Alen_W12				0.7986

Estrogen deficiency caused insignificant decreases in the moment of inertia at week 6 and week 12 (Table 4-30).

Table 4-30 P-value of statistical analysis (Exp3) of drug effect on moment of inertia (with sham data)

	OVX_W6	OVX_W12	E2_W12	Alen_W12	PTH_W12
Sham_W6	1.0000				
Sham_W12		0.9424	0.2798	0.9681	0.9932
OVX_W6			0.5482	0.8070	1.0000
OVX_W12			0.0254	1.0000	0.5986
E2_W12				0.0423	0.6774
Alen_W12					0.6910

E2 results in significant decrease in moment of inertia compared with OVX at week 12 (Table 4-31).

Table 4-31 P-value of statistical analysis (Exp3) of drug effect on moment of inertia (without sham data)

	OVX_W12	E2_W12	Alen_W12	PTH_W12
OVX_W6	0.6558	0.4966	0.7300	0.9997
OVX_W12		0.0384	1.0000	0.5394
E2_W12			0.0579*	0.6083
Alen_W12				0.6205

Estrogen deficiency caused insignificant decreases in the cross-sectional area at week 6 and week 12 (Table 4-32).

Table 4-32 P-value of statistical analysis (Exp3) of drug effect on cross-sectional area (with sham data)

	OVX_W6	OVX_W12	E2_W12	Alen_W12	PTH_W12
Sham_W6	0.9995				
Sham_W12		0.9809	0.2700	0.7025	1.0000
OVX_W6			0.4166	0.5273	1.0000
OVX_W12			0.0404	0.9830	0.9423
E2_W12				0.0075	0.3738
Alen_W12					0.5749

All treatment groups did not show any significant change in cross-sectional area compared with OVX at week 12 (Table 4-33).

Table 4-33 P-value of statistical analysis (Exp3) of drug effect on cross-sectional area (without sham data)

	OVX_W12	E2_W12	Alen_W12	PTH_W12
OVX_W6	0.8504	0.3769	0.4688	1.0000
OVX_W12		0.0523*	0.9481	0.8804
E2_W12			0.0133	0.3418
Alen_W12				0.5091

Estrogen deficiency caused insignificant decreases in the maximum tensile stress at week 6 and week 12 (Table 4-34).

Table 4-34 P-value of statistical analysis (Exp3) of drug effect on maximum tensile stress (with sham data)

	OVX_W6	OVX_W12	E2_W12	Alen_W12	PTH_W12
Sham_W6	0.8521				
Sham_W12		0.9990	0.7613	0.9934	0.9195
OVX_W6			0.0042	0.0306	0.0104
OVX_W12			0.9390	1.0000	0.9929
E2_W12				0.9838	0.9998
Alen_W12					0.9993

No statistically significant changes of treatments in maximum tensile stress were observed compared with OVX at week 12 (Table 4-35).

Table 4-35 P-value of statistical analysis (Exp3) of drug effect on maximum tensile stress (without sham data)

	OVX_W12	E2_W12	Alen_W12	PTH_W12
OVX_W6	0.0085	0.0007	0.0065	0.0020
OVX_W12		0.7530	0.9990	0.9349
E2_W12			0.8901	0.9940
Alen_W12				0.9860

CHAPTER 5. DISCUSSION

5.1 CANCELLOUS BONE SEGMENTATION METHOD

The new segmentation method offers a fast, automatic means to segment cancellous bone from cortical bone, and has the ability to determine the cavities in cortex automatically and objectively. Although the original image stacks (from computed tomography or MRI) provide 3D information, previous segmentation approaches are based on the 2D information of each single image slice and perform segmentation slice by slice according to this 2D information, which ignores the relationships between different slices. The difficulty of segmentation also comes from the complex structure of bone and the existence of the holes in the cortex. In some cases, it is difficult to know whether a cavity in a single image slice is a cavity in the cortex or a part of the marrow cavity. The insufficient information provided by the original image stack results in segmentation errors and limits the previous segmentation methods to be valid only in specific conditions. Unlike previous techniques, the method illustrated in this dissertation takes advantage of the 3D nature of the information, which is shown to have the advantage of giving more precise and accurate segmentation results.

If the ROI is connected to other bones in a single image stack, manual preprocessing is needed to delete the other bones from the ROI. An in-house program was created by Matlab for this purpose. The method is based on the observation that

cancellous bone is surrounded by a continuous marrow region and cortical bone is outside of this marrow region. The accurate designation of the marrow region is critical to the success of the method. There are three factors that affect the designation of marrow region: image quality, bone/non-bone segmentation and the definition of the WholeBoneMask.

Because trabeculae are very small, the present method requires high resolution of the original image stack so trabeculae can be separated from marrow. Higher image resolution leads to higher radiation dose and/or longer scanning times, which should be considered in *in vivo* study.

The segmentation of bone and non-bone is also critical. It is possible that cavities in the cortex are defined as marrow if the bone elements that are located between the cavities and the marrow are treated as non-bone elements, which leads to overestimation of the marrow region. Conversely, some marrow regions may be excluded from the definition of the main marrow region if a nonbone region appears to be disconnected from the main structure of marrow because of overestimation of the bone compartment.

The marrow region is the largest 3D cavity among the cavities found in the ROI. The cavities are defined by finding non-bone elements that are covered by the WholeBoneMask. In this dissertation, a dilating-filling-eroding method is used to create the WholeBoneMask if there are one or more cortex openings in a single image slice. Since the dilation smoothes the edges of the image, the outer contour of the WholeBoneMask is not exactly the same as that of the bone image, which causes false cavities along the outer surface of the bone compartment. If the false cavities are connected to the marrow region, they are false marrow and result in the inaccurate

definition of the marrow region. False marrow is on the image slices adjacent to or near the image slices with openings in the cortex. Since the segmentation is carried out based on the information of the marrow region, inaccurate definition of the marrow region causes errors in segmentation. Perfect WholeBoneMask is such that its contour is the same as that of the outer surface of cortex, so no false marrow exists. Different methods may be needed to find perfect WholeBoneMask for specific bone sample.

It works theoretically to find the largest object by the whole matrix method. However, the size of the 3D matrix, that is, the size of the bone sample, is limited to computer memory. To avoid this problem, the overlapping method was developed. Instead of handling the whole 3D matrix, overlapping method handles two image slices at one time, which results in more memory efficiency than the whole matrix method.

MarrowDiffL determines which bumps on the inner surface of cortex will be treated as trabeculae. MarrowDiffS delimits where to cut the trabeculae off. The value of MarrowDiffL and MarrowDiffS are determined by the bone structure in the study and are suggested to keep unchanged in a single longitudinal study, so no longitudinal error caused by these two parameters is involved.

There is no statistically significant difference between the segmentation results from the new method and those from a manual method, which demonstrates the accuracy of the new automatic segmentation method. However, the results calculated by the Helterbrand method are significantly different from those calculated by the manual method and by the new method. Using the manual work as gold standard, the new method is more accurate than the Helterbrand method.

The precision and repeatability of the new method are excellent. The precision of the new method is very high, ranging around 1%. The variance of the new method is statistically significantly smaller than that of the manual method, which means that the repeatability of the new method is better than the manual work. Theoretically, for a given image stack, the segmentation results will be the same no matter how many times the program is run if the program is totally automatic. The variance of the new method comes only from the scanning procedure: a single bone sample was loaded and scanned three times. The three data sets are not identical even though they come from the same bone sample because a bone sample cannot be fixed in the holder in exactly the same position twice.

In conclusion, the new method is more accurate than a previously published method (Helterbrand's method), and more precise and more repeatable than the manual method. The advantages of the method are: 1. It is automatic, accurate, precise and repeatable; 2. The segmentation is dependent on the bone architecture only, no assumption is needed; 3. The method has the potential to do segmentation even when the whole bone sample has complex structure and irregular shape; 4. The cavities in the cortex can be determined automatically and accurately. The prerequisite of the method is the high resolution of the image so that marrow region and cancellous compartment can be separated from each other.

5.2 ALENDRONATE STUDY

The volume fraction of the region of interest at week 0 approached 0.5 due to the young age of the rats and the ongoing growth and modeling of immature bone near the metaphysis. This also did not allow adequate registration of the serial images to include week 0.

OVX results in the negative basic multicellular units (BMUs) balance. It produces a net loss of bone from the skeleton with each remodeling event, which leads to the decrease of bone volume fraction. However, greater rates of bone loss and structural decay are more likely to be due to differences in remodeling rate than due to differences in remodeling imbalance (Seeman E, 2007). The situation may be explained by the regional difference of response to estrogen deficiency. It is well known that estrogen deficiency results in much greater bone loss in cancellous bone than in cortical bone. For the same bone volume, cancellous bone has much more bone surface than cortical bone, which indicates much greater remodeling rate in cancellous bone. Greater bone loss in cancellous bone reflects, at least partially, the greater influence of remodeling rate than the negative BMU balance.

This may explain the striking outcome of this study: alendronate causes such a large positive response in cancellous bone. The rats used in this study are 7-8 weeks old. The young animals are still growing rapidly and it is possible that the OVX operation results in higher remodeling rate in young animals. When anti-resorptive drug is given, the individuals with high baseline remodeling rate have more positive response than those with low baseline remodeling rate. The study of Greenspan et al. (Greenspan S et al.,

2006) showed that increases in BMD in those with a higher remodeling rate exceeded increases in BMD in those with low remodeling.

The dependence of the remodeling rate before treatment explains the effect of the young animals on the experimental results. The magnitude of increase of the bone volume fraction is also likely dependent on the inhibitory effect of the drug on resorption. Alendronate suppresses remodeling more than raloxifene (Allen M et al., 2006; Johnell O et al., 2002). The stronger the inhibitory effect of the drug on resorption, the greater the positive outcomes resulted by the drug. This is also supported by the experimental results of Alendronate Study. Based on the dose and schedule used in this study, it is clearly shown that alendronate resulted in significant higher cancellous bone volume fraction than E2. It may be tempting to conclude that alendronate has stronger inhibitory effect than E2 based on the experimental results of this Alendronate Study, but it needs be explored in future studies.

In Alendronate Study, alendronate has more positive effects on cancellous bone volume fraction than PTH as used in the young rat model. Because limiting the dose and frequency of PTH has some theoretical advantages, particularly with regard to cost (i.e. approximately US\$7200 per year for daily injections of PTH (Rosen CJ, 2004) and US\$635 drug cost per year of alendronate (Mobley LR et al, 2006)), combination therapy provides more economic choices. Rittmaster RS et al. (2000) have reported that postmenopausal osteoporotic women, who have been treated with alendronate given sequentially for 1 year after recombinant human PTH-(1–84) therapy, responded with an overall increase of 14.6% at the spine together with significant improvement in the femoral neck and total body calcium. Another possibility is that PTH was not given often

enough in Alendronate Study. PTH was administered only three times per week whereas other studies administered PTH more frequently (Baumann BD et al, 1995; Mosekilde L et al., 1995).

In summary, alendronate results in a greater increase of cancellous bone volume fraction than PTH in the model with high remodeling rate. Because the therapy of PTH is much more expensive, combination therapy of PTH followed by alendronate maybe a more economic choice as well as a more effective approach.

5.3 SENSITIVITY ANALYSIS

A novel indentation test method was developed during the Pradama Exp1. The animal samples of Pradama Exp1 were used to improve testing methods for the indentation testing and three-point breaking testing. Although exciting results in the Exp1 were obtained, the results of Exp1 were not very reliable because the Exp1 was more like a practicing. The sensitivity analysis was therefore based on Exp2 and Exp3.

A major drawback of the rat model is that rats continue to grow and do not ever completely fuse the epiphyses. This problem can be overcome by selecting cancellous bone sampling sites that are remodeling. For female Fischer rat model, the longitudinal bone growth in the proximal tibiae is $9.98\mu\text{m}/\text{day}$ at 6 months old and $3.3\mu\text{m}/\text{day}$ at 9 months old (Erben RG et al., 1996). In a 12-week (84 days) study, the proximal tibial growth will add less than 0.84 mm of new bone. Although the skeleton of Fischer rats may be more mature than skeleton in rat strains with a higher growth capacity, e.g., Sprague-Dawley or Wistar rats at a given age (Erben RG et al., 1996), the analysis with

ROI that begins at one mm distal to the growth plate of proximal tibia should be safe to avoid any new bone growth.

In both Exp2 and Exp3, there were no statistically significant differences between OVX and sham in the measurements of mid shaft of femur (bending force, moment of inertia, cross-sectional area and maximum tensile stress). The differences of some density measurements are detected and some not. For those densities with statistically significant differences, the differences between OVX and sham are in the range of 3.1% ~ 4.9%. Such small differences may be obscured because of issues of measurement precision, which challenges the three-point bending testing and Archimedes's method to be valid methods to evaluate OVX and treatment effects.

In Exp2, the difference in cancellous bone volume fraction between OVX and sham was 72.5% while the difference in whole bone volume fraction between OVX and sham was 19.9%. In Exp 3, the difference in cancellous bone volume fraction between OVX and sham was 55.8% while the difference in whole bone volume fraction between OVX and sham was 13.3%. No statistical significant difference in cortical bone between OVX and sham was detected. Estrogen deficiency increases the rate of bone remodelling and the negative bone balance in the BMUs. Remodeling occurs on bone surfaces. A volume of bone constructed with cancellous bone has more surface upon which remodeling can occur than the same volume of bone made up of cortical bone. Therefore, more cancellous bone is lost after OVX than cortical bone, which explains the better sensitivity of cancellous bone volume fraction to the differences between sham and OVX.

The indentation testing confirmed the dramatic effect of estrogen deficiency on cancellous bone in terms of corresponding changes in mechanical properties. OVX

resulted in 73.0% decrease in indentation force in Exp2 and 86.4% decrease in Exp3. Since there was little or no effect of estrogen deficiency on the cortical bone properties, which has been shown in the three-point bending testing, the excluding of cortical bone in the measurement increased the sensitivity in detecting changes of mechanical properties due to OVX or treatments.

The breaking testing measured mechanical properties of the whole bone of the proximal tibia metaphysis. The percent differences between sham and OVX obtained from the three-point breaking tests were about half of those from the indentation testing. The presence of cortical bone greatly reduced the sensitivity to detect changes in bone quality.

The difference in cancellous bone volume fraction between OVX and sham in Exp2 was greater than that in Exp3. Considering the fact that the distal part of the proximal metaphysis of tibia lost more cancellous bone after OVX operation, the result was not surprising because more distal part was included in the VOI of Exp2 than Exp3 (the VOI of Exp2 consisted of three hundred slices while the VOI of Exp3 consisted of two hundred slices).

Longer period of estrogen deficiency results in a greater bone loss. Because the indentation testing was performed at week 11 after OVX in Exp2 and week 12 after OVX in Exp3, it was not surprising that more difference was detected in indentation force in Exp 3 than in Exp2.

There have been many studies to explore the mechanical properties of cancellous bone by indentation testing. Some of these studies have identified regional variations of mechanical properties (Kato T, et al., 1996; Aitken GK, et al., 1985; Sumner DR, et al., 1994; Dunham CE et al., 2005). The bone samples for the studies, such as human patella,

distal human tibia, human humerus and adult male mongrel dog tibia, need to be big enough for the regional information. Indentation testing has also been used on small bone samples, like the rat model. An YH et al. (1997) reported the mechanical properties of rat epiphyseal cancellous bone. The indentation testing has also been used to evaluate mechanical properties of cancellous bone in the distal femoral metaphysis of rats (Shen V et al., 1995; Meng XW et al., 1996; Ke HZ et al., 1998). In Ke's study, OVX for 30 and 60 days induced significant decreases in the indentation force (-75%, and -82%, respectively) of cancellous bone as compared with sham control. Meng also reported the significantly lower load in OVX rats than in the sham animals. In all these previous studies, the exposed cancellous bone surface was completed by cutting the bone from the upper surface to a certain depth or by cutting directly proximal to the femoral condyle. Because the indentation testing results are very sensitive to the position of the exposed cancellous bone surface, the testing protocol is superior than other studies by providing consistent cuts with the help of CT scanning.

One other test method introduced in a previous study that indeed loaded only cancellous bone was the "reduced-platen" compression, which used platen sized and aligned to load only cancellous bone in the center of the sample (Hogan HA, et al., 2000). The maximum force, stiffness and energy absorbed were all diminished by roughly 60% as a result of the effect of 35 days of OVX on 14-week-old female Sprague-Dawley rats. This approach requires the cancellous bone surface on both top and bottom sides of the test specimens. In some cases when cancellous bone loss is severe, it is possible that there are just a few trabeculae or no cancellous bone on the bottom surface, which causes

trouble in the testing. In addition, the cutting position of exposed cancellous bone in Hogan's method was not sufficient.

Despite the promising results, the indentation testing protocol has its limitations. Specimen preparation is labor-consuming because of the bone embedding, CT scanning, saw-cut positioning and finally, cutting. Since the same indenter was used during the tests for all bone samples, the potential artifact introduced by the presence of the cortical bone that remains attached to the specimen during testing is different for different bone samples: the smaller the cross-area of the exposed cancellous surface, the greater the potential artifact. Unfortunately, the extent of this effect is unknown. This potential artifact was minimized by using a 1.5mm indenter, several times smaller than the metaphysis.

In summary, the changes of the mechanical properties of cancellous bone in the proximal tibia of the rat in different groups can be detected by the indentation testing; the evaluation of the whole bone properties at the proximal metaphysis can help people understand more about osteoporosis fracture. Based on the results and comparison with conventional methods (three-point bending testing, densities by Archimedes's method), the new methods (Cancellous bone volume fraction, indentation testing, three-point breaking testing) introduced here are more sensitive and useful to capture the changes in small bones of rat model.

5.4 LINEAR REGRESSION ANALYSIS

The selection of the ROI was better in Exp2 than in Exp3 because the start point of the ROI was more consistent in Exp2. In Exp2, A region located 0.98 mm (70 slices * 0.014 mm/slice) from the lower end of the growth plate and extending 4.2 mm (300 slices * 0.014 mm/slice) distally was chosen for evaluation. In Exp3, the ROI was chosen from the position where the lateral part of the cortex was just separated from the main part and extending 2.8 mm (200 slices * 0.014 mm/slice) distally.

The bone/non-bone segmentation was better in Exp3 than in Exp2. The global threshold method was used slice by slice to segment bone from nonbone in Exp2. The regional global threshold method was used slice by slice to segment bone from nonbone in Exp3. The better bone/non-bone segmentation resulted in better cortical and cancellous bone segmentation and finally better calculation of bone volume fraction. Due to some unknown reasons of scanning procedure, the lightness of the image slices changed a lot in a single image stack, which resulted in a wrong decision during bone/non-bone segmentation if the global threshold method was used. Moreover, since the cortical bone had higher gray values than cancellous bone, the global threshold method tended to lead to a bone/non-bone segmentation with thicker cortex and lost cancellous bone. These problems produced some poor results of cancellous and cortical bone segmentation, and finally some poor results of bone volume fraction. The regional global threshold method overcomes the problem of the lightness changing within a single image stack. In addition, regional global threshold method gave better decisions of cortical bone and cancellous bone definition than the global threshold method.

Because the bone/non-bone segmentation method had more effect on bone volume calculation than ROI selection, the results of Exp3 were considered closer to the real case and were used to explore the relationships between mechanical properties and bone volume fractions.

The indentation force was positively correlated with cancellous bone volume fraction and whole bone volume fraction. The R^2 (0.542) of the correlation between the indentation force and the cancellous bone volume fraction was a little lower than that (0.588) between the indentation force and the whole bone volume fraction. Because the indentation force was applied on the cancellous bone, it was expected that there would be better relationship between indentation results and cancellous bone volume fraction instead of whole bone volume fraction. One explanation to this phenomenon was that the whole bone volume fraction was also correlated with cancellous bone volume fraction ($R^2=0.503$). The bone loss or bone growth will happen on all parts of bone instead of some specific parts of bone. The second explanation to this phenomenon was the selection of the cancellous bone volume. The indentation force was applied on the cancellous bone surface that was just below the growth plate. The cancellous bone volume used in Exp3 was chosen lower than the growth plate. It is reasonable to predict the better correlation between the indentation force and the cancellous bone volume fraction if the cancellous bone volume was just below the growth plate, which needed to be confirmed in the future study. In addition, although the indentation force was applied on cancellous bone surface, the cancellous bone was attached to the cortical bone during the testing, which constrained lateral expansion of the loaded cancellous bone to some extent. This stiffer response led to the potential artifact, so the indentation force was not

only a response to the mechanical properties of the cancellous bone, but also to the cortical shell.

There was no correlation between the breaking results and cortical bone volume fraction. The breaking force was positively correlated with cancellous bone volume fraction and whole bone volume fraction. The R^2 (0.504) of the correlation between the breaking force and the cancellous bone volume fraction was a little lower than that (0.552) between the breaking force and the whole bone volume fraction. The yield breaking force was also positively correlated with cancellous bone volume fraction and whole bone volume fraction. The R^2 (0.542) of the correlation between the breaking yield force and the cancellous bone volume fraction was a little lower than that (0.552) between the breaking yield force and the whole bone volume fraction. Since three-point breaking testing evaluates the mechanical competence of whole bone, it was expected that there were better relationship between three-point breaking results and whole bone volume fraction instead of cancellous bone volume fraction and cortical bone volume fraction, which was shown in this experiment.

Although there was correlation between the bone mechanical strength and bone volume fraction, the R^2 value of around 0.55 was not strong enough to support the application of bone volume fraction alone to predict bone mechanical strength accurately. It may be explained by engineering perspective that mechanical competence is not only determined by the mass of the material but also determined by the spatial arrangement of the material, and the quality of the material, neither of which were considered. Pothuaud's study (Pothuaud L, et al., 2002) showed that in combining both morphological and topological explanatory powers, the normalized parameters were able

to increase the prediction of the elastic moduli compared to the prediction of BV/TV along. Shen (1995) also reported the mechanical strength was related to cancellous bone volume and connectivity parameters. So it is reasonable to expect that adding other structural parameters, such as trabecular thickness, trabecular number and trabecular separation etc, may result in better prediction, which needs to be shown in future studies.

5.5 PRADAMA DATA ANALYSIS (DRUG EFFECT)

The treatment effects of Estrogen, alendronate and PTH have also been evaluated here.

No drug significantly increased the cancellous bone volume fraction when compared with OVX control (Table 4-15). But the indentation testing showed that PTH resulted in the significant increase of mechanical strength of cancellous bone (Table 4-21). The discrepancy between the cancellous bone volume fraction and its mechanical strength caused by PTH therapy could be explained by the improvement of the bone structure or material. Previous studies (Sato M et al., 1997; Shen V et al, 1993) showed that PTH improved connectivity in the proximal tibiae and vertebrae. From a mechanical perspective, this is easy to understand because the strength of a structure is not only dependent on how much material is used to build the walls, but also dependent on the spatial arrangement of the materials.

PTH has been shown by others to significantly increase the cross-sectional area of cortical bone (Baumann BD et al, 1995; Mosekilde L et al., 1995). By contrast, Pradama Study did not show any significant differences in cross-sectional area and moment of

inertia. The different conclusions may be caused by the different treatment regimens. PTH was injected 5 days per week at a dose of 0.08 mg/kg BW in Baumann's study, 6 days per week at a dose of 0.08 mg/kg BW in Mosekilde's study, but only 3 days per week at a dose of 0.08 mg/kg BW in Pradama Study. In addition, the tibia diaphysis was evaluated in Baumann's study instead of the femur diaphysis, as in Pradama Study. The different site-specific responses to PTH have also been reported in other studies (Neer RM et al, 2001). Neer reported that the daily subcutaneous injections of PTH (1-34) increased bone mineral density by 9 and 13 more percentage points in the lumbar spine and by 3 and 6 more percentage points in the femoral, while decreased bone mineral density at the shaft of the radius by 2 more percentage points. Although the femur diaphysis was also evaluated in Moselilde's study, the treatment was initiated at 17 weeks of age in Moselilde's study and at 32 weeks of age in Pradama Study. The younger rat model may have more anabolic response to PTH treatment.

Although Roschger (Roschger P et al., 2001) reported that alendronate increased the degree and uniformity of mineralization in cancellous bone of osteoporotic women, there was no sign in Pradma Study that the intrinsic mechanical property (maximum tensile stress) was affected by the changes of material properties (if there was any change of material properties).

In the breaking tests, PTH significantly increased all measured parameters (breaking force, breaking yield force, breaking energy) compared with the OVX control group. Only breaking yield force was significantly increased by alendronate and no measured parameters were significantly increased by estrogen when compared with OVX control group. For the limited dosing that we investigated, the results of Pradama Study

suggest that PTH is superior to alendronate and estrogen in the restoring the mechanical strength in the proximal metaphysis of the rat tibia. However, it would be necessary to study each drug over a wide range of doses to find the optimum dose for each drug treatment. Then, when compared, the superiority of one drug over another may be determined. Considering the facts that there were not significant differences in the whole bone volume fraction between these three drug groups and the fact that PTH improved the bone structure, Pradama Study confirms the commonly accepted opinions that the bone volume fraction cannot predict the bone mechanical competence precisely. It is better to evaluate the bone structure together with the bone volume fraction to help people to understand the effect of osteoporosis and the treatments.

CHAPTER 6. CONCLUSION

The new cancellous and cortical bone segmentation method can segment cancellous bone from cortical bone automatically, accurately and precisely. There is no statistically significantly different between the result from the new method and that from the manual method. The variance of the results from the new method is significantly lower than that from manual method;

Alendronate was the only treatment that resulted in increased cancellous bone volume fraction and whole bone volume fraction in Alendronate Study, in which the young animals were used. This result has interesting implications for the possibility of early intervention to prevent osteoporosis while there is still enough remaining scaffold of cancellous bone for significant recovery to be possible;

The more traditional methods (Archimedes density measurements and three-point bending testing) show 5% or less differences between Sham group and OVX group. But for the same animals, the new methods (volume fraction, indentation testing, three-point breaking testing) can show up to 86% differences, indicating that the new methods are much more sensitive to distinguish the differences between sham, OVX and different drug treatments;

The correlations between indentation test and cancellous bone volume fraction, and between breaking force and whole bone volume fraction, and between breaking yield force and whole bone volume fraction are good. However, the correlation with R^2 around

0.55 is not strong enough to allow the sole application of bone volume fraction to predict mechanical properties accurately. For this reason, other image parameters are needed for the better correlation of destructive method using nondestructive method;

Bone volume fraction explains most of the differences in cancellous bone strength. But the spatial arrangement of bone material and the tissue quality also play important roles in bone quality. It is better to combine both image analysis and mechanical tests to understand osteoporosis in cancellous bone.

REFERENCE

- Aerssens J, Boonen S, Lowet G, Dequeker J. (1998) Interspecies difference in bone composition, density and quality; Potential implications for *in vivo* bone research. *Endocrinology* 139: 663-670.
- Aitken GK, Bourne RB, Finlay JB, Rorabeck CH, Andreae PR. (1985) Indentation stiffness of the cancellous bone in the distal human tibia. *Clin Orthop Relat Res.* 201: 264-70.
- Allen MR, Iwata K, Sato M, Burr DB. (2006) Raloxifene enhances vertebral mechanical properties independent of bone density. *Bone.* 39(5): 1130-5.
- An YH, Zhang J, Kang Q, Friedman RJ. (1997) Mechanical properties of rat epiphyseal cancellous bones studied by indentation testing. *J Mater Sci Mater Med* 8(8): 493-5.
- Augat P, Schorlemmer S. (2006) The role of cortical bone and its microstructure in bone strength. *Age Ageing* 35 Suppl 2: ii27-ii31.
- Azuma Y, Oue Y, Kanatani H, Ohta T, Kiyoki M, Komoriya K. (1998) Effects of continuous alendronate treatment on bone mass and mechanical properties in ovariectomized rats: comparison with pamidronate and etidronate in growing rats. *J Pharmacol Exp Ther.* 286(1):128-35.
- Baldock PAJ, Morris HA, Moore RJ, Need AG, Durbridge TC. (1998) Prepubertal oophorectomy limits the accumulation of cancellous bone in the femur of growing rats with long-term effects on metaphyseal bone architecture. *Calcif Tissue Int* 62: 244-249.
- Balena R, Toolan BC, Shea M, Markatos A, Myers ER, Lee SC, Opas EE, Seedor JG, Klein H, Frankenfield D, Quartuccio H, Fioravanti C, Clair J, Brown E, Hayes WC, Rodan GA. (1993) The effects of 2-year treatment with the aminobisphosphonate alendronate on bone metabolism bone histomorphometry and bone strength in ovariectomized nonhuman primates. *J Clin Invest* 92:2577-2586.
- Baumann BD, Wronski TJ (1995) Response of cortical bone to antiresorptive agents and parathyroid hormone in aged variectomized rats. *Bone* 16:247-253.

- Binkley N, Kimmel D, Bruner J, Haffa A, Davidowitz B, Meng C, Schaffer V, Green J. (1998) Zoledronate prevents the development of absolute osteopenia following ovariectomy in adult rhesus monkeys. *J Bone Miner Res* 13:1775-1782.
- Black, D. et al. (2003) The effects of PTH and alendronate alone or in combination in post-menopausal osteoporosis. *N. Engl. J. Med.* 349, 1207–1215.
- Borah B, Dufresne TE, et al. (2000) Evaluation of changes in trabecular bone architecture and mechanical properties of minipig vertebrae by three-dimensional magnetic resonance microimaging and finite element modeling. *J Bone Miner Res* 15(9): 1786-1797.
- Boyce RW, Franks AF, Jankowsky ML, Orcutt CM, Piacquadio AM, White JM, Bevan JA. (1990) Sequential histomorphometric changes in cancellous bone from ovariectomized dogs. *J Bone Miner Res* 5: 947-953.
- Boyd SK, Davison P, Muller R, Gasser JA. (2006) Monitoring individual morphological changes over time in ovariectomized rats by *in vivo* micro-computed tomography. *Bone* 39(4):854-862.
- Bronner, F. and Worrell, R. V., Eds. (1999) *Orthopaedics, Principles of Basic and Clinical Sciences*, CRC Press, Boca Raton, FL
- Buie HR, Campbell GM, Klinck RJ, Macneil JA, Boyd SK. (2007) Automatic segmentation of cortical and trabecular compartments based on a dual threshold technique for *in vivo* micro-CT bone analysis. *Bone*. 41(4):505-515.
- Burstein AH and Frankel VH. (1971) A standard test for laboratory animal bone. *J Biomech* 4:155–158.
- Clifford JR. (2004) What's new with PTH in osteoporosis: where are we and where are we headed? *TRENDS in Endocrinology and Metabolism*, Vol 15, NO. 5: 229-233.
- Consensus Development Conference, (1991) Prophylaxis and treatment of osteoporosis. *Am J Med* 90(1):107–110.
- Cummings SR, Melton LJ 3rd. (2002) Epidemiology and outcomes of osteoporotic fractures. *Lancet* 350: 1761-1767.
- Davidson MK, Lindsey JR, Davis JK. (1987) Requirements and selection of an animal model. *Isr J Med Sci* 23: 551-555.
- De Laet CE, van Hout BA, Burger H, Hofman A, Pols HA. (1997) Bone density and risk of hip fracture in men and women: cross sectional analysis. *BMJ* 315: 221–225.

- Dufresne T. (1998) Segmentation techniques for analysis of bone by three-dimensional computed tomographic imaging. *Technology and Health Care* 6: 351-359.
- Dunham CE, Takaki SE, Johnson JA, Dunning CE. (2005) Mechanical properties of cancellous bone of the distal humerus. *Clin Biomech (Bristol, Avon)*. 20(8):834-838.
- Elmoutaouskikil A, Peyrin F, Elkafi J, and Laval-Jeantet AM. (2002) Segmentation of cancellous bone from high-resolution computed tomography images: influence on trabecular bone measurements. *IEEE transactions on medical imaging*, Vol. 21, No. 4: 354-362.
- Engelke K, Kalender W (1998) Beyond bone densitometry: assessment of bone architecture by X-ray computed tomography at various levels of resolution. In: Genant HK, Guglielmi G, Jergas M (eds) *Bone Densitometry and Osteoporosis*. Springer, Berlin, pp 417-447.
- Erben RG. (1996) Trabecular and endocortical bone surfaces in the rat: modeling or remodeling. *Anat Rec* 246:39-46.
- Faugere MC, Okamoto S, DeLuca HF, Malluche HH. (1986) Calcitriol corrects bone loss induced by oophorectomy in rats. *Am J Physiol* 250:E35-E38.
- Feldkamp LA, Goldstein SA, Parfitt AM, Jesioil G, Kleerekoper M. (1989) The direct examination of three-dimensional bone architecture in vitro by computed tomography. *J. Bone Miner. Res.* 4: 3-11.
- Frost HM. (1998) Osteoporoses: New concepts and some implications for future diagnosis, treatment and research (based on insights from the Utah paradigm). Ernst Schering Research Foundation AG Lecture, Berlin: 7-57.
- Frost HM, Jee WSS. (1992) On the rat model of human osteopenias and osteoporoses. *Bone Miner* 18:227-236.
- Fox J, Miller MA, Newman MK, Metcalfe AF, Turner CH, Recker RR, Smith SY. (2006) Daily treatment of aged ovariectomized rats with human parathyroid hormone (1-84) for 12 months reverses bone loss and enhances trabecular and cortical bone strength. *Calcif Tissue Int.* 79(4):262-272.
- Genant HK, Engelke K, Fuerst T, Gluer CC, Grampp S, Harris ST, Jergas M, Lang T, Lu Y, Majumdar S, Mathur A, Takada M. (1996) Noninvasive assessment of bone mineral and structure: State of the art. *J Bone Miner Res* 11:707-730.
- Genant HK, Jiang Y. (2006) Advanced imaging assessment of bone quality. *Ann N Y Acad Sci.* 1068:410-428.

- Gilsanz V, Roe TF, Gibbens DT, Schulz EE, Carlson ME, Gonzalez O, Boechat MI. (1988) Effect of sex steroids on peak bone density of growing rabbits. *Am J Physiol* 255: E416-E421.
- Grardel B, Sutter B, Flautre B, Viguiier E, Lavaste F, Hardouin P. (1994) Effects of glucocorticoids on skeletal growth in rabbits evaluated by dual-photon absorptiometry, microscopic connectivity and vertebral compressive strength. *Osteoporosis Int* 4: 204-210.
- Greenspan S, Sebba A, Saag K, Thompson D, Rosenberg E, Chen EE, et al. (2006) Early reductions in bone turnover markers are associated with 24-month bone mineral density response and non-response in the Fosemanx Actonel Comparison Trial (FACT). Proceedings of the 28th annual meeting of the Am Soc Bone Mineral Res. Philadelphia USA Sept 15-19, 21(suppl 1). *J Bone Miner Res*; abst [M345].
- Haralick RM, and Shapiro LG. (1992) *Computer and Robot Vision, Vol. I*, Addison-Wesley: 158-205.
- Harrigan TP, Jasty M, Mann RW, (1988) Limitations of the continuum assumption in cancellous bone. *J. Biomech.*, 21, 269-275.
- Harvey EJ, Bobyn JD, Tanzer M, Stackpool GJ, Krygier JJ, Hacking SA. (1999) Effect of flexibility of the femoral stem on bone-remodeling and fixation of the stem in a canine total hip arthroplasty model without cement. *J Bone Joint Surg* 81-A: 93-107.
- Hazzard DG, Bronson RT, McClearn GE, Strong R. (1992) Selection of an appropriate animal model to study aging processes with special emphasis on the use of rat strains *J Gerontol: Biol Sci* 47: B63-64.
- Heaney RP. (1998) Bone mass, bone loss, and osteoporosis prophylaxis. [Editorial] *Ann Intern Med* 128(4):313-314.
- Hogan HA, Ruhmann SP, Sampson HW. (2000) The mechanical properties of cancellous bone in the proximal tibia of ovariectomized rats. *J Bone Miner Res.* 15(2):284-92.
- Helterbrand JD, Higgs RE Jr., Iversen PW, Tysarczyk-Niemeyer G, and Sato M. (1997) Application of Automatic Image Segmentation to Tibiae and Vertebrae From Ovariectomized Rats. *Bone*, Vol. 21, No. 5: 401-409.
- Hogan HA, Ruhmann SP, Sampson HW. (2000) The mechanical properties of cancellous bone in the proximal tibia of ovariectomized rats. *J Bone Miner Res.* 15(2):284-292.

- Hvid I, Hansen SL. (1985) Trabecular bone strength patterns at the proximal tibial epiphysis. *J Orthop Res.* 3(4):464-472.
- Jamsa T, Rho JY, Fan Z, MacKay CA, Marks SC Jr, Tuukkanen J. (2002) Mechanical properties in long bones of rat osteopetrotic mutations. *J Biomech.* 35(2):161-165.
- Jiang Y, Zhao J, Liao EY, Dai RC, Wu XP, Genant HK. (2005) Application of micro-CT assessment of 3-D bone microstructure in preclinical and clinical studies. *J Bone Miner Metab.* 23 Suppl:122-131.
- Jones G, Nguyen T, Sambrook PN, Kelly PJ, Gilbert C, and Eisman JA. (1994) Symptomatic fracture incidence in elderly men and women: The Dubbo osteoporosis epidemiology study (DOES). *Osteoporosis International*, Vol. 4, No. 5: 277-282.
- Johnell O, Scheel WH, Lu Y, Reginster J-Y, Need AG, Seeman E. (2002) Additive effects of raloxifene and alendronate on bone density and biochemical markers of bone remodelling in postmenopausal women with osteoporosis. *J Clin Endocrinol Metab* 87: 985-992.
- Kalu DN. (1991) The ovariectomized rat model of postmenopausal bone loss. *Bone Miner* 15:175-192.
- Katoh T, Griffin MP, Wevers HW, Rudan J. (1996) Bone hardness testing in the trabecular bone of the human patella. *J Arthroplasty* 11(4):460-468.
- Ke HZ, Shen VW, Qi H, Crawford DT, Wu DD, Liang XG, Chidsey-Frink KL, Pirie CM, Simmons HA, Thompson DD. (1998) Prostaglandin E2 increases bone strength in intact rats and in ovariectomized rats with established osteopenia. *Bone.* 23(3):249-255.
- Keenan MJ, Hegsted M, Jones KL, Delany JP, Kime JC, Melancon LE, Tulley RT, Hong KD. (1997) Comparison of bone density measurement techniques: DXA and Archimedes' principle. *J Bone Miner Res* 12:1903-1907.
- Kinney JH, Lane NE, Haupt DL. (1995) *In vivo*, three-dimensional microscopy of trabecular bone. *J Bone Miner Res* 10:264-270.
- Khodadadyan-Klostermann C, von Seebach M, Taylor WR, Duda GN, Haas NP. (2004) Distribution of bone mineral density with age and gender in the proximal tibia. *Clin Biomech (Bristol, Avon).* 19(4):370-376.
- Kimmel DB. (1991) The oophorectomized beagle as an experimental model for estrogen-depletion bone loss in the adult human. *Cells and Materials Suppl* 1: 75-84.

- Klotzbuecher CM, Ross PD, Landsman PB, et al. (2000) Patients with prior fractures have an increased risk of future fractures: a summary of the literature and statistical synthesis. *J Bone Miner Res*, Vol. 15: 721-739.
- Kohlbrenner A, Ruegsegger P. (1997) A high-speed 3D-pQCT system for structure analysis. *Osteoporosis Int*. 7: 268.
- Kuhn JL, Goldstein SA, Feldkamp LA, Goulet RW, Jesion G. (1990) Evaluation of a microcomputed tomography system to study trabecular bone structure. *J. Orthop. Res*. 8: 833-842.
- Lafage H-M, Balena R, Battle MA, Shea M, Seedor JG, Klein H, Hayes WC, Rodan G. (1995) Comparison of alendronate and sodium fluoride effects on cancellous and cortical bone in minipigs. *J Clin Invest* 95: 2127-2133.
- Lepola V, Vaananen K, and Jalovaara P. (1993) The effect of immobilization on the torsional strength of the rat tibia. *Clin Orthop* 297: 55-61.
- Li M, Shen Y, Qi H, Wronski TJ. (1996) Comparison study of skeletal response to estrogen depletion at red and yellow marrow sites in rats. *Anat Rec* 245:472-480.
- Li XJ, Jee WSS, Ke HZ, Mori S, Akamine T. (1991) Age related changes of cancellous and cortical bone histomorphometry in female Sprague-Dawley rats. *Cells Materials Suppl* 1:25-35.
- Lill CA, Gerlach UV, Eckhardt C, Goldhahn J, Schneider E. (2002) Bone changes due to glucocorticoid application in an ovariectomized animal model for fracture treatment in osteoporosis. *Osteoporos Int* 13: 407-414.
- Lill CA, Fluegel AK, Schneider E. (2002) Effect of ovariectomy, malnutrition and glucocorticoid application on bone properties in sheep: A pilot study. *Osteoporos Int* 13: 480-486.
- Lind PM, Lind L, Larsson S, Orberg J. (2001) Torsional testing and peripheral quantitative computed tomography in rat humerus. *Bone*. 29(3):265-270.
- Lindsay R. (1995) The burden of osteoporosis: cost. *Am J Med*, 98(2A): 9S-11S.
- Lindsay R, Silverman SL, Cooper C, et al. (2001) Risk of new vertebral fracture in the year following a fracture. *JAMA*, vol. 285, No. 3: 320-323.
- Lochmuller EM, Muller R, Kuhn V, Lill CA, Eckstein F. (2003) Can Novel Clinical Densitometric Techniques Replace or Improve DXA in Predicting Bone Strength in Osteoporosis at the Hip and Other Skeletal Sites? *J Bone Miner Res*, Volume 18, Number 5: 906-912.

- Ma YF, Ke HZ, Jee WSS. (1994) Prostaglandin E2 adds bone to a cancellous bone site with a closed growth plate and low bone turnover in ovariectomized rats. *Bone* 15:137-146.
- Maier GW, Kreis ME, Zittel TT, Becker HD. (1997) Calcium regulation and bone mass loss after total gastrectomy in pigs. *Ann Surg.* 225(2):181-192.
- Manolagas SC. (2000) Birth and death of bone cells: basic regulatory mechanisms and implications for the pathogenesis and treatment of osteoporosis. *Endocr Rev*, Vol. 21: 115-137.
- McNamara LM, Ederveen AG, Lyons CG, Price C, Schaffler MB, Weinans H, Prendergast PJ. (2006) Strength of cancellous bone trabecular tissue from normal, ovariectomized and drug-treated rats over the course of ageing. *Bone* 39(2):392-400.
- McNamara LM, Ederveen AG, Lyons CG, Price C, Schaffler MB, Weinans H, Prendergast PJ. (2007) Bone remodelling algorithms incorporating both strain and microdamage stimuli. *J Biomech.* 40(6):1381-1391.
- Meng XW, Liang XG, Birchman R, Wu DD, Dempster DW, Lindsay R, Shen V. (1996) Temporal expression of the anabolic action of PTH in cancellous bone of ovariectomized rats. *J Bone Miner Res.* 11(4):421-429.
- Melton LJ III, Thamer M, Ray NF, Chan JK, Chesnut CH III, Einhorn TA, Johnston CC, Raisz LG, Silverman SL, Siris ES. (1997) Fractures attributable to osteoporosis: Report from the National Osteoporosis Foundation. *J. Bone Miner. Res.* 12: 16-23.
- Melton LJ III, Atkinson EJ, Cooper C, et al. (1999) Vertebral fractures predict subsequent fractures. *Osteoporos Int*, Vol. 10: 214-221.
- Mobley LR, Hoerger TJ, Wittenborn JS, Galuska DA, Rao JK. (2006) Cost-effectiveness of osteoporosis screening and treatment with hormone replacement therapy, raloxifene, or alendronate. *Med Decis Making.* 26(2):194-206.
- Monier-Faugere M-C, Geng Z, Qi Q, Arnala I, Malluche HH. (1996) Calcitonin prevents bone loss but decreases osteoblastic activity in ovariohysterectomized beagle dogs. *J Bone Miner Res* 11: 446-455.
- Mosekilde L, Danielsen CC, Sogaard CH, McOsker JE, Wronski TJ (1995) The anabolic effects of parathyroid hormone on cortical bone mass, dimensions and strength-assessed in a sexually mature, ovariectomized rat model. *Bone* 16:223-230.
- Muller R, Ruegsegger P. (1997) Assessment of trabecular structure using high resolution magnetic resonance imaging. *Stud Health Technol Inform* 40:81-96.

- Nackaerts O, Jacobs R, Pillen M, Engelen L, Gijbels F, Devlin H, Lindh C, Nicopoulou-Karayianni K, van der Stelt P, Pavitt S, Horner K. (2006) Accuracy and precision of a densitometric tool for jaw bone. *Dentomaxillofac Radiol.* 35(4):244-248.
- National Osteoporosis Foundation, Washington D.C. (1996) Osteoporosis: the silent disease. Slide presentation #6.
- Neer RM, Arnaud CD, Zanchetta JR, Prince R, Gaich GA, Reginster JY, Hodsmann AB, Eriksen EF, Ish-Shalom S, Genant HK, Wang O, Mitlak BH. (2001) Effect of parathyroid hormone (1-34) on fractures and bone mineral density in postmenopausal women with osteoporosis. *N Engl J Med.* 344(19):1434-1441.
- NIH Consensus Development Panel on Osteoporosis Prevention, Diagnosis, and therapy. Osteoporosis prevention, diagnosis, and therapy. (2001) *JAMA*, 285: 785-795.
- Odgaard A, Andersen K, Melsen F, Gundersen HJ. (1990) A direct method for fast three-dimensional serial reconstruction. *J Microsc.* 159(Pt 3):335-342.
- Orsini LS, Rousculp MD, Long SR, Wang S. (2005) Health care utilization and expenditures in the United States: a study of osteoporosis-related fractures. *Osteoporosis international (Osteoporos. int.)*, Vol. 16, No. 4: 359-371.
- Otsu, N. (1979) A Threshold Selection Method from Gray-Level Histograms. *IEEE Transactions on Systems, Man, and Cybernetics*, Vol. 9, No. 1: 62-66.
- Parfitt AM. Skeletal heterogeneity and the purposes of bone remodelling: implications for the understanding of osteoporosis. In: Marcus R, Feldman D, Kelsey J, editors. *Osteoporosis*. San diego, CA: Academic; 1996. p. 315-329.
- Peng Z, Tuukkanen J, Zhang H, Jämsä T, Väänänen HK. (1994) The mechanical strength of bone in different rat models of experimental osteoporosis. *Bone* 15: 523-532.
- Peng Z-Q, Väänänen HK, Zhang HX, Tuukkanen J. (1997) Long-term effects of ovariectomy on the mechanical properties and chemical composition of rat bone. *Bone* 20: 207-212.
- Peyrin F, Salome M, Cloetens P, Laval-Jeantet AM, Ritman E, Rueggsegger P. (1998) Micro-CT examinations of trabecular bone samples at different resolutions: 14, 7 and 2 micron level *Technol Health Care* 6:391-401.
- Pothuaid L, Van Rietbergen B, Mosekilde L, Beuf O, Levitz P, Benhamou CL, Majumdar S. (2002) Combination of topological parameters and bone volume fraction better predicts the mechanical properties of trabecular bone. *J Biomech.* 35(8):1091-1099.

- Ray NF, Chan JK, Thamer M, Melton LJ III. (1997) Medical expenditures for the treatment of osteoporotic fractures in the United States in 1995: report from the National Osteoporosis Foundation. *J Bone Miner Res*, 12: 24-35.
- Rettmaster RS, Bolognese M, Ettinger MP, Hanley DA, Hodsmann AB, Kendler DL, Rosen CJ. (2000) Enhancement of bone mass in osteoporotic women with parathyroid hormone followed by alendronate. *J Clin Endocrinol Metab* 85: 2129-2134.
- Roschger P, Rinnerthaler S, Yates J, Rodan GA, Fratzl P, Klaushofer K. (2001) Alendronate Increases Degree and Uniformity of Mineralization in Cancellous Bone and Decreases the Porosity in Cortical Bone of Osteoporotic Women. *Bone*. 29(2):185-191.
- Rosen CJ. (2004) What's new with PTH in osteoporosis: where are we and where are we headed? *Trends Endocrinol Metab*.15(5):229-233.
- Rueggsegger P and Muller R. (1995) 3D-microtomography of human bones. Perth International Bone Meeting, Reth, Australia; 42.
- Rueggsegger P, Koller B and Muller R. (1996) A microtomographic system for the nondestructive evaluation of bone architecture. *Calcif. Tissue Int*. 58: 24–29.
- Sato M, Zeng GQ, Turner CH. (1997) Biosynthetic human parathyroid hormone (1-34) effects on bone quality in aged ovariectomized rats. *Endocrinology*. 138(10): 4330-4337.
- Sedgewick, Robert. (1998) *Algorithms in C*, 3rd Ed., Addison-Wesley, pp. 11-20.
- Seeman E. (2007) Is a change in bone mineral density a sensitive and specific surrogate of anti-fracture efficacy? *Bone*. 41(3): 308-317.
- Shen V, Birchman R, Xu R, Otter M, Wu D, Lindsay R, Dempster DW. (1995) Effects of reciprocal treatment with estrogen and estrogen plus parathyroid hormone on bone structure and strength in ovariectomized rats. *J Clin Invest*. 96(5):2331-2338.
- Soille P. (1999) *Morphological Image Analysis: Principles and Applications*, Springer-Verlag, pp. 173-174.
- Sogaard CH, Wronski TJ, McOsker JE, Mosekilde L. (1994) The positive effect of PTH on femoral neck bone strength in ovariectomized rats is more pronounced than that of estrogen or bisphosphonate. *Endocrinology* 134:650-657.
- Sturmer EK, Seidlova-Wuttke D, Sehmisch S, Rack T, Wille J, Frosch KH, Wuttke W, Sturmer KM. (2006) Standardized bending and breaking test for the normal and

osteoporotic metaphyseal tibias of the rat: effect of estradiol, testosterone, and raloxifene. *J Bone Miner Res.* 21(1):89-96.

Sumner DR, Willke TL, Berzins A, Turner TM. (1994) Distribution of Young's modulus in the cancellous bone of the proximal canine tibia. *J Biomech.* 27(8):1095-1099.

Trebacz H, Zdunek A. (2006) Three-point bending and acoustic emission study of adult rat femurs after immobilization and free remobilization. *J Biomech.* 2006;39(2):237-245.

Turner AS. (2001) Animal models of osteoporosis--necessity and limitations. *Eur Cell Mater.* Vol 1: 66-81.

Turner CH, Wang T, Hirano T. (1999) In primates, treatment with PTH (1-34), teriparatide, increases bone strength at trabecular bone sites without compromising the strength of cortical bone. *J Bone Miner Res* 14:S1;S414.

Turner RT, Maran A, Lotinun S, Hefferan T, Evans GL, Zhang M, Sibonga JD. (2001) Animal models for osteoporosis. *Rev Endocr Metab Disord.* 2(1):117-127.

Ulrich D, Hildebrand T, Van Rietbergen B, Muller R, Ruegsegger P. (1997) The quality of trabecular bone evaluated with micro-computed tomography, FEA and mechanical testing. *Stud Health Technol Inform.* 1997;40:97-112.

US Congress OoTA. (1994) Hip fracture outcomes in people aged fifty and over--background paper. OTA-BP-H-120. Washington, DC: US Government printing Office.

van den Boomgaard and van Balen. (1992) "Image Transforms Using Bitmapped Binary Images," *Computer Vision, Graphics, and Image Processing: Graphical Models and Image Processing*, Vol. 54, No. 3: 254-258.

Waarsing JH, Day JS, Weinans H (2004) An improved segmentation method for *in vivo* microCT imaging. *J Bone Miner Res.* 19(10):1640-1650.

Westerlind KC, Wronski TJ, Ritman EL, Luo Z-P, An K-N, Bell NH, Turner RT. (1997) Estrogen regulates the rate of bone turnover but bone balance in ovariectomized rats is modulated by prevailing mechanical strain. *Proc Natl Acad Sci USA.* 94: 4199-4204.

WHO Study Group. (1994) Assessment of fracture risk and its applications to screening for postmenopausal osteoporosis. WHO Technical Report Series 843, WHO, Geneva.

Wronski TJ, Cintron M, Dann LM. (1988) Temporal relationship between bone loss and increased bone turnover in ovariectomized rats. *Calcif Tissue Int.* 43(3):179-183.

- Wronski TJ, Dann LM, Scott KS, Cintron M. (1989) Long-term effects of ovariectomy and aging on the rat skeleton. *Calcif Tissue Int.* 45(6):360-366.
- Wronski TJ, Lowry PL, Walsh CC, Ignaszewski LA. (1985) Skeletal alterations in ovariectomized rats. *Calcif Tissue Int* 37:324–328.
- Wronski TJ, Yen CF. (1991) The ovariectomized rat as an animal model for postmenopausal bone loss. *Cells Materials Suppl* 1:69–74.
- Yang KH, Won JH, Yoon HK, Ryu JH, Choo KS, Kim JS. (2007) High concentrations of pamidronate in bone weaken the mechanical properties of intact femurs in a rat model. *Yonsei Med J.* 48(4):653-658.
- Yang S. 2006. Animal experiment (rabbit) to demonstrate changes in trabecular bone mechanical properties over time using finite element analysis. PhD Dissertation. Orthopaedic Bioengineering Laboratory. University of Louisville Press, Louisville, KY.

CURRICULUM VITAE

NAME: Qian Xu

ADDRESS: Department of Mechanical Engineering
J.B. Speed School of Engineering
University of Louisville
Louisville, Kentucky 40292

EDUCATION

&TRAINING: Ph.D., (Doctoral candidate) Mechanical Engineering
University of Louisville, Louisville, KY
2003 - 2008

Masters, Engineering, Mechanical Engineering
Beijing University of Chemical Technology, Beijing, China
1993 - 1996

B.S., Mechanical Engineering
Daqing Petroleum Institute, Province of Heilongjiang, China
1989 - 1993

AWARDS: Hsing Chuang Award for Excellence in Graduate Study
University of Louisville
2006

Graduate Assistantship
Orthopaedic Bioengineering Laboratory
University of Louisville
2003 - 2008

PUBLICATIONS:

Xu, Q; Voor, MJ; Merten K; Pierce WM., (2008) Cancellous bone quality differences between osteoporosis therapies. Transactions of the Southeastern Meeting of the American Society of Biomechanics, Birmingham, Alabama.

Xu, Q; Voor, MJ; Waddell, S W; Burden, R L, Jr., (2007) Marrow space used for high resolution image segmentation of cancellous and cortical bone. Transactions of the 31st Annual Meeting of the American Society of Biomechanics, Stanford University, Palo Alto, California.

Voor, MJ; **Xu, Q**; Burden RL Jr; Neale, J; Carter, H; Yang S; Waddel, SW; Pierce, WM., (2007) Alendronate is strongly anabolic in a young rat model of ovariectomy induced osteoporosis whereas hormone-based treatments have little effect. Transactions of the 53rd Annual Meeting of Orthopaedic Research Society, San Diego, California.